2009

Investigation Of Damage Detection Methodologies For Structural Health Monitoring

Mustafa Gul
University of Central Florida

INVESTIGATION OF DAMAGE DETECTION METHODOLOGIES FOR STRUCTURAL HEALTH MONITORING

by

MUSTAFA GÜL
B.S. Boğaziçi University, 2002
M.Sc. Boğaziçi University, 2004

A dissertation submitted in partial fulfillment of the requirements
for the degree of Doctor of Philosophy
in the Department of Civil, Environmental and Construction Engineering
in the College of Engineering and Computer Science
at the University of Central Florida
Orlando, Florida

Summer Term
2009

Major Professor: F. Necati Çatbaş

ABSTRACT

Structural Health Monitoring (SHM) is employed to track and evaluate damage and deterioration during regular operation as well as after extreme events for aerospace, mechanical and civil structures. A complete SHM system incorporates performance metrics, sensing, signal processing, data analysis, transmission and management for decision-making purposes. Damage detection in the context of SHM can be successful by employing a collection of robust and practical damage detection methodologies that can be used to identify, locate and quantify damage or, in general terms, changes in observable behavior. In this study, different damage detection methods are investigated for global condition assessment of structures. First, different parametric and non-parametric approaches are re-visited and further improved for damage detection using vibration data. Modal flexibility, modal curvature and un-scaled flexibility based on the dynamic properties that are obtained using Complex Mode Indicator Function (CMIF) are used as parametric damage features. Second, statistical pattern recognition approaches using time series modeling in conjunction with outlier detection are investigated as a non-parametric damage detection technique. Third, a novel methodology using ARX models (Auto-Regressive models with eXogenous output) is proposed for damage identification. By using this new methodology, it is shown that damage can be detected, located and quantified without the need of external loading information. Next, laboratory studies are conducted on different test structures with a number of different damage scenarios for the evaluation of the techniques in a comparative fashion. Finally, application of the methodologies to real life data is also presented along with the capabilities and limitations of each approach in light of analysis results of the laboratory and real life data.

To my family, whom I love more than everything

ACKNOWLEDGMENTS

First and foremost, I would like to express my thanks and my deepest gratitude to Dr. F. Necati Çatbaş; for his guidance as well as his friendship throughout this study. He has made this whole experience possible and enjoyable. None of this would have been possible without his mentorship and help.

I would also like to thank to the members of my dissertation committee, Dr. Manoj Chopra, Dr. Shirley Dyke, Dr. Michael Georgiopoulos, and Dr. Kevin Mackie for their time and feedback. I am grateful to Dr. Georgiopoulos also for his help and feedback during various parts of this study.

I would like to thank to the current and former members of our research team, Ricardo Zaurin, Burak Gokce, Taha Dumlupinar, Ozerk Sazak, Jason Burkett, Kevin Francoforte, Danny Meier, Tom Terrell, and Marcus Lisicki for their collaboration and help. I also would like to thank my friends for their support during this study. I thank GW for his friendship and continuous support. Finally, I would like to thank Maral, who has been one of the biggest supports during the most difficult times of this study.

And last, but most certainly not the least, I would like to express my deepest love and gratitude to my family; I cannot thank them enough for their love and support.

TABLE OF CONTENS

LIST OF FIGURES

LIST OF TABLES

CHAPTER 1. INTRODUCTION

1.1. Structural Health Monitoring (SHM)

Structural Health Monitoring (SHM) is the research area focusing on condition assessment of different types of structures including aerospace, mechanical and civil structures. Though the earliest SHM applications were in aerospace engineering, mechanical and civil applications have gained momentum in the last few decades.

Different definitions of SHM can be found in the engineering literature. For example, Aktan et al. (2000) defined SHM as follows; SHM is the measurement of the operating and loading environment and the critical responses of a structure to track and evaluate the symptoms of operational incidents, anomalies, and/or deterioration or damage indicators that may affect operation, serviceability, or safety and reliability. Another definition was given by Farrar et al. (1999) and Sohn et al. (2001) where the researchers stated that SHM is a statistical pattern recognition process to implement a damage detection strategy for aerospace, civil and mechanical engineering infrastructure and it is composed of four portions: (1) operational evaluation, (2) data acquisition, fusion and cleansing, (3) feature extraction, and (4) statistical model development.

By its nature, SHM is a highly interdisciplinary area involving experimental testing of the structure, acquisition, storing and managing of the data, digital signal processing and system identification, feature extraction, modeling and simulation, and statistical analysis. The socio-organizational and non-technical challenges also constitute a big part of a complete and successful SHM application. Fundamental needs, technology needs and socio-organizational

challenges for routine health monitoring applications are highly interrelated and they have to be carefully addressed (Catbas et al. (2004)). These challenges are summarized in Figure 1.

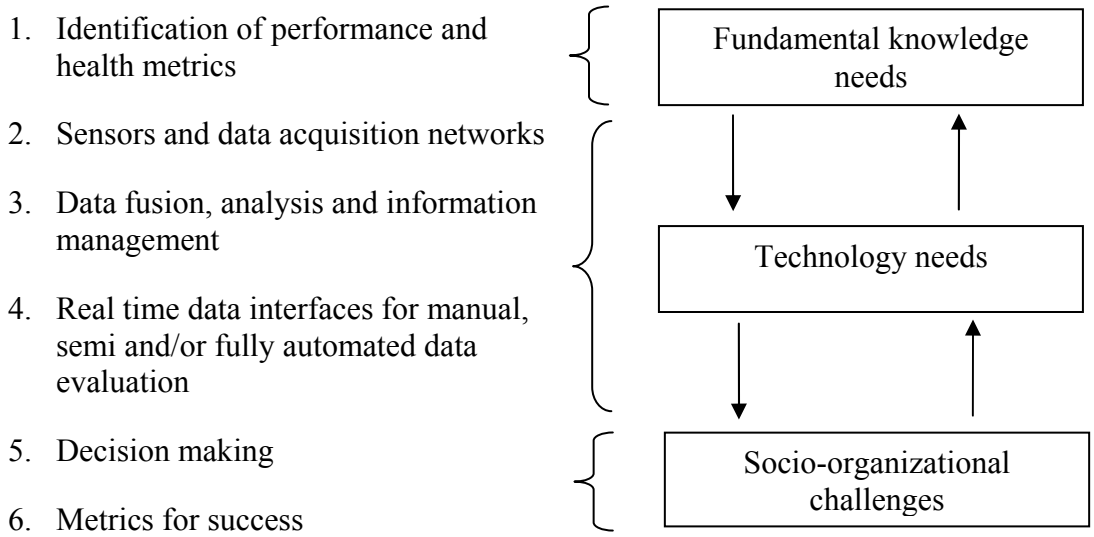

Figure 1. Main components of a health monitoring design (adapted from Catbas et al. (2004))

1.2. SHM Implementations in General

The starting point of an SHM system may be considered as the sensing and data acquisition step. The properties of the data acquisition system and the sensor network are rather application specific. The number and types of the sensors have a direct effect on the accuracy and the reliability of the monitoring process. The data collected during an SHM process generally include the response of the structure at different locations and information about the environmental and operational conditions. The measurements related to the structural response may include strain, displacement, acceleration, rotation and others. On the other hand, data related to environmental and operational conditions may include temperature, humidity and wind speed and direction measurements.

After collection, the SHM data can be analyzed by means of various methodologies to obtain useful information about the structure and its performance. With the recent technological developments in reduced cost sensing technologies, large amounts of data can be acquired easily with different types of sensors. Unless effective data analysis methodologies are implemented to an SHM system, problems related to data management will be inevitable, which may not only cause an overwhelming situation for handling large amounts of data effectively but also cause missing critical information. In addition to the analysis of experimental data, interpretation might require modeling and simulation where the analytical and numerical results may be combined or compared with experimental findings. Finally, information extracted from the data is used for decision-making about the safety, reliability, maintenance, operation and future performance of the structure.

SHM has been applied to many different structures including aerospace structures, automotive structures, rotating machinery, wind turbine blades, offshore platforms, civil infrastructures and others. Implementation of SHM to civil infrastructure systems is rather recent. The civil infrastructure includes components such as critical buildings, roads and highways, bridges, tunnels, dams, pipelines and water systems. All of these components are very critical for a reliable civil infrastructure network and adequate effort has to be spent for the life-cycle safety, operation and maintenance of these structures, which are essential components for the quality of life in a modern society.

In civil engineering community, a lot of attention has been directed to SHM implementations to bridges (Toksoy and Aktan 1994; Brownjohn et al. 1995; Aktan et al. 1996; Catbas et al. 1997; Enright and Frangopol 1999; Lus et al. 1999; Farhey et al. 2000; Chang et al.

2001; Fujino 2002; Casas and Cruz 2003; Dyke et al. 2003; Maeck and De Roeck 2003; Ko and Ni 2005; Catbas et al. 2007). The reason of this interest in bridge health monitoring is mainly the fact that bridges are critical components of the transportation network for every nation. As an example, many of the 600,000 highway bridges existing today in the US were constructed from 1950 to 1970 for the interstate system. Having an approximately 50-year design life, most of these bridges are either approaching or have surpassed their intended design life. Many old bridges are likely to be load-posted to prevent heavy trucks from crossing them. Highway agencies are struggling to keep up with the increasing demands on their highways and deteriorating bridges are becoming severe choke points in the transportation network. In 2008, 151,391 of 601,411 (25.17%) bridges were rated as structurally deficient or functionally obsolete (Federal Highway Administration (FHWA) 2008). With a rapidly aging infrastructure, a key approach to improving and maintaining highway bridges will be the use of innovative inspection, monitoring, and testing technologies to assess objectively their actual condition for decision-making.

1.3. Use of SHM for Damage Detection

Although sometimes SHM is used (rather incorrectly) as synonymous to damage detection, it actually refers to a much broader research area that can be employed for different purposes such as validation of the properties of a new structures, long-term monitoring of an existing structure, structural control and many others. Brownjohn et al. (2004) presents a good review of civil infrastructure SHM applications. On the other hand, it should also be emphasized that damage detection is a very critical component of SHM. Identifying the presence of the damage might be considered as the first step to take preventive actions and to start the process

towards understanding the root causes of the problem.

Before continuing with discussions about damage detection, it might be necessary to define what is meant by damage. Damage may roughly be defined as any structural or material change that affects the behavior of the structure adversely and shortens its operation life. A widely accepted definition of the levels of damage detection was provided by Rytter (1993). Rytter defined four levels of damage identification, which are (1) detection of the damage, (2) localization of the damage, (3) quantification of damage and (4) decision-making. One of the major challenges in damage detection of civil structures is that change in behavior due to reasons such as environmental inputs can be misinterpreted as damage. It is critical to be able to differentiate these changes from real damage, which has direct impact on the safety and reliability of the structure, and/or warrants some type of maintenance and rehabilitation to fulfill performance requirements.

Various methodologies have been proposed for detecting damage using SHM data. For global condition assessment, most of these methodologies employ vibration data by using one or a combination of different time domain and/or frequency domain algorithms. The aim is to extract features that will be sensitive to the changes occurring in the structure and relatively insensitive to other interfering effects (e.g. operational and environmental effects). Some of these methodologies can be found in literature and the references therein (Hogue et al. 1991; Toksoy and Aktan 1994; Doebling et al. 1996; Worden et al. 2000; Sohn and Farrar 2001; Bernal 2002; Catbas and Aktan 2002; Chang et al. 2003; Kao and Hung 2003; Sohn et al. 2003; Giraldo and Dyke 2004; Lynch et al. 2004; Alvandi and Cremona 2005; Nair and Kiremidjian 2005; Catbas et al. 2006; Sanayei et al. 2006; Carden and Brownjohn 2008; Gul and Catbas 2009).

1.4. Objective and Scope

As mentioned above, SHM is a multidisciplinary and broad research area, which offers great promise on effective management of civil infrastructure systems when implemented effectively. It is widely accepted that a particular sensing technology or data analysis method cannot be an answer to every SHM problem. There should be an arsenal of methodologies to be available for implementation. Therefore, this study is devoted to reviewing, improving and developing some damage detection techniques in the context of SHM. Different parametric and non-parametric approaches for damage detection are studied. For parametric methodologies, modal parameter based indices are used as damage indicating features. For the non-parametric approach, first improvement of a statistical pattern recognition technique for damage detection is presented. Second, a novel methodology is developed for detection, localization and quantification of damage by using time series modeling. Theoretical backgrounds of the methodologies are discussed. The effectiveness of each approach is demonstrated by using laboratory experiments. Finally, results of a real life application are presented in a comparative fashion. The scope of the dissertation is shown schematically in Figure 2.

1.5. Organization of the Dissertation

The organization of the dissertation is as follows.

In *Chapter 2*, a parametric approach for damage detection is described. Modal parameter based damage indices are used for parametric damage detection. Since the damage features are derived from modal parameters and their derivatives, some of the time and frequency domain parameter identification methods to obtain modal (i.e. dynamic) properties are reviewed. Another

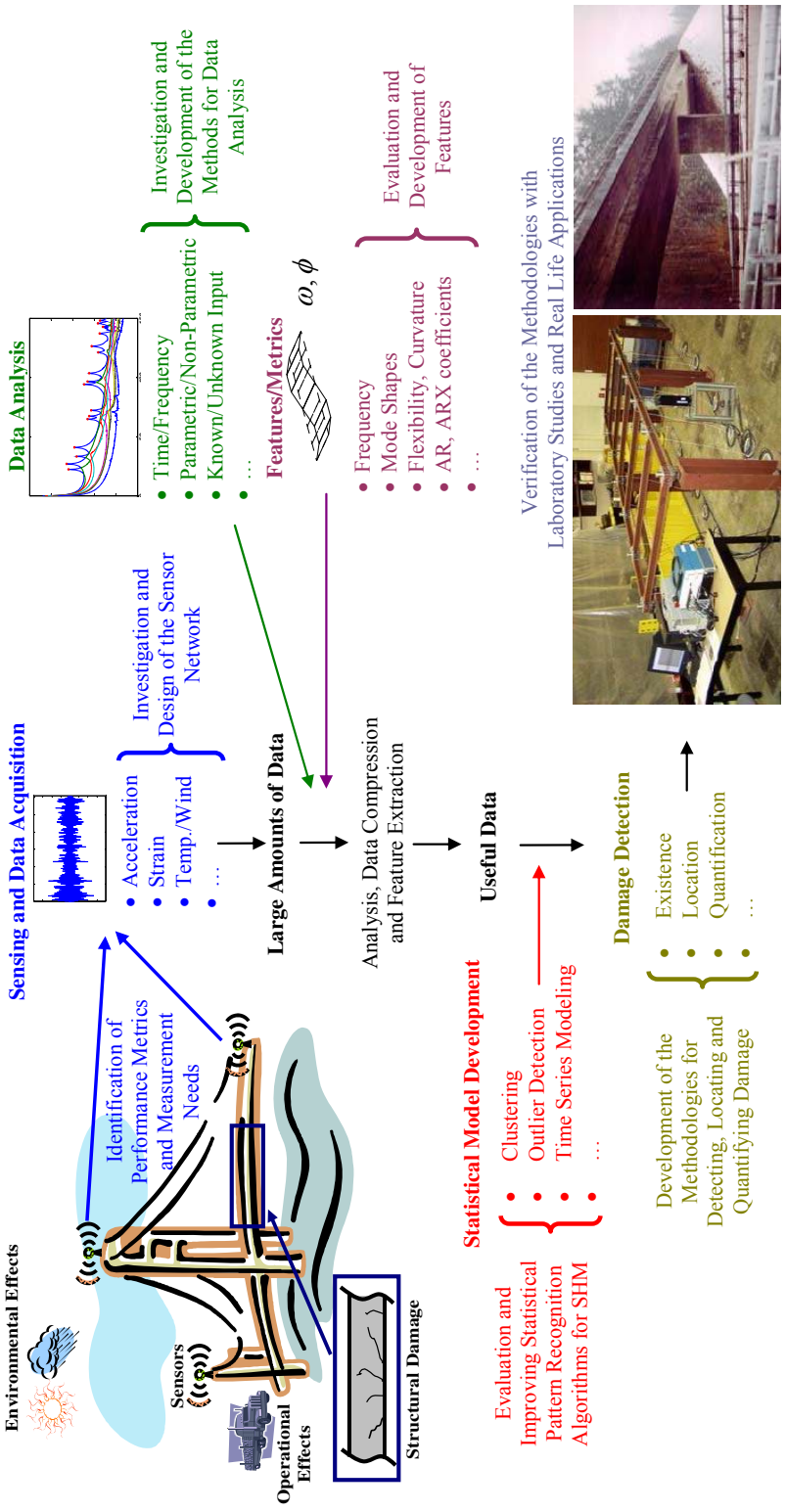

Figure 2. The scope of the dissertation

topic discussed in this chapter is a robust and practical methodology for condition assessment by using ambient vibration data. The development of these damage features are discussed along with the theoretical backgrounds followed by the experimental results and discussions. The laboratory structure and the damage simulations, which are used throughout this study, are explained also in this chapter.

Chapter 3 presents a non-parametric approach for damage detection. In this approach, statistical pattern recognition techniques are adapted for damage detection. Time series analysis along with its implementation with outlier detection for damage detection is discussed. The studies presented in this chapter incorporate a different approach as a complement to commonly employed methods. Experimental studies are presented at the end of this chapter.

In *Chapter 4,* a new non-parametric methodology using ARX (Auto-Regressive model with eXogenous output) analysis of vibration data for damage detection is introduced. The capability of this approach for identifying the existence, location and severity of the damage is discussed. After discussing the theoretical background, verification with numerical models are presented. Finally, experimental studies and the analysis of the data are given along with the results and interpretations.

Chapter 5 is dedicated mainly to the verification of the damage identification methodologies with real life data. First, design of an SHM system implemented to a movable bridge is discussed. For damage detection purposes, forced and ambient vibration data coming from the Z24 Bridge Benchmark are used. The methodologies discussed in Chapters 2, 3 and 4 are implemented for damage detection. The performance of each approach for this real life

application is presented in a comparative fashion.

Finally, *Chapter 6* provides the summary and presents the conclusions after theoretical and applied studies are given in the dissertation. General comments about the methodologies described in this study are reviewed along with recommendations and possible directions for future research.

CHAPTER 2. PARAMETRIC EVALUATION METHODOLOGIES FOR DAMAGE DETECTION

2.1. General Remarks

A number of different methodologies have been introduced for damage detection by using the SHM data. A considerable number of them can be considered as parametric methods in the sense that these methods generally assume that the *a priori* model representing the system is known. The aim of such methods is usually to compute the unknown parameters of this model. These parameters are mostly related to physical quantities such as mass, damping and stiffness of the system and the change in these parameters is used for damage detection.

Modal parameter estimation is one of the commonly used parametric system identification approaches where the aim is to identify the unknown parameters of a modal model (modal frequencies, damping ratios, mode shape vectors and modal scaling) of the system from given input-output or output only data sets. One of the advantages of using the modal parameters is that they can easily be related to the physical characteristics of the structure. Therefore, a large body of research effort has been conducted investigating the modal parameter based damage indices for SHM. A very comprehensive and highly referenced review by Doebling et al. (1996) discusses and summarizes different methodologies to identify the damage by using the modal parameters and modal parameter based damage indices.

Modal parameter estimation research has yielded different methods and approaches especially for mechanical and aerospace engineering applications in the last four to five decades. More recently, research for civil infrastructure applications using different forms of input-output, or output only dynamic tests has contributed new and/or revised algorithms, methods and

methodologies. These can be mainly grouped in two categories according to their working domain, i.e. time and frequency. In this study, a frequency domain methodology, which is suitable for time-varying nature of civil infrastructure, is used to obtain the modal parameters. The method is referred as Complex Mode Indicator Function (CMIF) method and detailed discussions are given in the following sections. Before the review of CMIF, some other common time domain and frequency domain methods are also briefly reviewed in the following sections. There are also very good review studies in the literature that would provide insightful information about different methods (Maia and Silva 1997; Allemang and Brown 1998; Ewins 2000; Fu and He 2001; Peeters and Ventura 2003; Alvandi and Cremona 2005).

2.2. Modal Parameter Identification Methodologies

Dynamic testing has been shown to be one of the most effective methods for SHM applications. Dynamic methods are commonly used because modal data can be acquired without any need of fixed reference. The data provide global properties with few measurements as well as the local behavior if spatial resolution is sufficient. From experimental point of view, there are mainly two types of modal analysis in terms of the availability of the input force. The ideal case is that both the input and output data are acquired for multiple input multiple output (MIMO) analysis. There have been numerous examples of MIMO testing and applications on large structures such as bridges; however, for most of the real life applications to civil structures, it is generally not practical or possible to excite the large constructed structures with a known input. Therefore, research studies with ambient vibration testing gained considerable attention as a means for civil infrastructure testing. The MIMO or ambient vibration (also known as output only) data can then be used to identify the modal parameters with a suitable modal parameter

estimation method. A brief review of the common methodologies is given in the following sections.

2.2.1. Review of the Time Domain Methodologies

Time domain methods, as the name implies, extract the information from the time history data. These methods are generally developed from control theory concepts. The starting point of these methodologies is usually the free response or the pulse response of the system. However, most of these methodologies can be used with ambient vibration data after some pre-processing of the raw data to obtain an estimation of the free decay time response data.

Although these methodologies are usually numerically stable and give satisfactory results, their application to heavily damped systems is limited since they require a large amount of time domain data. Some of the widely used methods include Complex Exponential Algorithm (CEA), Polyreference Time Domain (PTD) method, Ibrahim Time Domain (ITD) method and Eigensytem Realization Algorithm (ERA). Detailed discussions about the time domain methodologies can be found in the literature including Maia and Silva (1997), Allemang and Brown (1998), Allemang (1999), and Peeters and Ventura (2003).

CEA (or damped CEA) is a high order time domain method (Allemang and Brown 1987) and it uses the free response or unit impulse response of the system to calculate the modal parameters. The term high order is used to indicate the order of the matrix polynomial equations that are to be solved to obtain the modal parameters. One of the advantages of the CEA is that it is simple and fast. One of the disadvantages is that since it is a high order algorithm, a number of noise modes are identified along with the real modes. Eliminating the noise modes can be a very

challenging issue for some complex and time variant systems. The PTD, ITD and ERA methodologies are developed based on CEA and they are discussed in the following sections.

PTD is a more general implementation of CEA to MIMO data sets and it was developed by Vold et al. (1982). PTD accounts for the multiple reference data at the same time and therefore it can be considered as the first algorithm able to solve for closely spaced or repeated modes (Allemang 1999).

ITD is a low order CEA based method initially introduced by Ibrahim and Mikulcik (1977) to identify the modal parameters from the free decay responses. The modal parameters are identified from the Hankel matrix by decomposing it to modal observability and controllability matrices. Since ITD is a low order algorithm, meaning that a small number of time points are sufficient to determine the modal parameters, it can be used for highly damped systems.

ERA was developed by Juang and Pappa (1985) and is based on the minimal realizations to obtain a state space system with minimum orders to represent a given set of input output relations. ERA can also be considered as the multiple reference version of ITD. Since ERA is one of the widely used time domain modal parameter identification methods and it provides a generic framework for CEA and ITD, it is discussed in more detail in the following.

A discrete time n^{th} order state space system with r inputs and m outputs can be written as

$$\begin{aligned} x(k+1) &= A_D x(k) + B_D x(k) \\ y(k) &= C_D x(k) + D_D u(k) \end{aligned} \tag{1}$$

where $y_{m\times 1}(k)$ is the output vector, $u_{r\times 1}(k)$ is the input vector, $x_{n\times r}(k)$ is the state vector

and $A_{D\,n\times n}$, $B_{D\,n\times r}$, $C_{D\,m\times n}$ and $D_{D\,m\times r}$ the time invariant system matrices. If the system is assumed to be excited with a unit impulse function and if the initial conditions of the system are zero as shown in Eqn. (2), then the response of the system can be calculated as written in Eqn. (3).

$$\begin{aligned} u(k) = 1,\ x(k) = 0 \quad for \quad k = 0 \\ u(k) = 0,\ x(k) \neq 0 \quad for \quad k \neq 0 \end{aligned} \tag{2}$$

$$y(0) = D_D, \quad y(1) = C_D B_D, \quad y(2) = C_D A_D B_D, \quad \cdots, \quad y(k) = C_D A_D^{k-1} B_D, \tag{3}$$

The parameters shown in Eqn. (3) are known as Markov parameters. These parameters are collected in a so-called Hankel matrix, denoted with Π, as in Eqn. (4). Substituting the Markov parameters to Eqn. (4), the Hankel matrix in Eqn. (5) is obtained.

$$\Pi(0) = \begin{bmatrix} y(1) & y(2) & \cdots & y(i) \\ y(2) & y(3) & \cdots & y(i+1) \\ \vdots & \vdots & \ddots & \vdots \\ y(j) & y(j+1) & \cdots & y(i+j-1) \end{bmatrix} \tag{4}$$

$$\Pi(0) = \begin{bmatrix} C_D B_D & C_D A_D B_D & \cdots & C_D A_D^{i-1} B_D \\ C_D A_D B_D & C_D A_D^2 B_D & \cdots & C_D A_D^i B_D \\ \vdots & \vdots & \ddots & \vdots \\ C_D A_D^{j-1} B_D & C_D A_D^j B_D & \cdots & C_D A_D^{j+i-2} B_D \end{bmatrix} \tag{5}$$

where i and j are the number of the columns and rows in the Hankel matrix, respectively. After building the Hankel matrix, the system matrices are retrieved by using Singular Value Decomposition (SVD) of the Hankel matrix.

$$\Pi(0) = USV^T = \begin{bmatrix} U_1 & U_2 \end{bmatrix} \begin{bmatrix} S_1 & 0 \\ 0 & 0 \end{bmatrix} \begin{bmatrix} V_1^T \\ V_2^T \end{bmatrix} \tag{6}$$

where U and V are unitary matrices and S is a square diagonal matrix. The system matrices can be obtained by using the following

$$A_D = S_1^{-1/2} U_1^T \Pi(1) V_1 S^{-1/2} \tag{7}$$

$$B_D = S_1^{1/2} V_1^T E_r \tag{8}$$

$$C_D = E_m U_1 S_1^{1/2} \tag{9}$$

where $E_r = \begin{bmatrix} I_{r\times r} & 0 & \cdots & 0 \end{bmatrix}$ and $E_m = \begin{bmatrix} I_{m\times m} & 0 & \cdots & 0 \end{bmatrix}$. The natural frequencies can be obtained directly from the eigenvalues of the system matrix A_D. The mode shapes can be computed by multiplying the corresponding eigenvectors of A_D with the output matrix C_D.

2.2.2. Review of the Frequency Domain Methodologies

Frequency domain methods transform the time histories to frequency domain and extract the modal parameters in the frequency domain. These methodologies use the FRFs (Frequency Response Functions) to compute the modal parameters. One of the main advantages of the frequency domain methodologies is that less computational modes (noise modes) are obtained in comparison with time domain algorithms. Some of the disadvantages of these methodologies are due to the restrictions of the FFT (Fast Fourier Transform). For example, leakage is one of the commonly encountered problems because FFT assumes the signal is periodic within the observation time. The effect of leakage can be eliminated by using windowing functions but it cannot be avoided completely.

One of the simplest frequency domain methods is Peak Picking method where the modes are selected from the peaks of the FRF plots. If the system is lightly damped and if the modes are well separated, the natural frequencies (eigenfrequencies) can be estimated from the FRF plots. The damping ratios can be determined by using the half power method.

Rational Fraction Polynomial is a high order frequency domain methodology where the following formulation is used to identify the modal parameters. The coefficients of these polynomials can be estimated from the FRF measurements by using a linear least squares solutions. Then the modal parameters are computed by using the polynomial coefficients.

$$H(j\omega) = \frac{\left[(j\omega)^p \beta_p + (j\omega)^{p-1} \beta_{p-1} + \cdots + \beta_0\right]}{\left[(j\omega)^p I + (j\omega)^{p-1} \alpha_{p-1} + \cdots + \alpha_0\right]} \tag{10}$$

where H is the FRF, ω is the frequency in radians and α, β are the polynomial coefficients.

Another method called Frequency Domain Decomposition (FDD) has also been used for ambient analysis by using Singular Value Decomposition (SVD) of the output spectrum matrix (Brincker et al. 2000). This method is very similar to Complex Mode Indicator Function (CMIF) where both of the methodologies identify the modal parameters by using the SVD of the output spectrum matrix. The CMIF method is described in detail in the following since it is the methodology used for modal parameter identification in this study.

Shih et al. (1988; 1988) initially introduced CMIF as a mode indicator function for MIMO data to determine the number of modes for modal parameter estimation. Then, CMIF was successfully used as a parameter estimation technique to identify the frequencies and un-scaled

mode shapes of idealized test specimens (Shih et al. 1988; Fladung et al. 1997). Recently, Catbas et al. (1997; 2004) modified and further extended CMIF to identify all of the modal parameters including the modal scaling factors from MIMO test data. In these studies, it was shown that CMIF is able to identify physically meaningful modal parameters from the test data, even if some level of nonlinearity and time variance were observed. Figure 3 shows the basic steps of the methodology. Further details are discussed in the following sections.

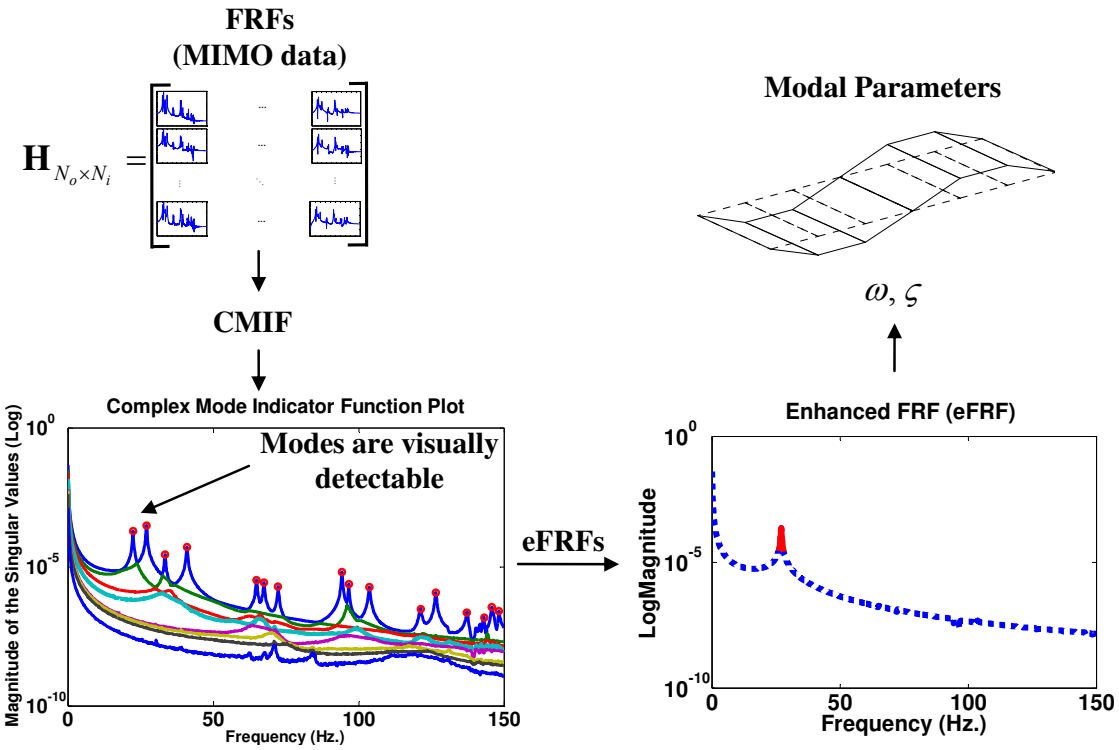

Figure 3. Summary of CMIF method

The first step of the CMIF method is to compute the Singular Value Decomposition (SVD) of FRF matrix, which is given with Eqn. (11).

$$[H(\omega_i)]_{(N_o \times N_i)} = [U]_{(N_o \times N_i)} [S]_{(N_i \times N_i)} [V]^H_{(N_i \times N_i)} \tag{11}$$

where $[S]$ is singular value matrix, $[U]$ and $[V]$ are left and right singular vectors respectively and $[V]^H$ indicates the conjugate transpose of $[V]$. The above equation shows that the columns of the FRF matrix $[H(\omega_i)]$ are linear combination of the left singular vectors and similarly, the rows of the FRF matrix are linear combination of the right singular vectors. Since the left and right singular vectors are unitary matrices, the amplitude information of the FRF matrix is carried within the singular value matrix. The CMIF plot is that of singular values as a function of frequency. The number of singular values at a spectral line and therefore the number of lines in the CMIF plot depends on the number of excitation points, N_i in Eqn. (11) assuming that N_i is smaller than N_o. For this reason, MIMO data CMIF plots indicate multiple lines enabling tracking of the actual physical modes of the structure. The FRF matrix can be expressed in a different way than Eqn. (11) in terms of modal expansion using individual real or complex modes as given in Eqn. (12).

$$[H(\omega_i)]_{(N_o \times N_i)} = [\Psi]_{(N_o \times 2N)} [\frac{1}{j\omega_i - \lambda_r}]_{(2N \times 2N)} [L]^T_{(2N \times N_i)} \qquad (12)$$

where ω is frequency, λ_r is r^{th} complex eigenvalue or system pole, $[\Psi]$ is the mode shapes and $[L]$ is the participation vectors. Note that while Eqn. (11) is a numerical decomposition, Eqn. (12) incorporates the physical characteristics, such as mode shapes and frequencies. As mentioned before the left and right singular vector matrices $[U]$ and $[V]$ are unitary matrices in SVD formulation. Furthermore, $[\Psi]$ and $[L]$ are constant for a particular mode. The system pole and the driving frequency are closer along the frequency line near resonance, which results in a local maximum in CMIF plot. Therefore, it is a very high

possibility that the peak singular values in CMIF plot are the pole locations of the system. In addition, since the left singular vector is the response at the resonance, it is a good approximation of the modal vector at that frequency. Then these modal vectors are used as modal filters to condense the measured response to as many SDOF (Single Degree Of Freedom) systems as the number of selected peaks. This, in fact, is a transformation of the response from physical coordinates to the modal coordinates. After the transformation is completed, enhanced Frequency Response Functions (eFRFs) are calculated for each SDOF system. Then the entire system is uncoupled to a vector of SDOF system for mode m with Eqn. (13).

$$eH(\omega_i)_m = \{U\}_m^H \left[[\Psi] \left[\frac{1}{j\omega_i - \lambda_r} \right] [L]^T \right] \{V\}_m \qquad (13)$$

The level of the enhancement depends on the inner product of the left singular vector and the modal vector $[\Psi]$. If the modal vectors are mutually orthogonal, then the eFRF will be completely uncoupled, showing a single mode FRF with a strong peak. However, if some of the modes are non-orthogonal, then those modes will have some contribution to the eFRF, which will cause another peak or peaks to appear.

After obtaining the set of SDOF systems, the second part of the method is about determining the modal frequency, damping and modal scaling for each separate mode. Since the system is now transformed to a set of SDOF systems using the eFRFs, the following equation can be written in the frequency domain to compute the system poles.

$$[(j\omega_i)^2 \alpha_2 + (j\omega_i)\alpha_1 + \alpha_0]\{eH(\omega_i)\} = [(j\omega_i)^2 \beta_2 + (j\omega_i)\beta_1 + \beta_0]\{R(\omega_i)\} \qquad (14)$$

In Eqn. (14), $\{R(\omega)\}$ is the index vector showing the coordinates of the forcing locations

and α and β are unknown coefficients. Since the eFRF matrix is generated in the first phase, $eH(\omega)$ and $(j\omega)$ are now known quantities. If there is no noise or residual terms in the data sets just β_0 is sufficient, but to handle the noise β_1 and β_2 can be added to the right hand side of the equation to enhance the results (Catbas et al. 1997; Fladung et al. 1997). If either α_0 or α_2 is assumed to be unity a least square solution can be applied and then the eigenvalue problem can be formulated and solved for the poles of the SDOF system. The poles $(\lambda_r = \sigma_r + j\omega_r)$ of the system are determined on a mode-by-mode basis.

2.2.3. Ambient Vibration Data Analysis

As mentioned above, the ideal case for modal parameter identification is one where both the input and output data are available. However, for most of the real life applications such an experimental setup cannot be realized since it is generally neither feasible nor possible to excite the large constructed structures with a known input especially if the structure is tested during usual operation hours particularly in the case of existing bridges. Therefore, identification of modal parameters from ambient vibration test data has attracted attention in the last decades and several studies are available in the literature (Beck et al. 1994; Brincker et al. 2000; Peeters and De Roeck 2001; Brownjohn 2003; Caicedo et al. 2004; Yang et al. 2004; Catbas et al. 2007; Gul and Catbas 2008).

Several methods have been proposed to identify the modal parameters of the structures with output only data. These methods are usually based on the methods discussed in previous sections of this text where data is pre-processed with different methodologies to obtain output spectra, un-scaled FRFs or un-scaled free responses. For example, Peak Picking method which

was mentioned in the previous sections can be used for ambient data analysis. However, for output only analysis, the auto and cross power spectral densities of the ambient outputs are used instead of FRFs (Ren et al. 2004). Another method called Frequency Domain Decomposition (FDD) has also been used for ambient analysis by using Singular Value Decomposition (SVD) of the output spectrum matrix (Brincker et al. 2000, Peeters and De Roeck 2001). This method is also referred as CMIF (Catbas et al. 1997, Peeters and De Roeck 2001). A difference between the previous application of the FDD and the CMIF method presented in this study is that here un-scaled FRFs (will be explained in later sections in detail) are used instead of power spectral densities. The un-scaled FRFs obtained from Random Decrement analysis provided very clean data compared to power spectral densities especially when the sufficient excitation is exerted. Rodrigues et al. (2004) used a similar approach and combined Random Decrement (RD) with frequency domain methodologies (i.e. FDD), where the authors obtained the modal parameters of a shear type, 4-story laboratory structure by using ambient data.

There are a number of different approaches for ambient vibration data analysis. One example of time domain methods for ambient data analysis is the ITD used in conjunction with RD (Huang et al. 1999). In another approach, Caicedo et al. (2004) combined the Natural Excitation Technique with ERA to identify the modal and stiffness parameters. Stochastic Subspace Identification (SSI) is another commonly used method (Van Overschee and De Moor 1996; Peeters and De Roeck 2001; Ren et al. 2004) which is based on writing the first order state space equations for a system by using two random terms, i.e. process noise and measurement noise, which are assumed to be zero mean and white. After writing the first order equations, the state space matrices are identified by using SVD. Then, the modal parameters are extracted from

the state space matrices (Peeters and De Roeck 2001).

In this study, CMIF is utilized together with Random Decrement (RD) where applicable to obtain modal properties of a structural system under ambient excitation. By using the RD technique, the un-scaled impulse response of the system is computed from the ambient vibration data. Then these impulse responses are converted to un-scaled FRFs by taking the Fast Fourier Transform (FFT). After obtaining the un-scaled FRFs, they are fed to the CMIF algorithm to obtain the modal parameters as detailed in the following sections. It should be noted that for lightly excited modes, Power Spectral Densities (PSD) can be used to see these modes, even though PSD based CMIF plots seem to have more noise.

2.2.4. Using Random Decrement (RD) for Ambient Vibration Data Analysis

Traditionally, un-scaled FRFs of a structure are estimated by using auto and cross power spectra of the time history data after application of certain windowing functions. However, several problems due to using these spectral densities can be experienced during the analysis, such as leakage and computational complexity. Some of these issues could be mitigated by using the RD technique as discussed in detail by Asmussen (1997). For example, since the un-scaled free response obtained with RD will decay to zero, the leakage problem can be eliminated even without windowing functions (for long data sets). Furthermore, since the data is averaged in the time domain, the RD method is computationally more efficient. Another advantage brought by time domain averaging is that the noise in the data can be minimized. It should be noted here that while this is a major advantage to minimize noise, it might have adverse effects on lightly excited modes.

The RD technique was introduced by Cole (1968) for transformation of random time series into a free decay response, which contains only the information about the structure, to eliminate the effect of the random loading on the signal (Asmussen 1997). The basic idea behind the RD is that the random response of a system at the time $t_0 + \tau$ consists of three components, which are the step response due to the initial displacements at the time t_0, the impulse response from initial velocity at time t_0, and a random part due to the load applied to the structure between t_0 and $t_0 + \tau$. By taking average of time segments, every time the response has an initial displacement bigger than the trigger level given in Eqn. (15), the random part due to random load will eventually die out and become negligible. Additionally, since the sign of the initial velocity can be assumed to vary randomly in time, the resulting initial velocity will be zero (Asmussen 1997).

$$T_{x_i} = \{a_1 \le x_i(t) < a_2\} \tag{15}$$

In Eqn. (15), $x_i(t)$ represents the time response for the channel i, and a_1 and a_2 show the lower and upper bounds for the trigger. The trigger level for the averaging process can be determined in different ways (Asmussen et al. 1996). The most commonly used triggering condition is referred as level crossing triggering condition where a_1 is set as a threshold value. Another triggering condition is zero crossing triggering condition, which implies that the structure is assumed excited every time the acceleration at the reference channel crosses zero with a positive slope. In this study, the level crossing triggering condition is used while applying RD. Eqn. (16) shows the averaging of the data channel p for reference channel q. When p is equal to q, Eqn. (16) is referred as auto RD function, whereas it is called cross RD function for

p different than q. This process is applied to all data channels and repeated for every reference channel. As a result, an un-scaled yet full MIMO data matrix is generated.

$$\hat{h}_{pq}(\tau) = \frac{1}{N}\sum_{k=1}^{N} x_p(t_k : t_k + \tau) \Big| \{ a_1 \le x_q(t_k) < a_2 \} \tag{16}$$

In Eqn. (16), N is the total number of trigger crossings, $x_p(t_k : t_k + \tau)$ is the k^{th} time segment of channel p (the values between $x_p(t_k)$ and $x_p(t_k + \tau)$) when the response at channel q is in the trigger level. The un-scaled impulse responses are shown as $\hat{h}_{pq}$ in Eqn. (16). Then, the un-scaled FRFs (shown with $\hat{H}_{pq}$) are computed by taking FFT of the corresponding un-scaled impulse function. Finally, the pseudo (un-scaled) FRFs ($\hat{H}_{N_o \times N_i}$) for N_o outputs and N_i inputs (references) are obtained by applying RD to all the output channels for each reference channel. If RD is implemented for all measurement channels as $N_i = N_o$, the un-scaled FRF matrix is $\hat{H}_{N_o \times N_o}$. The process of ambient data with RD is summarized in Figure 4. The full un-scaled FRF matrix is then fed to CMIF algorithm as input to identify the modal parameters as discussed in the previous sections. Figure 5 shows how the un-scaled FRFs are used in conjunction with CMIF. Note the similarity of Figure 5 with Figure 3.

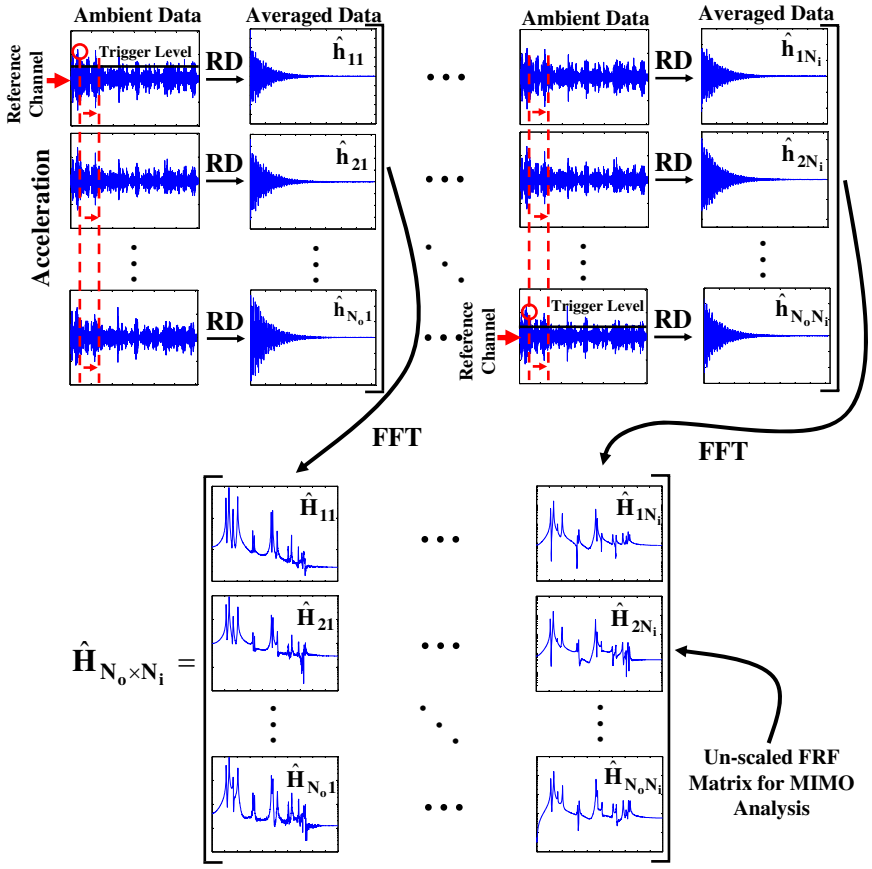

Figure 4. Generating un-scaled FRF matrix for MIMO data

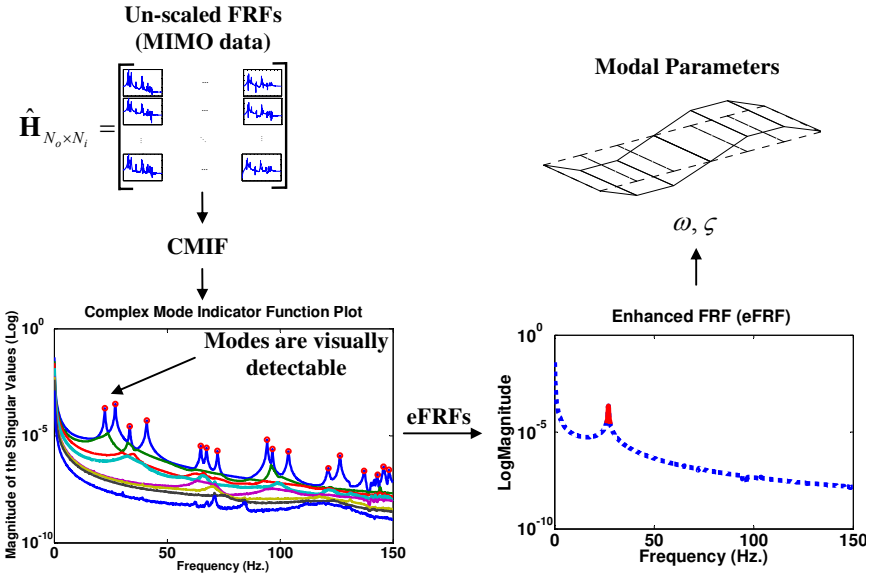

Figure 5. CMIF method used in conjunction with RD for ambient vibration data

2.3. Evaluation and Development of Damage Features with Dynamic Testing

2.3.1. Overview of the Common Damage Features

After obtaining the modal parameters, the modal parameters or their derivatives can be used as damage sensitive metrics. Some of the common modal parameter based features may be summarized as the natural frequencies, mode shapes and their derivatives, modal flexibility matrix, modal curvature and others. It has been shown that natural frequencies are very sensitive to environmental conditions, especially to temperature changes, yet they are not sufficiently sensitive to damage. In addition, since most of time, damage is a local phenomenon, the lower frequency modes are usually not affected by the damage. The higher frequency modes may indicate the existence of the damage because they generally represent local behavior but it is more difficult to identify those modes compared to identification of lower frequency modes.

Unlike natural frequencies, which do not usually provide any spatial information, mode shapes provide such information and thus they are generally a better indicator of damage than natural frequencies. In theory, mode shapes would indicate the location of the damage; however a dense array of sensors may be needed to capture those modes. Modal Assurance Criterion (MAC) is one of the commonly used modal vector comparison tool (Allemang and Brown 1982). Modal curvature, which is usually obtained by taking derivative of the mode shapes, has also been used for damage detection purposes. Modal flexibility is another damage indicator, which can be obtained by using the frequencies and mass normalized mode shapes. A review of these damage features was given by Doebling et al. (1996) and Carden and Fanning (2004).

The damage features presented in this chapter are derived from the identified modal

parameters using FRF measurement data. One of the assumptions for modal parameter estimation using FRF data is that the structure is linear and time invariant. This brings the question as to how FRF based data can be used for damage detection. When a structure is damaged, it is possible to assume that it behaves piecewise linear in that damaged state if the applied load levels are not in the range of non-linear load-displacement levels. Provided that this condition is satisfied, the proposed features can be expected to perform successfully. Special care must be taken while applying these linear methodologies to real-life structures. A practical approach to validate the linearity is to perform a linearity check where the structure is excited under different levels of excitations and the corresponding FRFs are compared. In addition, reciprocal FRFs can be compared. In this study, linearity and reciprocity were checked and were observed to satisfy the linearity assumption.

2.3.2. Modal Flexibility and Modal Curvature

As damage features, modal flexibility and modal curvature are obtained from the MIMO data sets with CMIF. The general overview of the methodology used in this study is summarized in Figure 6. The details and formulations of these damage features are explained below.

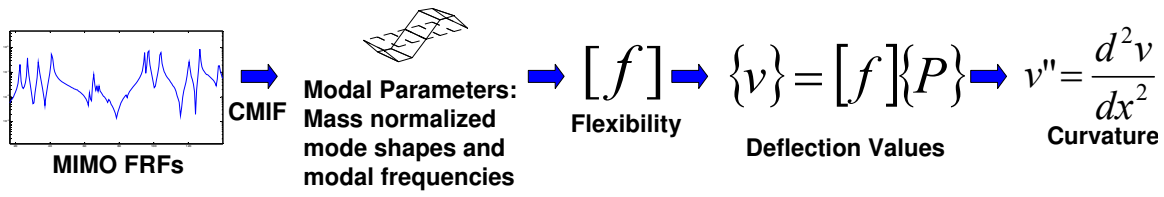

Figure 6. Obtaining the modal flexibility and modal curvature

Modal Flexibility

First developed by Maxwell (Maxwell 1864), the flexibility is a displacement influence

coefficient of which the inverse is stiffness. Flexibility is a significant index as it characterizes input-output relationship for a structure. It has been shown to be a robust and conceptual condition index for constructed facilities. To find the modal flexibility of a structure, one can use modal parameters from dynamic testing. Flexibility has been proposed and shown as a reliable signature reflecting the existing condition of a bridge. For this reason, flexibility based methods in bridge health monitoring are promising. Flexibility has been extracted and used in a number of different ways and further studies can be found in Toksoy and Aktan (1994), Catbas and Aktan (2002), Bernal (2002), Bernal and Gunes (2004), Alvandi and Cremona (2005), Huth et al. (2005), Catbas et al. (2004; 2006; 2008), Gao and Spencer (2006). If an approximation to real structural flexibility is needed, the input force must be known in order to obtain the scaling of the matrix. In addition, it is always an approximate index since not all the modes can ever be included in the calculation of the flexibility matrix (Catbas et al. 2006).

One of the objectives of this study is to implement the results of the impact tests for condition evaluation using modal flexibility. In this current study, scaled dynamic flexibility is obtained by using impact test results as a result of the following relationship between flexibility and FRF matrices. An FRF between point p and q can be written in partial fraction form as in Eqn. (17)

$$H_{pq}(\omega) = \sum_{r=1}^{m} \left[\frac{(A_{pq})_r}{j\omega - \lambda_r} + \frac{(A_{pq}^*)_r}{j\omega - \lambda_r^*} \right] \tag{17}$$

where $H_{pq}(\omega)$ is FRF at point p due to input at point q, ω is frequency, λ_r is r^{th} complex eigenvalue or system pole, $(A_{pq})_r$ is residue for mode r, and $(^*)$ indicates the

complex conjugate. Eqn. (17) can be rewritten by using the modal parameters as in Eqn. (18).

$$H_{pq}(\omega) = \sum_{r=1}^{m} \left[\frac{\psi_{pr}\psi_{qr}}{M_{Ar}(j\omega - \lambda_r)} + \frac{\psi^*_{pr}\psi^*_{qr}}{M^*_{Ar}(j\omega - \lambda^*_r)} \right] \tag{18}$$

where ψ_{pq} is the mode shape coefficient between point p and q for the r^{th} mode and M_{Ar} is the modal scaling for the r^{th} mode. Finally, the modal flexibility matrix can be computed by evaluating $H_{pq}(\omega)$ at $\omega = 0$ as in Eqn. (19).

$$H_{pq}(\omega = 0) = \sum_{r=1}^{m} \left[\frac{\psi_{pr}\psi_{qr}}{M_{Ar}(-\lambda_r)} + \frac{\psi^*_{pr}\psi^*_{qr}}{M^*_{Ar}(-\lambda^*_r)} \right] \tag{19}$$

The flexibility formulation is an approximation to actual flexibility matrix because only a finite number of modes can be included in the calculations. The number of modes, *m*, is to be determined such that sufficient modes are selected (i.e. temporal truncation is minimized) and a good approximation to actual flexibility is achieved. Catbas et al. (2006) used a modal convergence criterion to determine the number of the modes necessary to construct a reliable flexibility matrix. In this current study, around 15 modes are used to construct the flexibility matrices for each case. The modal flexibility matrix can also be written as in Eqn. (20). After obtaining the scaled modal flexibilities, the deflections under static loading can be calculated easily for any given loading vector $\{P\}$, which is shown in Eqn. (21).

$$[H] = \begin{bmatrix} H_{11}(\omega = 0) & H_{12}(\omega = 0) & .. & H_{1N}(\omega = 0) \\ H_{21}(\omega = 0) & .. & .. & .. \\ .. & .. & .. & .. \\ H_{N1}(\omega = 0) & .. & .. & H_{NN}(\omega = 0) \end{bmatrix} \tag{20}$$

$$\{deflection\} = \{v\} = [H]\{P\} \tag{21}$$

Modal Curvature

Curvature is commonly used in mechanics of materials and structural analysis. Curvatures of modal vectors have been presented in the literature (Pandey et al. 1991; Maeck and De Roeck 1999; Maeck and De Roeck 2003). However, there is little work done for obtaining curvatures from deflection patterns. Here, the deflections and curvatures are created from the modal flexibility. These indices are implemented in this study in terms of displacement vectors resulting from uniform loads applied to the modal flexibility matrices. In other words, the novelty of this methodology is that the modal curvature is obtained from the deflected shape of the structure, which is obtained by using modal flexibility. However, the limitations of the curvature method are to be recognized. First, the spatial resolution (i.e. number of sensors) should be sufficient to describe a deflection pattern along a girder line. In order to obtain a good approximation to actual flexibility, both dynamic input and output are to be measured. In addition, modal truncation is to be minimized since modal flexibility has to approximate actual flexibility. Finally, taking derivatives of the data which include random noise and experimental errors might create numerical errors (Chapra and Canale 2002). However, the derivation is based on the combination of all modes and associated deflections in this study. Therefore, the random numerical errors are averaged out and may have less effect than taking the derivative of a single mode shape.

As given in mechanics theory, curvature and deflection are related for a beam type by Eqn. (22).

$$v'' = \frac{d^2 v}{dx^2} = \frac{M}{EI} \tag{22}$$

where v'' is the curvature at a section, M is the bending moment, E is the modulus of elasticity, and I is the moment of inertia. The relationship between loading, deflected shape, moment distribution and curvature is shown in Figure 7 for a beam type structure. Since curvature is a function of stiffness, any reduction in stiffness due to damage should be observed by an increase in curvature at a particular location. The basic assumption for applying this relation to bridges is that the deformation is a beam type deformation along the measurement line. This assumption can yield reasonably good approximation for bridges with girder lines. However, if it is to be used for damage identification for a two-way plate type structure, the curvature formulation should be modified to take two directions into account.

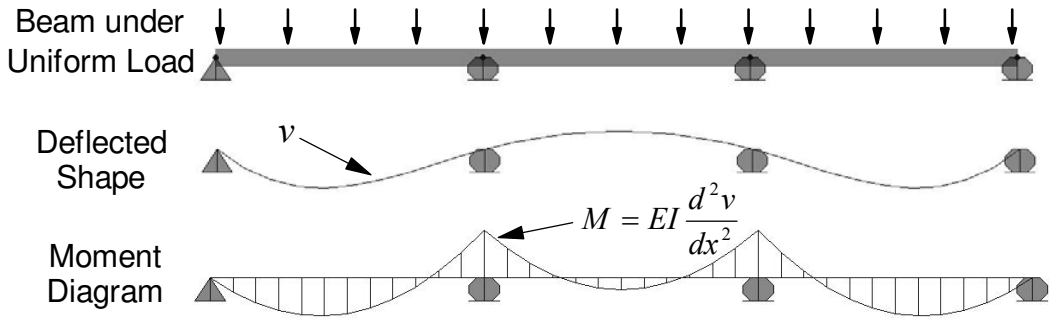

Figure 7. The relationship between deflected shape, moment and curvature for a beam type structure

To calculate the curvature of the displacement vectors, the central difference approximation is used for numerical derivation as in Eqn. (23).

$$v''_{q,i} = \frac{v_{q-1,i} - 2v_{q,i} + v_{q+1,i}}{\Delta x^2} \tag{23}$$

where q represents the elements of the i^{th} displacement vector and Δx is the length between measured displacement points.

2.3.3. Un-scaled (pseudo) Flexibility

For the known input case, the modal flexibility and modal curvature were used as damage features. However, these features cannot be extracted from ambient vibration data since modal scaling cannot be computed if the input is unknown. Therefore, another feature that will be referred as pseudo-flexibility (un-scaled flexibility) is investigated for damage detection with ambient data.

The procedure for obtaining modal flexibility in MIMO testing was explained in the previous sections. It was shown that the modal flexibility matrix can be written by evaluating $H_{pq}(\omega)$ at $\omega = 0$ as

$$H_{pq}(\omega = 0) = \sum_{r=1}^{m} \left[\frac{\psi_{pr}\psi_{qr}}{M_{Ar}(-\lambda_r)} + \frac{\psi^*_{pr}\psi^*_{qr}}{M^*_{Ar}(-\lambda^*_r)} \right] \tag{24}$$

Unlike the MIMO testing case, the modal scaling factor M_{Ar} cannot be determined as a system property for the ambient test case since input force is not measured. The $\hat{H}_{pq}(\omega = 0)$ with an arbitrary scaling can be reconstructed by using the identified mode shapes and poles from the ambient tests. If the same arbitrary scaling is consistently used for different ambient tests, comparable matrices can be obtained. As a result, the mode shape vector and the poles of the structure, which are obtained using the CMIF-based method, can be used to define an un-scaled flexibility, $\hat{H}_{pq}(\omega = 0)$ as given in Eqn. (25). In this formulation, the modal scaling

factors, M_{Ar}, are assumed to be unity.

$$\hat{H}_{pq}(\omega = 0) = \sum_{r=1}^{m} \left[\frac{\varphi_{pr}\varphi_{qr}}{(-\lambda_r)} + \frac{\varphi^*_{pr}\varphi^*_{qr}}{(-\lambda^*_r)} \right] \tag{25}$$

where φ_{pr} is the arbitrarily scaled mode shape coefficient at point *p* for the r^{th} mode. After obtaining the scaled and un-scaled flexibilities, the deflections under static loading can be calculated easily for any given force vector $\{P\}$.

$$\{deflection\} = [\hat{H}]\{P\} \tag{26}$$

It should be noted that the deflection obtained in Eqn. (26) is also a pseudo-deflection, combining the effects of all modes obtained during modal identification. Scaling values obtained from FE models can be used for more accurate deflections. On the other hand, using arbitrary (but consistent) scaling for each mode, pseudo flexibility can be tracked over time as ambient vibration data is collected and modal parameters are identified.

Here, the discussions about the theoretical background of the parametric methods for damage detection end. The following sections discuss the experimental studies conducted for verification of these methods and damage features. The laboratory structure and the damage simulations which are used throughout this study are explained in the next section. Finally, the experimental results are discussed at the end of this chapter.

2.4. Experimental Studies

Before the routine application of SHM systems to real-life structures, the methodologies

should be verified on analytical and physical models. Although analytical studies are necessary in the first phases of verification, laboratory studies with complex structures are also essential. Laboratory studies with large physical models are a vital link between the theoretical work and field applications if these models are designed to represent real structures where various types and levels of uncertainties can be incorporated. A brief review of laboratory studies recently conducted by different researchers is presented in the following.

Motavalli and Gsell (2004) aimed to close the gap between complex, real-world applications and simplified laboratory experiments with a 1/1 scale model, cable stayed glass fiber reinforced polymer-bridge. Due to complexities in scaling a structure, the decision was made to design a 1/1 model, which was most practical for a footbridge. The model was 63 ft long by 5 ft wide and its height was 25 ft. The design considerations included bolted connections so that members can be replaced with pre-damaged members and loosening of connections to simulate damage. Lee et al. (2003) developed a 1/15 scale model of Korea's Yeongjong Bridge floor system for investigating local damage detection. The scaled model dimensions were approximately 11 ft by 8 ft in plan view. Using an impact hammer and forty-eight channels of dynamic strain gages, the structure was tested to examine 12 different damage cases. Dyke et al. (2001) tested a 4-story, 2-bay by 2-bay steel frame at the University of British Columbia. The model was 8.20 ft x 8.20 ft in plan and was 11.81 ft tall. Six damage cases were induced to the structure by loosening bolts and removing braces. Different researchers used different methodologies to analyze the data obtained from the structure for a benchmark study.

Two phenomenological models were created at the University of Cincinnati and Drexel University to study the challenges limiting successful SHM applications (Ciloglu et al. 2001).

The grids were representative of the large population of medium-span bridges. While these two models could be utilized for various studies, these models were single span models where damage can be identified relatively easily compared to multi-span redundant structures.

2.4.1. Steel Grid Structure

A steel grid structure was designed, constructed, and used for the experimental studies discussed in this dissertation. This model is a multi-purpose specimen enabling researchers to try different technologies, sensors, algorithms, and methodologies before real life applications. The physical model has two clear spans with continuous beams across the middle supports. It has two 18 ft girders (S3x5.7 steel section) in the longitudinal direction. The 3 ft transverse beam members are used for lateral stability. The grid is supported by 42 in tall columns (W12x26 steel section). The grid is shown in Figure 8 and more information about the specimen can be found in Burkett (2005), Caicedo et al. (2006), Gul and Catbas (2007), and Catbas et al. (2008).

Figure 8. The steel grid model used for the experimental studies

A very important characteristic of the grid structure is that it can be easily modified for

different test setups. For example, with specially designed connections (Figure 9) various damage cases can be simulated. In addition, several different boundary conditions and damage cases (e.g., pin supports, rollers, fixed support, and semi-fixed support) can be simulated by using the adjustable connections.

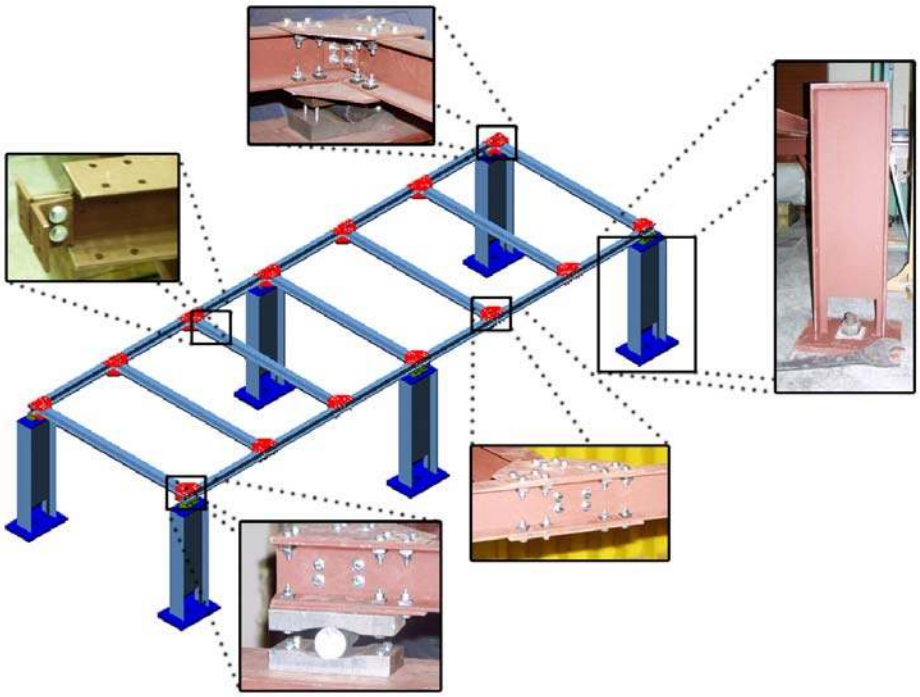

Figure 9. CAD drawing and representative pictures showing the details of the grid.

The grid structure can be instrumented with a number of sensors for dynamic and static tests. The instrumentation for the dynamic tests that are in the scope of this study is summarized as follows. The grid is instrumented with 12 accelerometers in vertical direction at each node (all the nodes except N7 to N14 in Figure 10). The accelerometers used for the experiments are ICP/seismic type accelerometers (Figure 11) with a 1000 mV/g sensitivity, 0.01 to 1200 Hz frequency range, and ∓ 2.5 g of measurement range. To record the dynamic response, an acquisition system from VXI and Agilent Technologies is used. The MTS-Test software package

was used for acquisition control of the impact tests.

For the impact tests, the grid was excited at nodes N2, N5, N6, and N12 and 5 averages were used to obtain the FRFs as it is suggested in the literature. The sampling frequency is 400 Hz. For the impact tests, an exponential window is applied to both input and output data sets whereas a force window is applied only to the input set. Both time history and FRF data from MTS software were recorded. The ambient vibration was created by random tapping of two researchers with fingertips simultaneously. The researchers were continuously moving around the structure to make the excitation as random as possible. The ambient data was recorded by using VXI DAQ Express software.

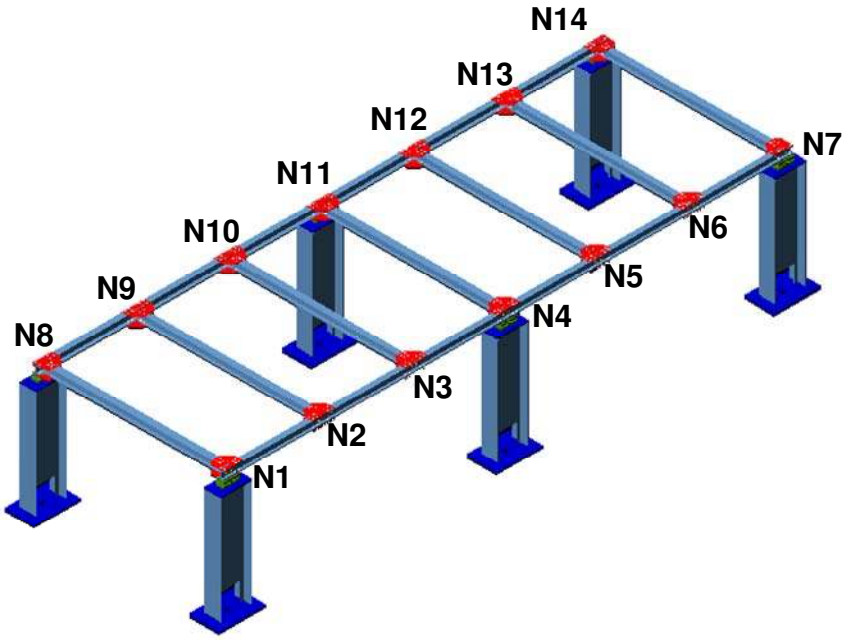

Figure 10. Node numbers for the steel grid

Figure 11. Accelerometers used in the experiments

2.4.2. Damage Simulations

A number of different damage scenarios were applied to the grid. These damage cases are simulated to represent some of the problems commonly observed by bridge engineers and Department of Transportation officials (Burkett 2005). Four different damage cases are investigated in this study and they are summarized below. Two of these damage cases are devoted to local stiffness loss whereas the other two cases are simulated for boundary condition change.

Baseline Case (BC0)

Before applying any damage, the structure is tested to generate the baseline data so that the data coming from the unknown state can also be compared to the baseline data for damage detection.

Damage Case 1 (DC1): Moment release at N3 and N10

The integrity of steel bridges is usually threatened by local stiffness losses due to different reasons such as fatigue cracking, bolt shear, and corroded elements. All of these

phenomena might change the behavior of the structure. The reduced stiffness damage scenarios are intended to correspond to these problems and they are investigated in two parts (DC1 and DC2). For DC1, the moment connection of the transverse member at N3 and N10 is released by removing the bolts that are connecting the transverse member to the main girder (Figure 12). In real life, this corresponds to slight local stiffness loss due to loosening or removing the bolts at that connection. Eight bolts at two connections (16 bolts in total) are removed for this case.

Figure 12. Removal of the bolts at N3 and N10 for DC1

Damage Case 2 (DC2): Moment release and plate removal at N3

DC2 is another case to simulate local stiffness loss. The bottom and top gusset plates at node N3 are removed in addition to all bolts at the connection (Figure 13). However, the bolts or plates at N10 are not removed. This is an important damage case since gusset plates are very critical parts of steel structures. Furthermore, it has been argued that inadequate gusset plates might have contributed to the failure of the I-35W Mississippi River Bridge (Holt and Hartmann 2008).

Figure 13. Plate removal at N3 for DC2

Damage Case 3 (DC3): Scour at N4

Boundary condition change can affect the behavior of a structure considerably. Therefore, DC3 and DC4 are dedicated to simulate such changes in the grid structure. Pile loss is an important problem faced in real life. The term pile loss may not always mean the failure of the bridge column. For example, a loss of contact between the column and bridge deck due to excessive settlement might also induce such damage to the bridge. To simulate the pile loss case, the roller support at N4 is removed (Figure 14).

Figure 14. Removal of the roller support at N4 for DC3

Damage Case 4 (DC4): Boundary restraint at N7 and N14

The second boundary condition change is DC4. This damage case is created to simulate some unintended rigidity at a support caused by different reasons such as corrosion. The oversized through-bolts were used at N7 and N14 to introduce fixity at these two supports. Although these bolts can create considerable fixity at the supports, it should be noted that these bolts cannot guarantee a perfect fixity.

Figure 15. Boundary fixity at N7 and N14 for DC4

2.4.3. Experimental Results for MIMO Testing

In this section, the experimental results are discussed in the context of damage detection. Starting with the modal flexibility and curvature, the performance of different damage features are presented in a comparative fashion. The modal parameters are identified by using CMIF based parameter estimation method. These modal parameters are then used to obtain the damage features (i.e. the modal flexibility and modal curvature). Detailed discussions about the results are presented below.

Baseline Case (BC0)

The first step in damage detection is generally to define the baseline state. Therefore, the damage features are first evaluated for the healthy case. The modal parameters of the healthy structure are identified by using CMIF. Sample FRFs and the CMIF plot for BC0 are shown in Figure 17 and Figure 18. There are 17 vertical modes identified for this case and the first 10 vertical modes are shown in Figure 19.

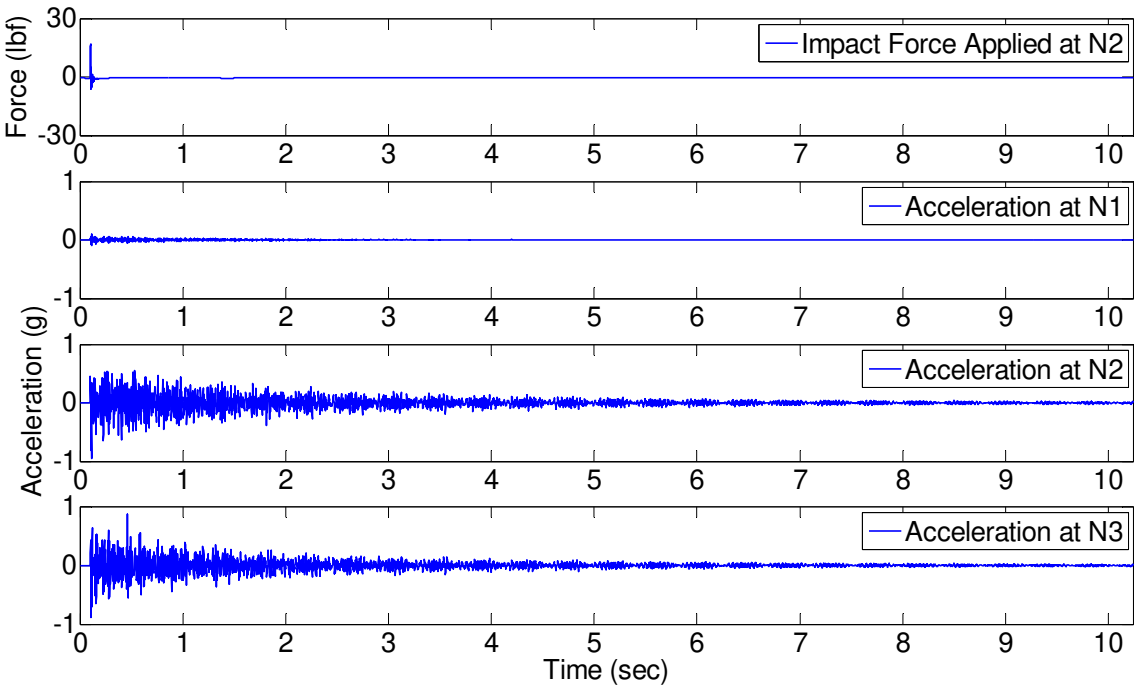

Figure 16. Sample data from impact testing for BC0

Note from the mode shapes that middle supports seem to be moving in some of the modes (see Mode 6 in Figure 19). This is somewhat unexpected for two span case. Therefore, the possible reasons for this discrepancy were investigated after the analysis and it was observed that there were some imperfections at the supports due to partial contact at the middle supports. The sensors at that location were on top of the area where the contact was lost. This essentially made

the sensor vibrate as opposed to being a node point on top of the middle support (Figure 20). This phenomenon was observed during various stages of the testing at different supports and it should be noted that it made the damage detection process considerably more challenging.

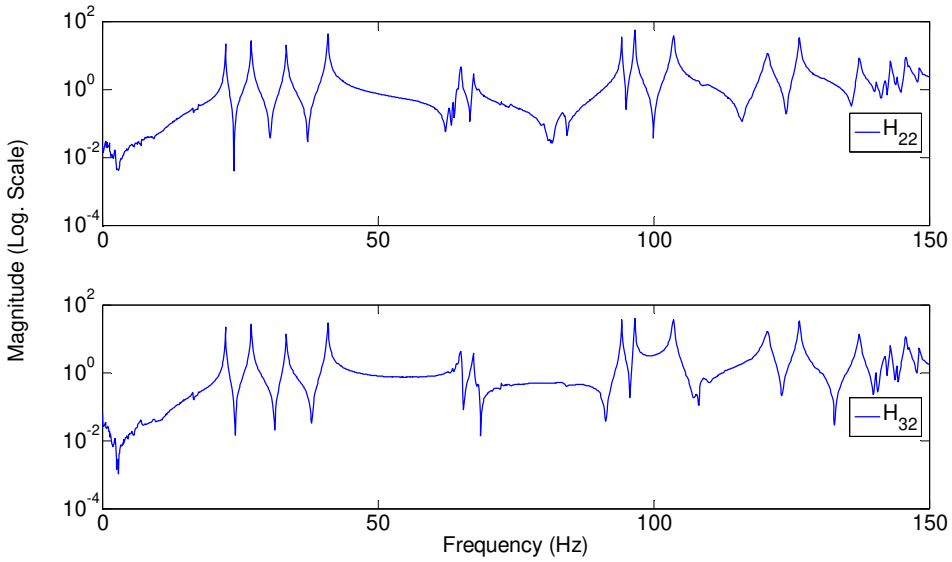

Figure 17. Sample FRF data obtained from impact testing for BC0

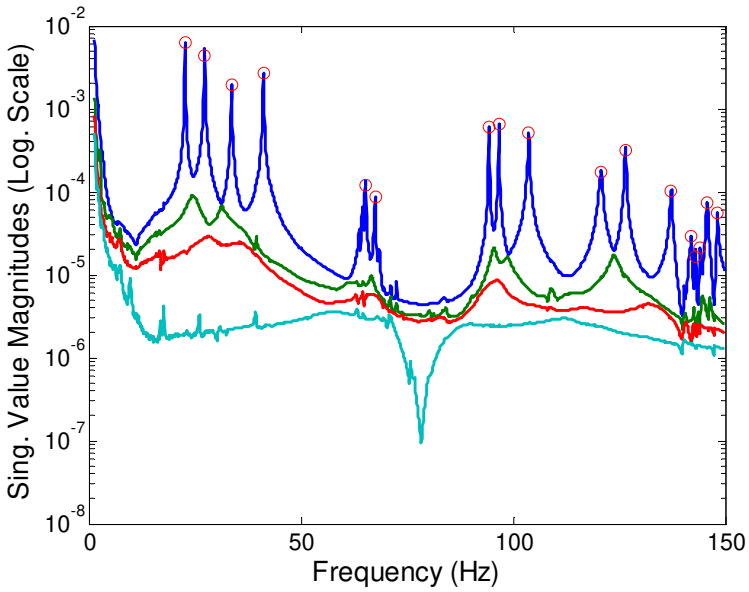

Figure 18. The CMIF plot for BC0 obtained with impact testing

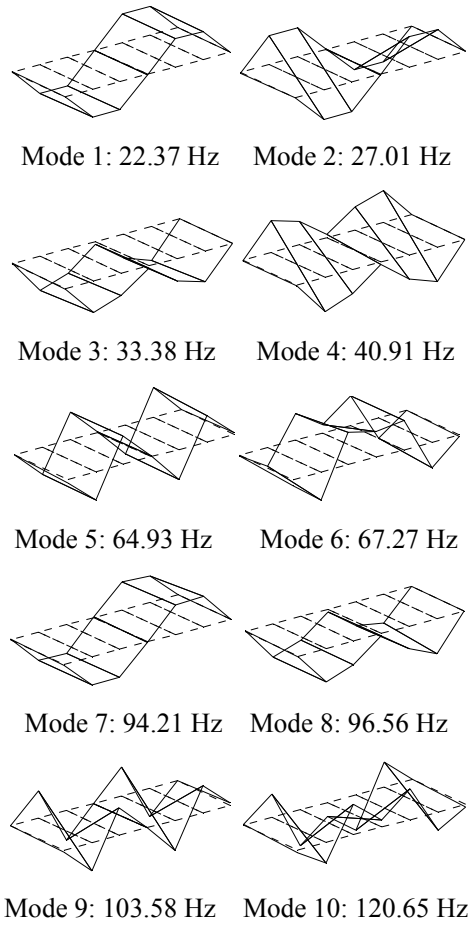

Figure 19. The first 10 vertical modes for BC0 obtained with impact testing

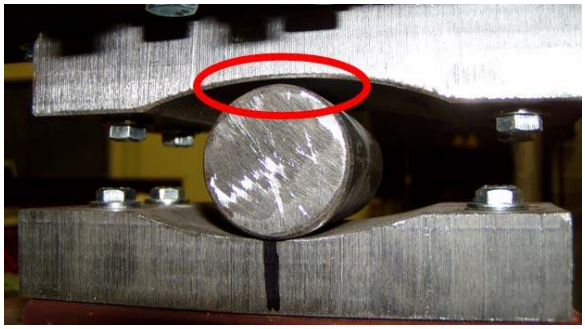

Figure 20. Picture showing the loss in the support contact.

After the modal parameters were identified, the modal flexibility was calculated. The deflection profile obtained with modal flexibility is shown in Figure 21. The deflected shape is

obtained by applying a 100 lb uniform load to the measurement locations (i.e. 100 lb at each node).

A preliminary finite element (FE) model was also employed to check the deflection profile obtained using modal flexibility. This comparison is conducted to globally cross-check the experimental results. The dynamically obtained deflection profile and its counterpart obtained with the FE model are illustrated in Figure 22. The consistency of the deflected shape is apparent although there are slight numerical differences (5-15%) due to experimental and modeling uncertainties and errors. It should also be noted that the FE model is not a calibrated model and calibration to minimize the discrepancy could be achieved to further improve the FE model results; however, it is beyond the scope of this study.

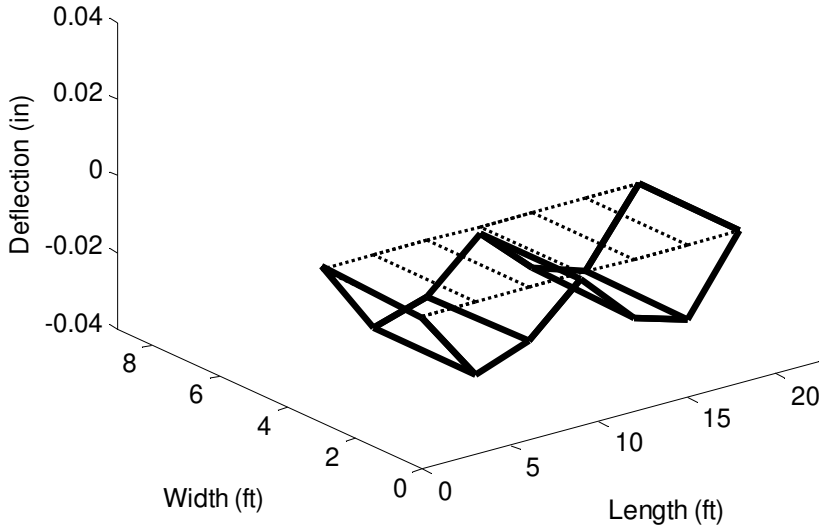

Figure 21. Deflection profile obtained using the modal flexibility for BC0

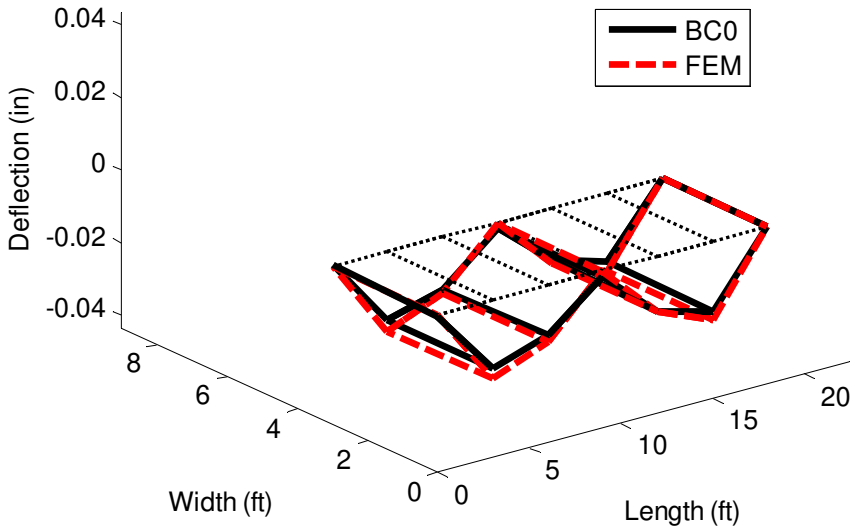

Figure 22. Comparison with FE model deflected shape

After obtaining the deflections, the curvature is obtained by using the deflected shapes as was shown in Eqn. (23). The modal curvature of the baseline case is shown in Figure 23. Moreover, the curvature values coming from experiments and FE model are compared in Figure 24. It is shown that the curvature obtained from modal flexibility based deflections is in good agreement with the values obtained from the FE model. It should be noted that the spatial resolution of the sensors would affect the quality of the curvature data considerably. A denser sensor array would further improve the results. However, the sensor spatial resolution in this study is defined so that it represents a feasible sensor distribution for real life applications on short and medium span bridges. Another consideration for modal curvature calculation is that there is no curvature value at the beginning and end measurement locations due to the numerical approximation of the central difference formula. The curvatures at the supports are assumed to be zero since the roller supports cannot resist moment thus indicating that there cannot be any curvature at these points. Finally, the curvature plot is very similar to that of a moment diagram

(*M/EI*) for a girder under uniform load. As such, the interpretation and evaluation of the curvature plot becomes very intuitive for structural engineers as in the case of deflected shapes.

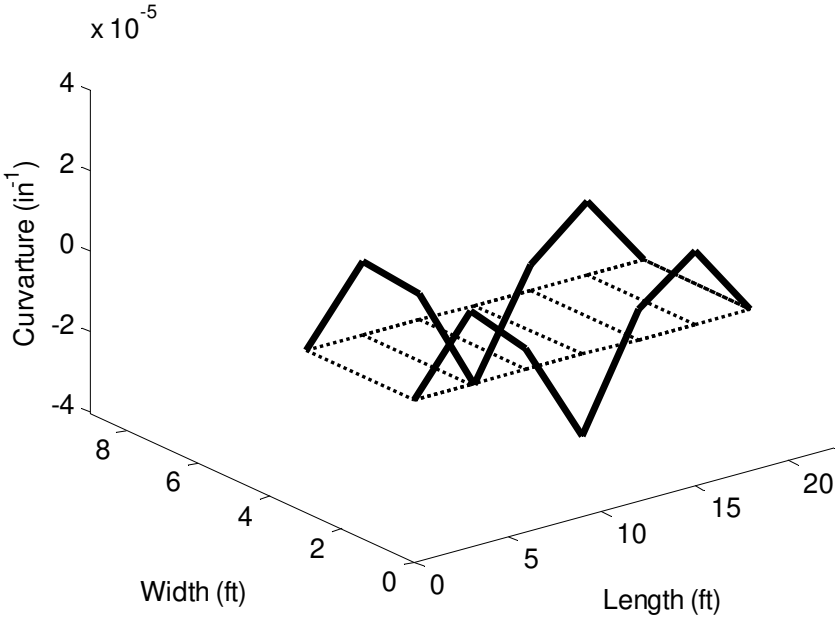

Figure 23. Curvature profile obtained using the modal curvature for BC0

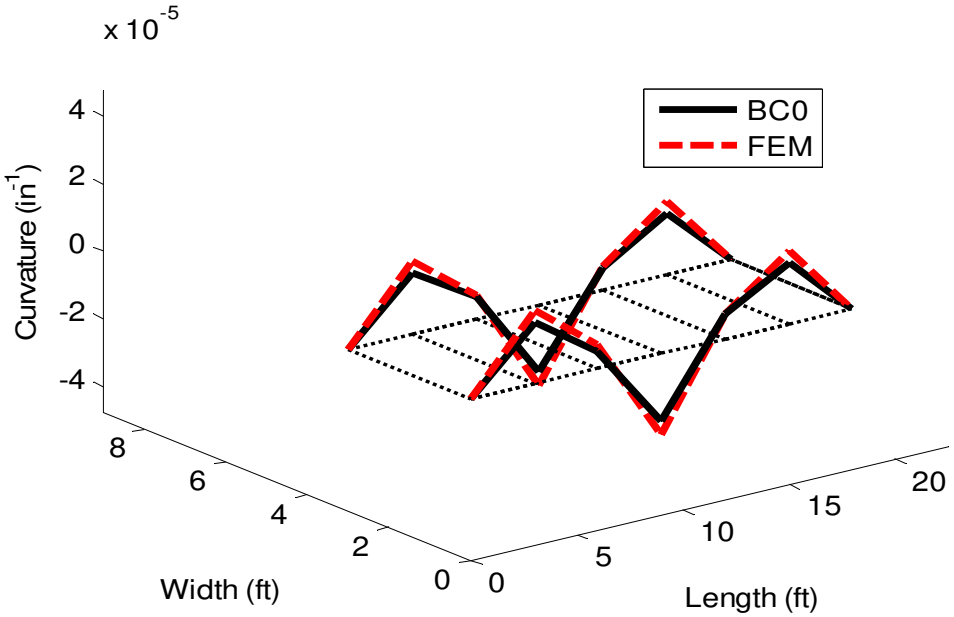

Figure 24. Comparison with FE curvature

Damage Case 1 (DC1): Moment release at N3 and N10

The deflected shape comparison of the BC0 and DC1 does not give any significant information about the slight damage occurred at N3 and N10 (Figure 25). The changes in the deflections under uniform loading for all nodes except the support nodes are around 1-2%. On the other hand, looking at the modal curvatures of the two main girders, it is observed that the modal curvature is increased 3.1% at N3 and 12.8% at N10. Although the change at N3 is not very significant, the change at N10 clearly points the change at that node. Similar results were obtained using other methodologies with numerical and experimental data when the same damage case is considered and are discussed in the following chapters.

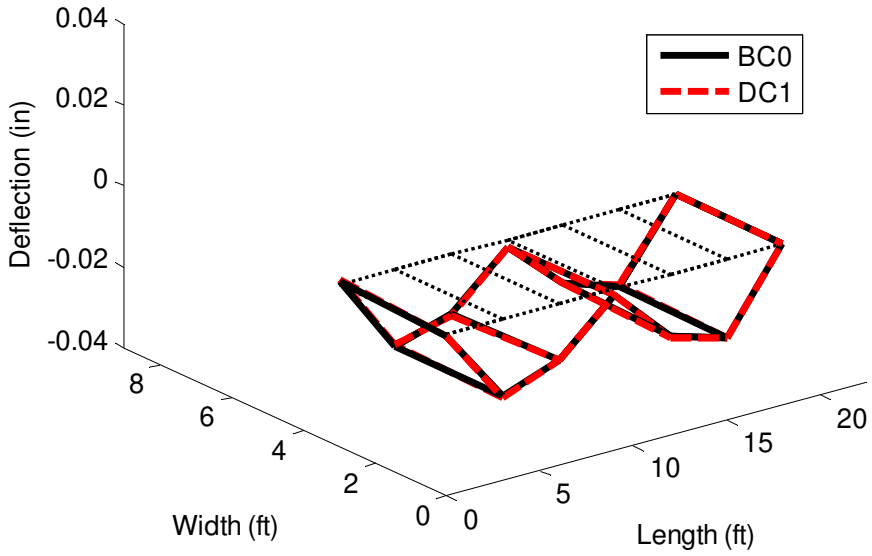

Figure 25. Deflection comparison for BC0 and DC1

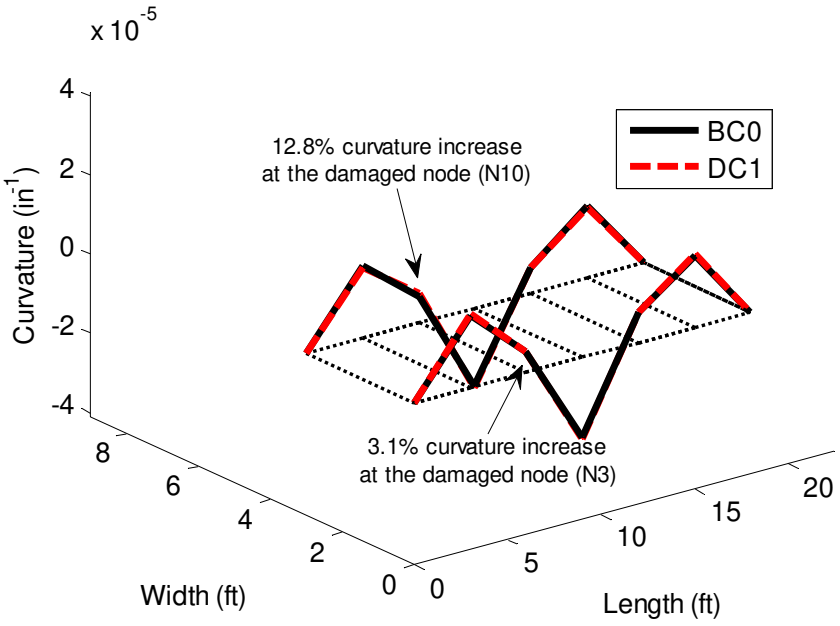

Figure 26. Curvature comparison for BC0 and DC1

Damage Case 2 (DC2): Moment release and plate removal at N3

It is seen from Figure 27 that the maximum deflection change obtained is at the damage location (N3) and is around 2.8%. The changes at the other nodes are around 1-2%. Although this change may possibly be considered as an indicator of the damage occurred at N3 for this laboratory case, it should also be noted that a 3% change in the flexibility coefficients might not be a clear indicator of the damage, especially for real life applications. Looking at the curvature comparisons, Figure 28 shows that the maximum curvature change is around 10.7% and is obtained at the damage location. The changes in the curvature for other points are less than 1-3% except at N12 where 4.7% increase in the curvature is computed.

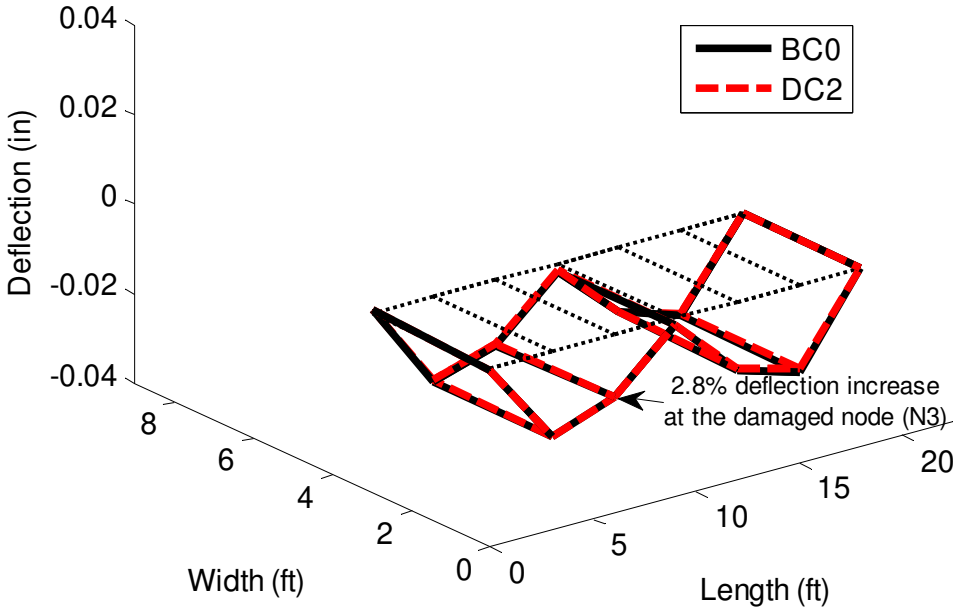

Figure 27. Deflection comparison for BC0 and DC2

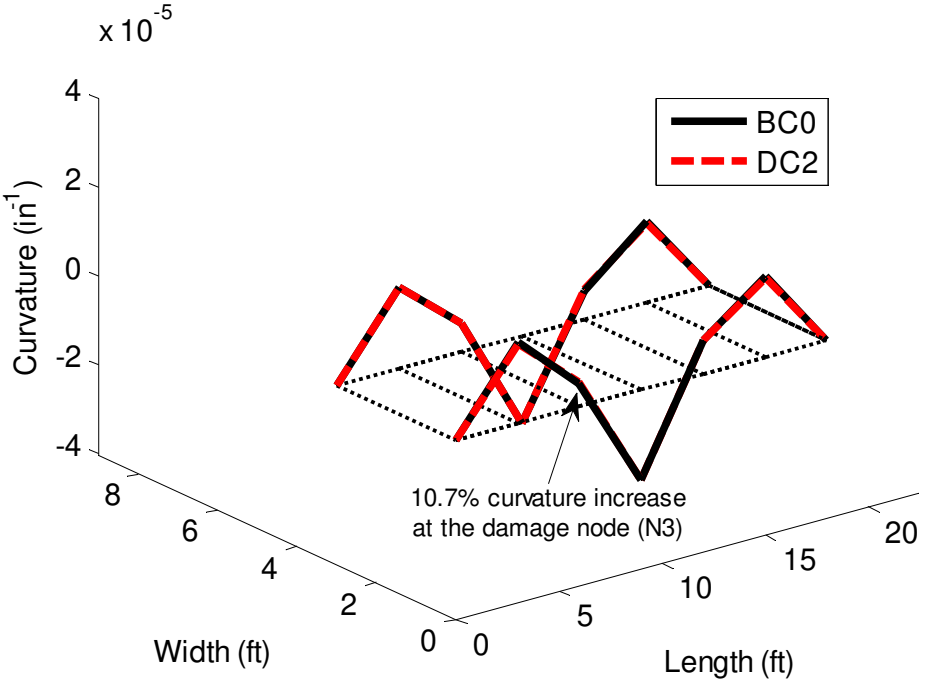

Figure 28. Curvature comparison for BC0 and DC2

Damage Case 3 (DC3): Scour at N4

DC3 is a relatively easier damage example to identify since removing the roller support changes the behavior of the structure significantly. The deflection changes at the right span in Figure 29 obviously show the removal of the roller support at N4. There is a significant deflection change (from 0.02 in to approximately 1 in) on the damaged side. The change is also clearly observable from the curvature plots in Figure 30. Therefore, without further discussion, it can be concluded that the damage is detected, located, and quantified successfully by using modal flexibility and curvature.

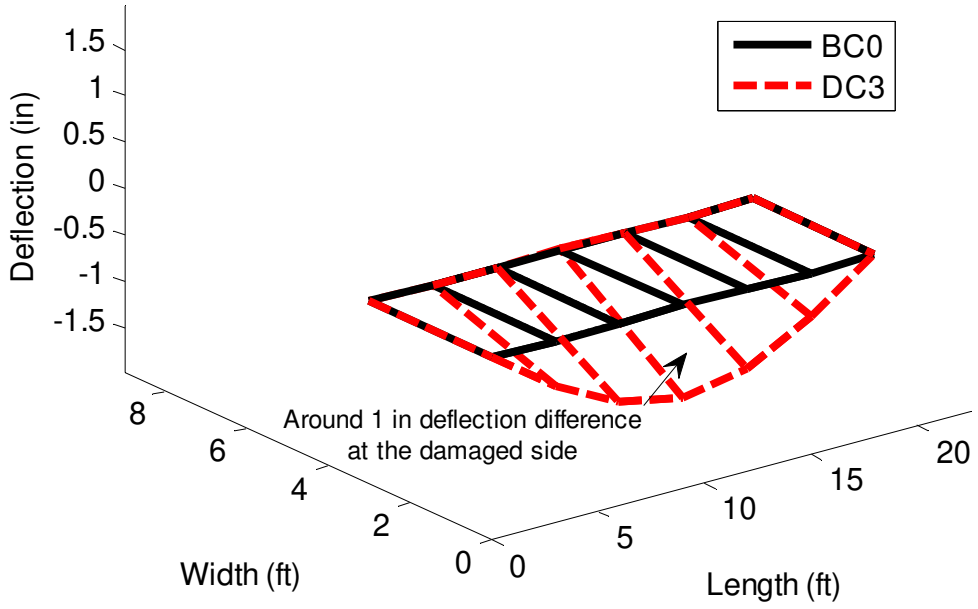

Figure 29. Deflection comparison for BC0 and DC3

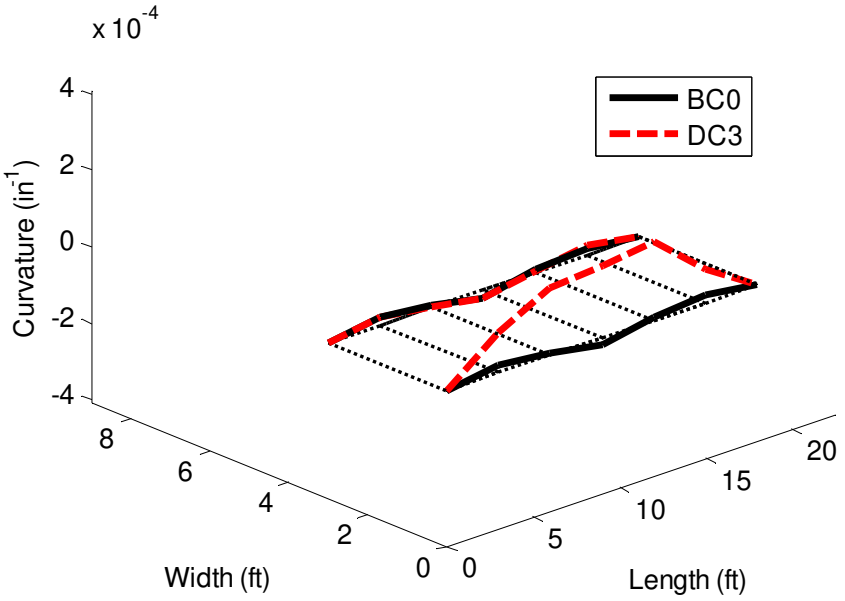

Figure 30. Curvature comparison for BC0 and DC3

Damage Case 4 (DC4): Boundary restraint at N7 and N14

For DC4, the damage can be visually observed from the deflection patterns as seen in Figure 31. It should be noted that this damage case can be considered as a symmetric damage case (both N7 and N14 are restrained) and thus a clear change in the deflected shapes is observable for both of the girders. The deflection reduced by about 30-50% at the span where joint restraint damage scenario was implemented.

Curvature from the deflected shapes was determined subsequently for DC4. As was mentioned before, the curvature at the roller supports was assumed zero for pin-roller boundary conditions. For the restrained case however, this assumption is not correct for N7 and N14 since the moment at these fixed supports is non-zero. However, for visualization purposes, the curvatures at N7 and N14 are still assumed as zero. It is seen from Figure 32 that a clearly observable 30% decrease in the curvature exists near the damage location. Here, we see a

decrease in the curvature because the structure with restrained support is stiffer than the baseline with roller supports. It is clear that a finer resolution of sensors, especially around the end supports, would yield more accurate results in terms of curvature.

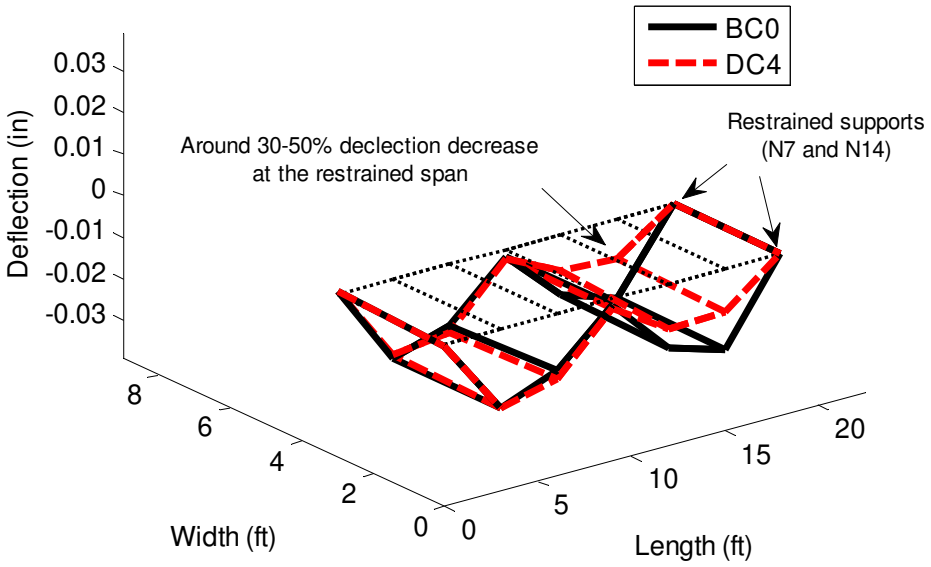

Figure 31. Deflection comparison for BC0 and DC4

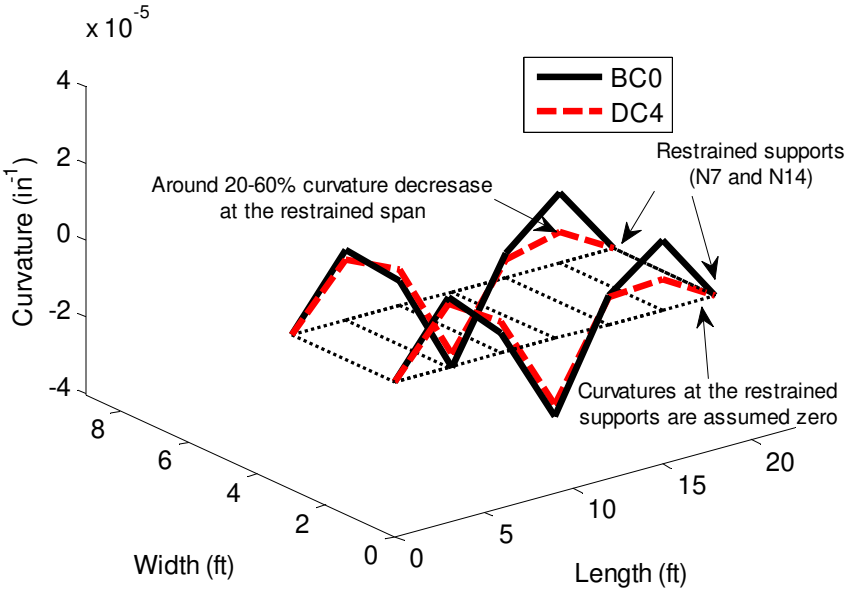

Figure 32. Curvature comparison for BC0 and DC4

2.4.4. Experimental Results for Ambient Testing

For the ambient testing, the grid is excited by randomly tapping the structure with fingertips as mentioned before. Data sets used for this part of the study contains 120,832 data points which approximately corresponds to 5 minutes of recording with a sampling frequency of 400 Hz. RD technique is applied to each channel for every reference channel to obtain the un-scaled impulse functions. All channels except the support channels are selected as reference channels (eight channels). For RD analysis, 4096 point windows are used and level crossing triggering condition is applied, i.e. $a_1 = 0$ and $a_2 \approx \infty$ (refer to Eqn. (15)). For illustration purposes, the ambient data for two span case and its analysis with RD is shown in Figure 33 to Figure 35. These figures show the raw ambient, averaged, and windowed data for N2 where the reference channel is also N2. Note from Figure 35 that an exponential window function is applied to the averaged data in order to mitigate any leakage during the FFT process.

After obtaining the pseudo-free responses by using the RD method, the unscaled FRFs are computed taking the FFT of the pseudo-free responses. Then, these FRFs are fed to the CMIF algorithm as a MIMO data set. Sample FRFs and CMIF plots of the baseline for the ambient test is shown in Figure 36 and Figure 37. Note from the figure that there are eight lines in the plot showing that eight references were used during the RD process. Also, note the similarity of this plot with the one shown for the impact case (Figure 17 and Figure 18). The first ten vertical modes obtained with ambient tests are shown in Figure 38. The consistency of the frequencies and mode shapes of ambient case with MIMO case is observed from Table 1.

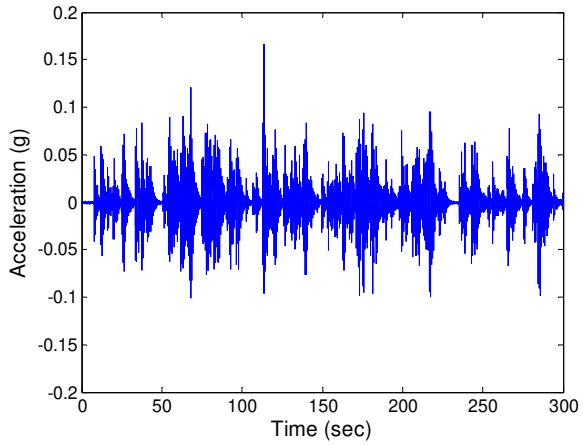

Figure 33.Ambient vibration data

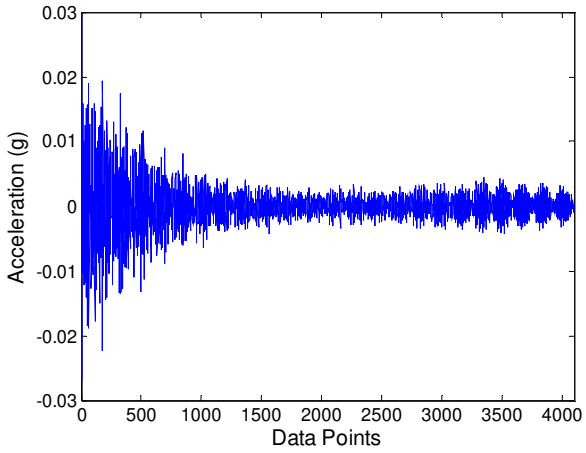

Figure 34.Ambient vibration data after averaging with RD

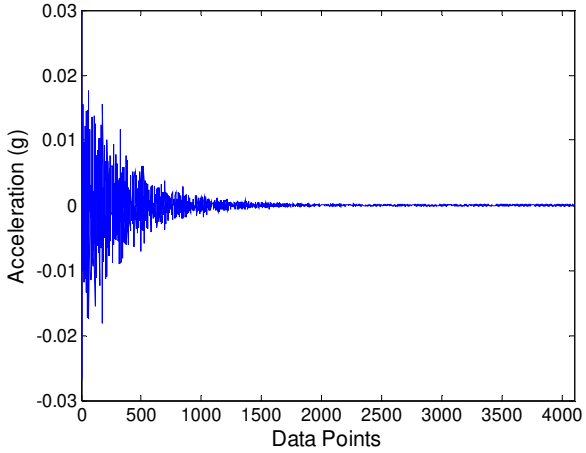

Figure 35.Averaged data after applying exponential window

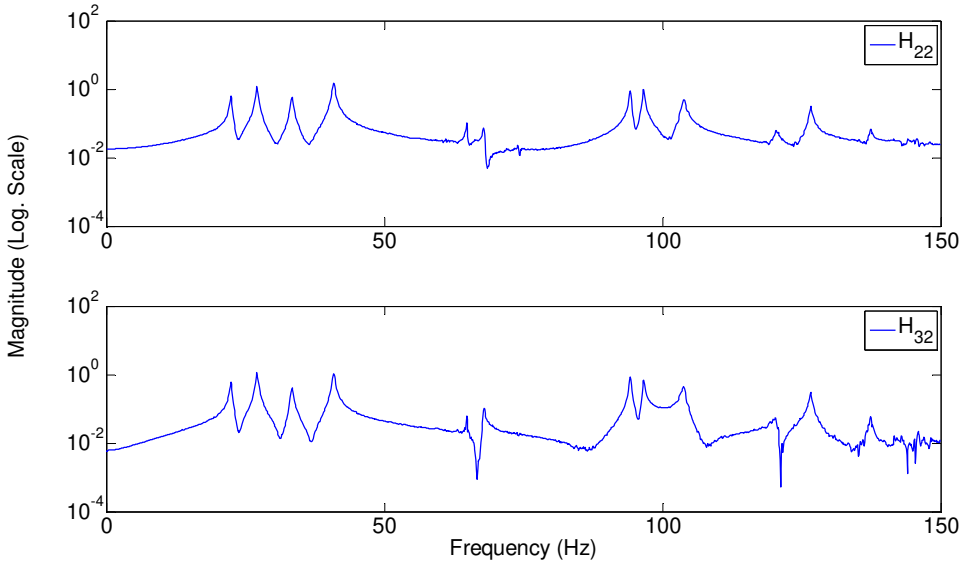

Figure 36. Sample FRF data obtained from ambient testing for BC0

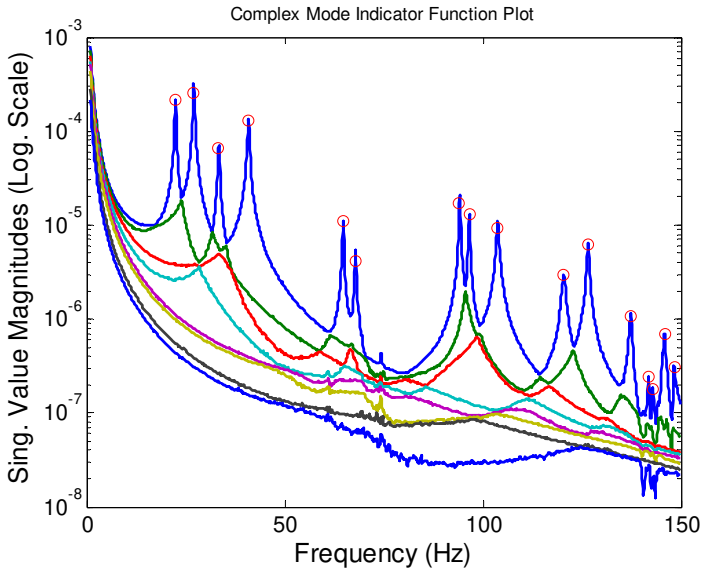

Figure 37. The CMIF plot of the baseline case obtained with ambient tests

By using the un-scaled modal parameters, the pseudo-flexibility instead of the modal flexibility is computed. The deflection pattern under uniform loading for BC0 obtained with the pseudo-flexibility is shown in Figure 39. Note that although the deflection pattern is nearly same

as MIMO testing results, values are significantly different because the scaling information cannot be obtained with ambient testing.

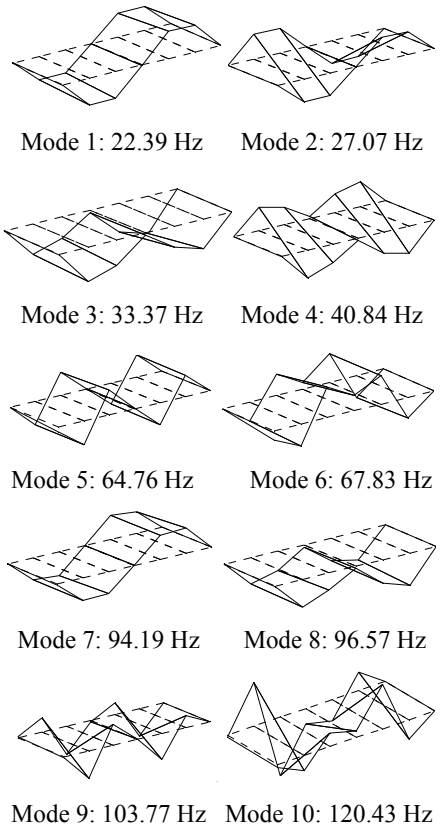

Figure 38. The first ten vertical modes of the baseline case obtained with ambient testing

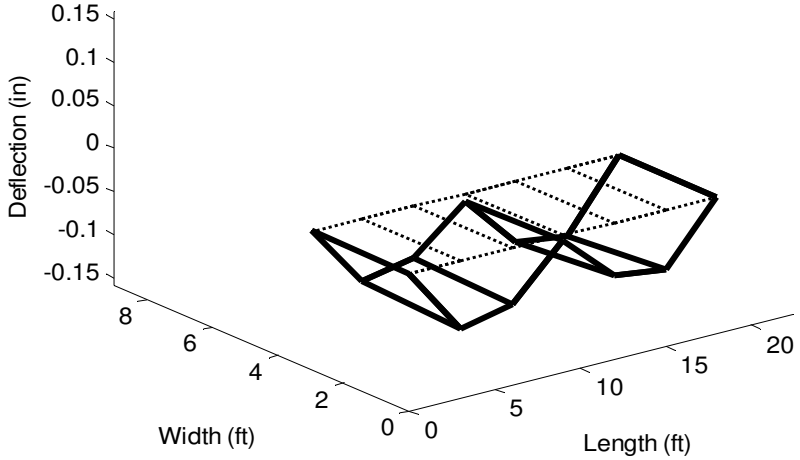

Figure 39. Deflection profile of BC0 for ambient testing

Table 1. Comparison of the first 10 modes identified with impact and ambient testing

Mode No	Frequency (Hz)			MAC
	Impact	Ambient	Diff. (%)	
1	22.37	22.39	0.12	0.999
2	27.01	27.07	0.23	0.999
3	33.38	33.37	-0.04	0.987
4	40.91	40.84	-0.16	1.000
5	64.93	64.76	-0.26	0.992
6	67.27	67.83	0.85	0.914
7	94.21	94.19	-0.01	0.999
8	96.56	96.57	0.01	0.998
9	103.58	103.77	0.18	0.995
10	120.65	120.43	-0.19	0.987

Damage Case 1 (DC1): Moment release at N3 and N10

The deflection pattern for DC1 obtained with pseudo-flexibility is compared with BC0 in Figure 40. It is observed that the there are notable differences at different nodes that are most likely not due to the damage. These changes are probably because of the errors encountered while obtaining the pseudo-flexibility. Therefore, it can be concluded that the pseudo-flexibility based deflections performed poorly for identification of the slight damage for DC1.

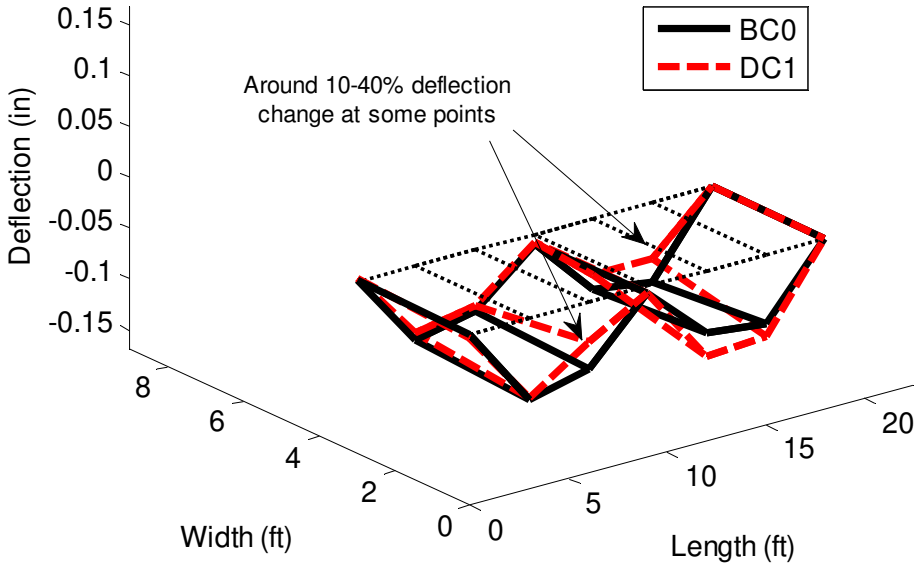

Figure 40. Deflection comparison for BC0 and DC1 for ambient testing

Damage Case 2 (DC2): Moment release and plate removal at N3

The pseudo-flexibility based deflections for BC0 and DC2 are compared in Figure 41. It is observed that there are slight changes in the deflection profiles. However, these changes cannot be attributed to the damage easily. Therefore, the local damage applied at N3 could not be identified by using ambient data where pseudo-flexibility based deflections are used as a damage index.

Damage Case 3 (DC3): Scour at N4

The comparison of the deflected shapes for BC0 and DC3 clearly shows the occurrence and location of the damage as presented in Figure 42. Furthermore, the severity of the damage is also apparent since the un-scaled deflection values increased more than 10 times. The global condition change in the structure is therefore successfully identified by using the pseudo-flexibility.

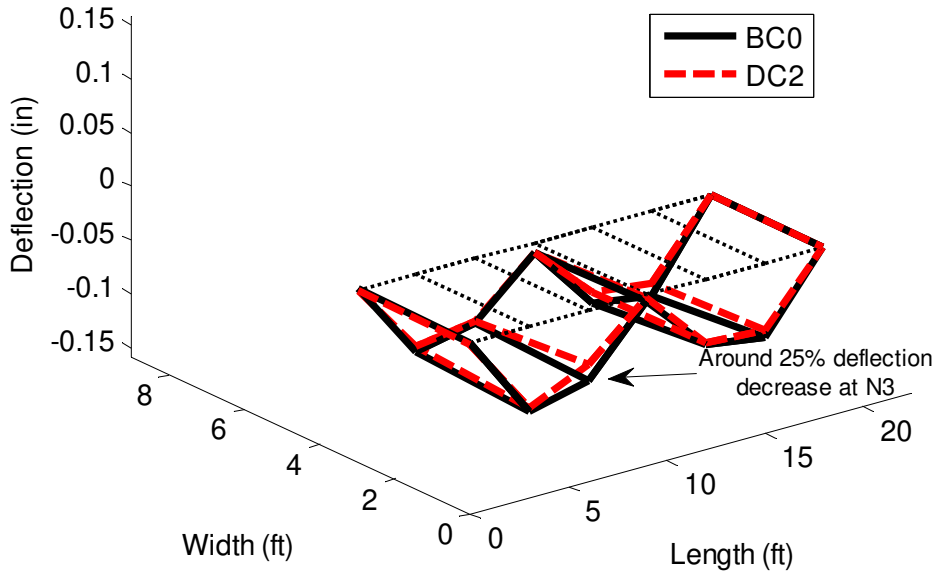

Figure 41. Deflection comparison for BC0 and DC2 for ambient testing

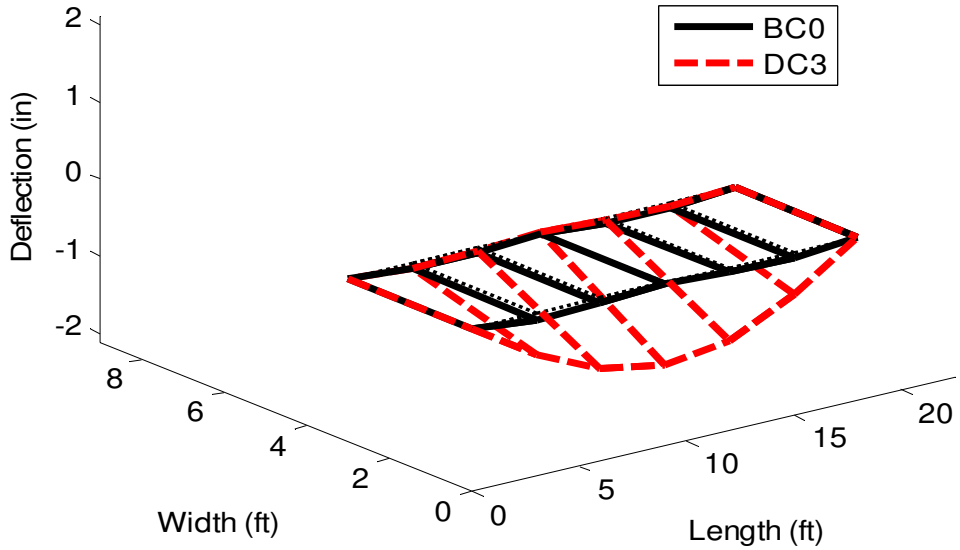

Figure 42. Deflection comparison for BC0 and DC3 for ambient testing

Damage Case 4 (DC4): Boundary restraint at N7 and N14

Figure 43 shows the un-scaled flexibilities coming from the healthy and damaged (DC4) structure. It is clearly seen that the deflection at the restrained span is less than the other span where all the joints have roller supports. The comparison of two un-scaled deflected shapes not only indicates that there has been a structural change, but it also gives us spatial information about the location of the damage.

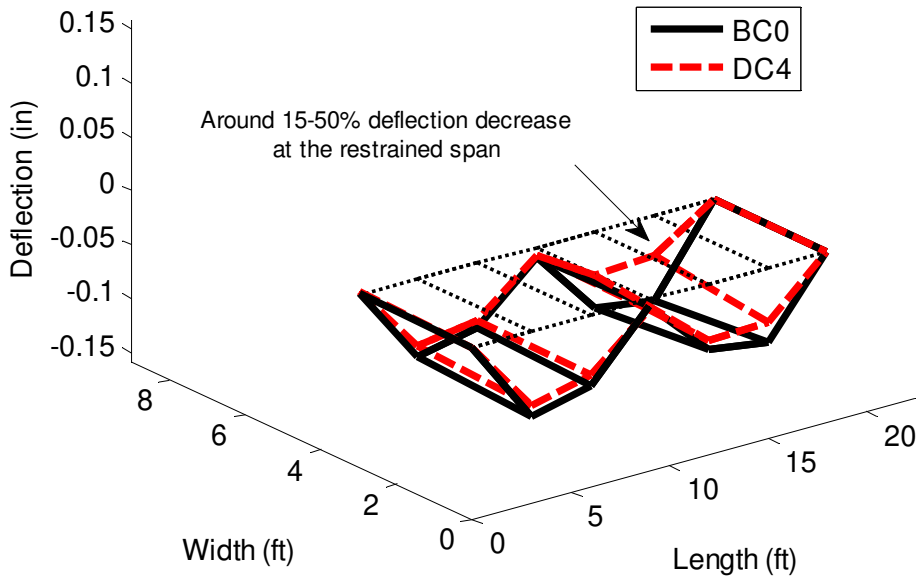

Figure 43. Deflection comparison for BC0 and DC4 for ambient testing

2.5. Summary

In this chapter, some parametric damage features obtained from MIMO and ambient vibration testing are employed. The damage detection capabilities of modal flexibility, modal curvature, and pseudo-flexibility are investigated by using dynamic data coming from a steel grid structure for different damage simulations.

In the first part, MIMO acceleration data is analyzed with CMIF to obtain the modal

parameters. Then the modal flexibility is obtained by using the modal parameters. Finally, deflected shape and modal curvature is obtained by applying a pseudo-loading to the modal flexibility. The damage simulations showed that both modal flexibility and modal curvature performed well for localized and global damage cases. It was also noted that change in the modal curvature was a better indicator for the localized damage cases.

In the second part, a conceptual methodology for system identification and structural condition assessment using ambient vibration data is presented. The CMIF was used in conjunction with RD for identification of the modal parameters from ambient vibration data. For the condition assessment of the structures, the deflection profiles obtained from the un-scaled (pseudo) flexibility is presented as a conceptual indicator. It was shown that, although the pseudo-flexibility performed satisfactorily for global damage cases (DC3 and DC4), it was not successful at identification of the localized damage (DC1 and DC2).

CHAPTER 3. NON-PARAMETRIC EVALUATION WITH STATISTICAL PATTERN RECOGNITION FOR DAMAGE DETECTION

3.1. General Remarks

Use of statistical pattern recognition methods offers promise for handling large amounts of data while taking into account variations in the data. Farrar and Sohn (2000) further describe SHM as the observation of a system over time using periodically sampled dynamic response measurements from an array of sensors, the extraction of damage sensitive features from these measurements and the statistical analysis of these features to determine the current state of system health. Most of the studies focusing on statistical pattern recognition applications on SHM use a combination of time series modeling with a statistical novelty detection methodology (e.g. outlier detection). One of the main advantages of such methodologies is that they require only the data from the undamaged structure in the training phase (i.e. unsupervised learning) as opposed to supervised learning where data from both undamaged and damaged conditions is required to train the model. The premise of the statistical pattern recognition approach is that as the model is trained for the baseline case, new data coming from the damaged structure will likely be classified as outliers in the data.

Most of these statistical models are used to identify the novelty in the data by analyzing the feature vectors, which include the damage sensitive features. For example, Sohn et al. (2000) used a statistical process control technique for damage detection. Coefficients of Auto-Regressive (AR) models were used as damage-sensitive features and they were analyzed by using X-bar control charts. Different levels of damage in a concrete column were identified by using the methodology. Worden et al. (2000) and Sohn et al. (2001) used Mahalanobis distance-

based outlier detection for identifying structural changes in numerical models and in different structures. Worden et al. (2000) used transmissibility function as damage sensitive features whereas Sohn et al. (2001) used the coefficients of the AR models. Manson et al. (2003) also used similar methodologies to analyze data coming from different test specimens including aerospace structures.

In another study, Omenzetter and Brownjohn (2006) used Auto-Regressive Integrated Moving Average (ARIMA) models to analyze the static strain data coming from a bridge during its construction and when the bridge was in service. The authors were able to detect different structural changes by using the methodology. They also mentioned the limitations of the methodology, for example, it was unable to detect the nature, severity, and location of the structural change. Nair et al. (2006) used an Auto-Regressive Moving Average (ARMA) model and used the first three AR components as the damage sensitive feature. The mean values of the damage sensitive features were tested using a hypothesis test involving the t-test. Furthermore, the authors introduced two damage localization indices using the AR coefficients. They tested the methodology using numerical and experimental results of the ASCE benchmark structure. It was shown that the methodology was able to detect and locate even different types of damage scenarios for numerical case. However, it was concluded by the authors that more investigations were needed for analysis of experimental data.

Another methodology was proposed by Zhang (2007) where the author used a combination of AR and ARX (Auto-Regressive model with eXogenous output) models for damage detection and localization. The standard deviation of the residuals of the ARX model was used as damage sensitive feature. Although the methodology was verified by using a

numerical model, the author indicated that further studies should be conducted to make the methodology applicable in practice. In a recent study, Carden and Brownjohn (2008) used ARMA models and a statistical pattern classifier, which uses the sum of the squares of the residuals of the ARMA model. The authors stated that the algorithm was generally successful in identifying the damage and separating different damage cases from each other. However, the authors noted that the vibration data was coming from forced excitations tests and the methodology may not be applicable for structures with only ambient dynamic excitation.

As summarized above, there are a number of different approaches utilizing time series modeling in conjunction with an outlier detection or novelty measurement methodology to identify structural change. It is observed, however, that most of these methodologies need more investigation by means of additional experiments. Therefore, in this chapter, we employ experimental data coming from different test structures and damage cases to examine a statistical pattern recognition approach for SHM. The methodology uses Auto-Regressive models in conjunction with a Mahalanobis distance-based outlier detection algorithm. In the proposed methodology, Random Decrement technique is used to obtain free vibration response from the ambient vibration data. After obtaining the normalized data with RD, AR models are fitted to the data. Finally, the coefficients of these models are used for Mahalanobis distance-based outlier detection. The methodology is investigated by using experimental data from the two different test structures for a number of different structural configurations. Various damage conditions are simulated and the advantages and drawbacks of the methodology are discussed in light of the experimental results.

3.2. Review and Formulations of Time Series Modeling

Time series modeling (or analysis) is statistical modeling of a sequence of data points that are observed in time. It has been used in many different fields including structural dynamics and system identification. In the following sections, a brief discussion about time series modeling is given. A more detailed discussion about the theory of the time series modeling is beyond the scope of this study and can be found in the literature (Pandit and Wu 1993; Box et al. 1994; Ljung 1999).

A linear time series model representing the relationship of the input, output and the error terms of a system can be written with the difference equation shown in Eqn. (27) (Ljung 1999). A more compact form of this equation is shown in Eqn. (28)

$$\begin{aligned} &y(t) + a_1 y(t-1) + \cdots + a_{n_a} y(t-n_a) \\ &\quad = b_1 u(t-1) + \cdots + b_{n_b} u(t-n_b) + e(t) + d_1 e(t-1) + \cdots + d_{n_d} e(t-n_d) \end{aligned} \tag{27}$$

$$A(q)y(t) = B(q)u(t) + D(q)e(t) \tag{28}$$

where, $y(t)$ is the output of the model, $u(t)$ is the input to the model and $e(t)$ is the error term. The unknown parameters of the model are shown with a_i, b_i, and d_i and the model orders are shown with n_a, n_b and n_d. $A(q)$, $B(q)$ and $D(q)$ in Eqn. (28) are polynomials in the delay operator q^{-1} as shown below in Eqn. (29). The model shown in Eqn. (28) can also be referred as an ARMAX model (Auto-Regressive Moving Average model with eXogenous input) and a block diagram of an ARMAX model can be shown as in Figure 44.

$$A(q) = 1 + a_1 q^{-1} + a_2 q^{-2} + \cdots + a_{n_a} q^{-n_a}$$
$$B(q) = b_1 q^{-1} + b_2 q^{-2} + \cdots + b_{n_b} q^{-n_b} \quad (29)$$
$$D(q) = 1 + d_1 q^{-1} + d_2 q^{-2} + \cdots + d_{n_d} q^{-n_d}$$

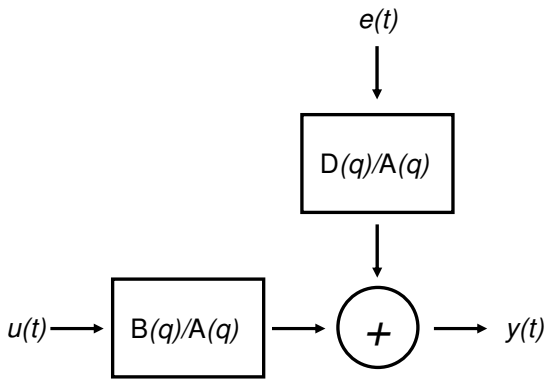

Figure 44. The block diagram of an ARMAX model (adapted from Ljung (1999))

By changing the model orders of an ARMAX model, different types of time series models can be created. For example, if $n_b=n_d=0$, the model is referred as an AR model, whereas an ARMA model is obtained by setting n_b to zero. The structure of an AR model is shown in Eqn. (30) whereas the block diagram of the model is shown in Figure 45.

$$A(q)y(t) = B(q)u(t) + e(t) \quad (30)$$

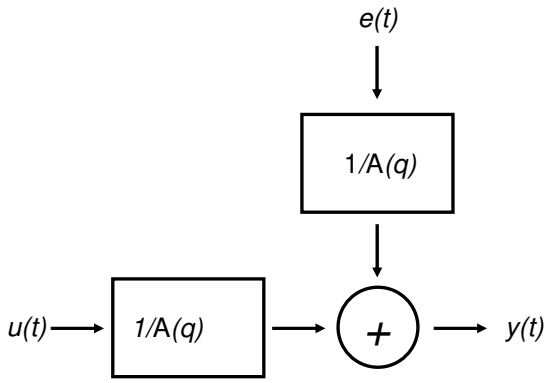

Figure 45. The block diagram of an AR model (adapted from Ljung (1999))

Estimating the unknown parameters of a time series model from the input-output data set (i.e. system identification) is of importance since the identified model can be used for many different purposes including prediction and novelty detection. To estimate the unknown parameters, the difference equation of an ARX model can be written as in Eqn. (31).

$$y(t) = -a_1 y(t-1) - \cdots - a_{n_a} y(t-n_a) + b_1 u(t-1) + \cdots + b_{n_b} u(t-n_b) + e(t) \tag{31}$$

The equation shown in Eqn. (31) can be written for the previous time step as in Eqn. (32).

$$\begin{aligned} y(t-1) = -a_1 y(t-2) - \cdots - a_{n_a} y(t-n_a-1) \\ + b_1 u(t-2) + \cdots + b_{n_b} u(t-n_b-1) + e(t-1) \end{aligned} \tag{32}$$

Considering that these equations can be written for each time step, the equations can be put in a matrix form as in Eqn. (33).

$$Y = X\theta + E \tag{33}$$

where

$$Y = \begin{bmatrix} y(t) & y(t-1) & \cdots & y(t-n+1) \end{bmatrix}^T \tag{34}$$

$$X = \begin{bmatrix} -y(t-1) & \cdots & -y(t-n_a) & u(t-1) & \cdots & u(t-n_b) \\ -y(t-2) & \cdots & -y(t-n_a-1) & u(t-2) & \cdots & u(t-n_b-1) \\ \vdots & \vdots & \vdots & \vdots & \vdots & \vdots \\ -y(t-n) & \cdots & -y(t-n_a-n) & u(t-n) & \cdots & u(t-n_b-n) \end{bmatrix} \tag{35}$$

$$\theta = \begin{bmatrix} a_1 & \cdots & a_{n_a} & b_1 & \cdots & b_{n_b} \end{bmatrix}^T \tag{36}$$

$$E = \begin{bmatrix} e(t) & e(t-1) & \cdots & e(t-n+1) \end{bmatrix}^T \tag{37}$$

where n is the number of the equations. It is observed that Eqn. (33) is a linear matrix

equation and the vector θ containing the unknown parameters can be estimated by using linear regression as shown in Eqn. (38).

$$\theta = \left(X^T X\right)^{-1} X^T Y \tag{38}$$

This solution also guarantees that the error vector *E* is minimized.

3.3. Time Series Modeling in Conjunction with Novelty Detection

3.3.1. Implementation of RD for Data Normalization

The theoretical background and formulations of RD technique was given in the previous chapter. This section details its implementation before using the time series modeling. The RD method is used to normalize the data and obtain the pseudo free responses from the ambient data. By doing so, the effect of the operational loadings on the data is minimized. Therefore, different data sets coming from different operational conditions can be compared more reliably. The proposed methodology is illustrated in Figure 46.

3.3.2. Auto Regressive (AR) Models for Normalized Data

After obtaining the pseudo free response functions, AR models of these free responses are created. Although a more detailed discussion about Time Series Modeling was given in the previous sections, a brief discussion about AR models is given here. An AR model estimates the value of a function at time t based on a linear combination of its prior values. The model order (generally shown with p) determines the number of past values used to estimate the value at t (Box et al. 1994). The basic formulation of a p^{th} order AR model is defined in Eqn. (39).

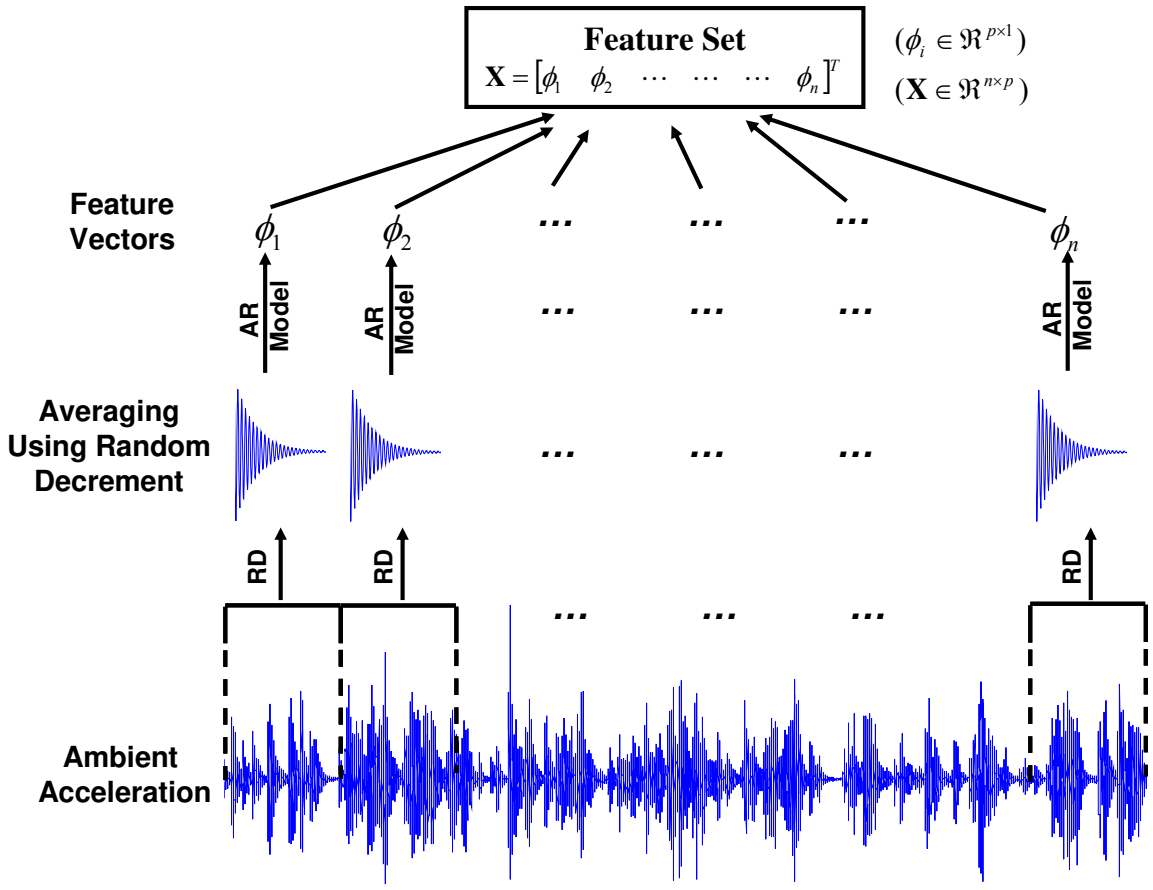

Figure 46. Implementing RD to ambient acceleration data before obtaining the feature sets using time series modeling

$$x(t) = \sum_{j=1}^{p} \phi_j x(t - j\Delta t) + e(t) \tag{39}$$

where $x(t)$ is the time signal, ϕ is the model coefficients and $e(t)$ is the error term. After obtaining the coefficients of the AR models, they are fed to the outlier detection algorithm where the Mahalanobis distance between the two different data sets is calculated.

3.3.3. Mahalanobis Distance-Based Outlier Detection using AR Coefficients

After obtaining the AR model coefficients for different data sets, these coefficients are now used for outlier detection. Outlier detection can be considered as the detection of clusters,

which deviate from other clusters so that they are assumed to be generated by another system or mechanism. Outlier detection is one of the most common pattern recognition concepts among those applied to SHM problems. In this study, Mahalanobis distance-based outlier detection is used to detect the novelty in the data.

The outlier detection problem for univariate (1D) data is relatively straightforward (e.g., the outliers can be identified from the tails of the distribution). There are several discordance tests, but one of the most common is based on deviation statistics and it is given by Eqn. (40).

$$z_i = \frac{d_i - \bar{d}}{\sigma} \tag{40}$$

where, z_i is the outlier index for univariate data, d_i is the potential outlier and, $\bar{d}$ and σ are the sample mean and standard deviation, respectively. The multivariate equivalent of this discordance test for $n \times p$ (n is the number of the feature vectors and p is the dimension of each vector) data set is known as the Mahalanobis squared distance (Mahalanobis 1936). The Mahalanobis squared distance will be referred as Mahalanobis distance after this point and it is given by Eqn. (41)

$$Z_i = (x_i - \bar{x})^T \Sigma^{-1} (x_i - \bar{x}) \tag{41}$$

where, Z_i is the outlier index for multivariate data, x_i is the potential outlier vector and $\bar{x}$ is the sample mean vector and Σ is the sample covariance matrix. By using the above equations, the outliers can be detected if the Mahalanobis distance of a data vector is higher than a pre-set threshold level.

Determining this threshold value is very critical and an example framework was

presented by Worden et al. (2000) where the authors used a Monte Carlo simulation to determine the threshold. In this study a similar methodology is adapted as follows. First, a $n \times p$ normal data set with zero mean and unit standard deviation is created. Then the exclusive measures of the Mahalanobis distance for each feature vector is calculated. Here, exclusive measure implies that the corresponding feature vector is excluded from the data set during the computation of the Mahalanobis distance. After calculating the Mahalanobis distances for all the feature vectors, the maximum of these values is stored. This process is repeated for 1000 times and the value above which only 1 % of the trials occur is selected, i.e. 99% confidence threshold. After determining the numerical threshold value, it is checked by using experimental data sets.

3.4. Experimental Studies

In this section, the capability of the methodology to separate different structural configurations is investigated by using experimental data. The first test specimen is a steel beam where different boundary conditions are applied. The second test structure is the steel grid, which was discussed in detail in the previous chapter. The same damage cases used in the previous chapter are used in this chapter.

3.4.1. Test Beam

The model used for the first set of experiments is a simply supported steel W8x13 I-beam. The clear span of the beam is 144 in, while the overall length is 156 in. The beam sits on two steel sawhorses each measuring 3 ft in height. The setup can be seen in Figure 48 and more information can be found in Francoforte et al. (2007).

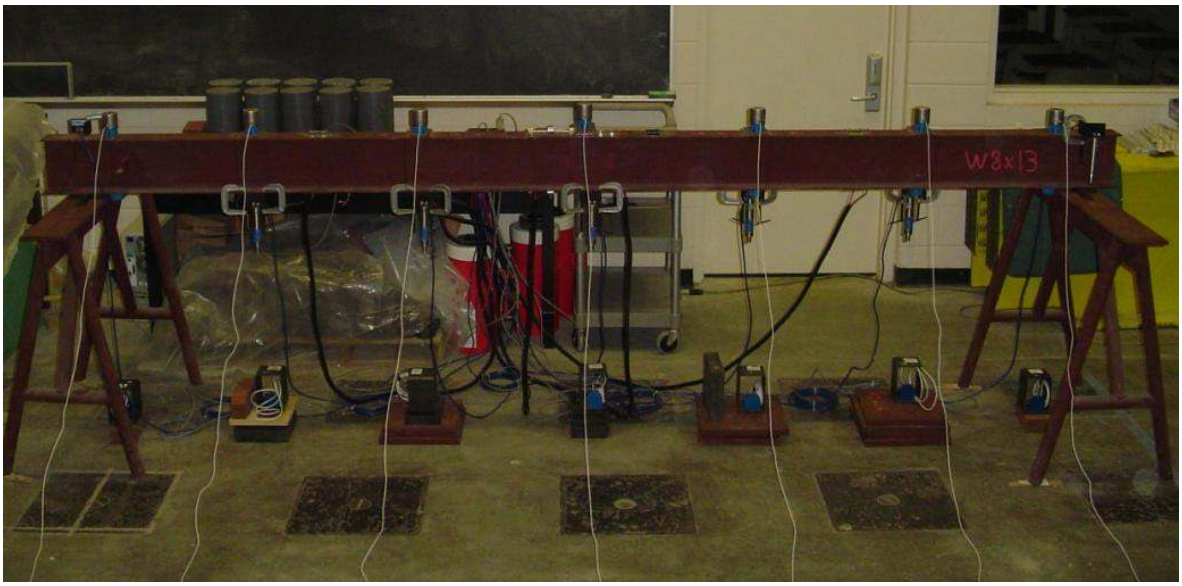

Figure 47. Test setup and the instrumented steel beam

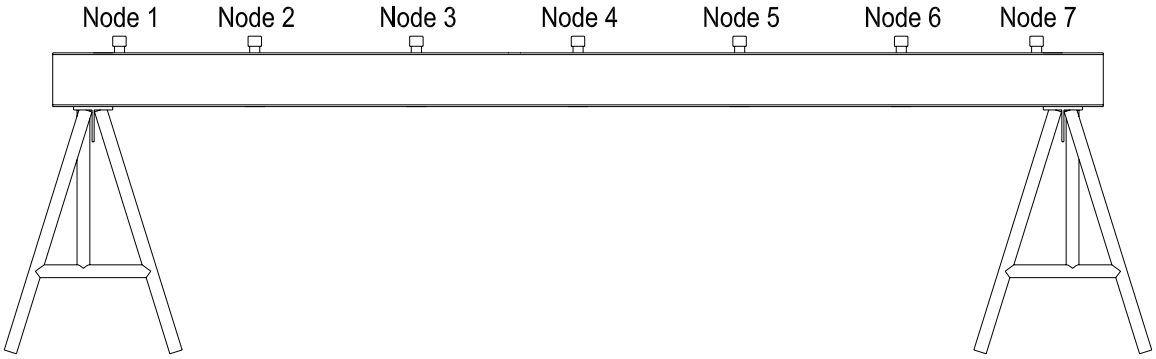

Figure 48. The node numbers of the beam

Although it is a simple laboratory specimen, the beam is densely instrumented with a number of sensors and it is tested for many different structural configurations. The beam is tested for different boundary conditions (Table 2). The total number of dynamic and static sensors is 29 (i.e. seven accelerometers, seven displacement gages, seven tiltmeters and eight strain gages (Figure 48)). However, only acceleration data is collected during the ambient vibration tests. The results presented in this study are obtained by using the ambient acceleration data, which was

generated by random hand tapping of two researchers simultaneously. Figure 49 (a) shows the pin support for BC1 where Figure 49 (b) shows BC2 and Figure 49 (c) shows five Duro70 pads for BC4.

(a)

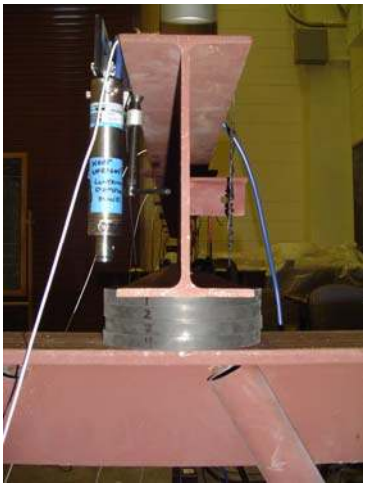

(b)

(c)

Figure 49. Example pictures showing different BC (a) the pin support for BC1 (b) four Duro50 pads for BC2 (c) five Duro70 pads for BC4

Table 2. Boundary conditions of the test beam

Name	Boundary Condition (BC)
BC1	Pin supports at each support
BC2	4 Duro50 pads at node 1; Pin/shims at node 7
BC3	5 Duro50 pads at each support
BC4	5 Duro70 pads at each support

As discussed in previous sections, the ambient vibration data is first processed (averaged) by using RD to obtain pseudo (un-scaled) free responses. Then, the AR models are fitted to the averaged data to obtain the condition indicating features. There are a number of different crucial parameters for the analysis such as the size of the data blocks, the reference channel for the RD and the model order of AR models. A sensitivity analysis concerning these parameters can reveal important information about the effects of these parameters on the identified features; however, it is beyond the scope of this study.

The ambient data is collected from each channel for approximately ten minutes with a sampling frequency of 800 Hz. 23 blocks of 20000 points with 50% overlap are used for each boundary condition. Reference channel for RD is Node 6 and each data block has 1024 points after averaging with RD. The model order p for AR models is three and obtained by using partial auto-correlation function (Box et al. 1994). Figure 50 (a) shows an example of the ambient data collected from the beam. Figure 50 (b) shows the pseudo impulse function obtained with RD, which is plotted on top of the pseudo impulse function estimated using the AR model. As it can

be seen from Figure 50 (b) and (c), the averaged and estimated data match almost perfectly, which indicates that the AR model fitted to the data is working reasonably well.

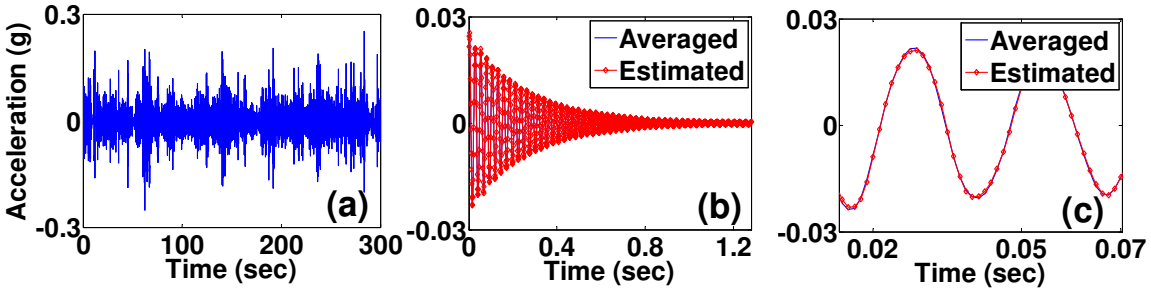

(a) (b) (c)

Figure 50. Time history data (a) Ambient data (b) Data after averaging with RD plotted with the data estimated with AR model (c) A closer look at the figure in (b)

After constructing the AR models, the coefficients of these models are used as the damage indicating features. Note that, for each BC, there are 23 data blocks, which means there are 23 sets of feature vectors each containing three AR coefficients. Then, all of these features are used to calculate the Mahalanobis distance between the features coming from different BC. The threshold value for the separation is obtained by using the methodology described in the previous sections and it is set as 35. Before discussing the results coming from different BC, the validity of the threshold value is investigated by using the experimental data. Figure 51 shows the Mahalanobis distance of two baseline data sets (first and second half of one data set). It is observed that most of the values are under the threshold value verifying the numerically obtained threshold value. Figure 52 compares the features coming from BC1 and BC2 for the seven nodes. The first half of the features (stars) is coming from BC1 whereas second half (circles) represents the BC2. It is clearly seen from the plots that the two BC can be well separated by using Mahalanobis distance. In another study, the authors also used K-Means clustering to

separate the same data however it was shown that K-Means clustering did not perform satisfactorily for this case (Gul et al. 2007). An important point to notice from Figure 52 is that although the difference between data sets is clearly seen, no information about the location of the change is obtained. Similar plots are shown in Figure 53 and Figure 54 where BC 1 vs. BC 3 and BC1 vs. BC4 are presented respectively. It is observed that different boundary conditions are successfully differentiated by using the methodology described in this text. An important point to re-emphasize is that the location of the change is not revealed from the results. It is observed that the separation is better for the data coming from the inner nodes compared to the support nodes. It is evident from the figures that as the vibration level increases for a node, a better separation is obtained. For example, looking at Node 1 and Node 7 in Figure 53 and Figure 54, it is seen that the features are not separated clearly, even though the change has been made at these locations.

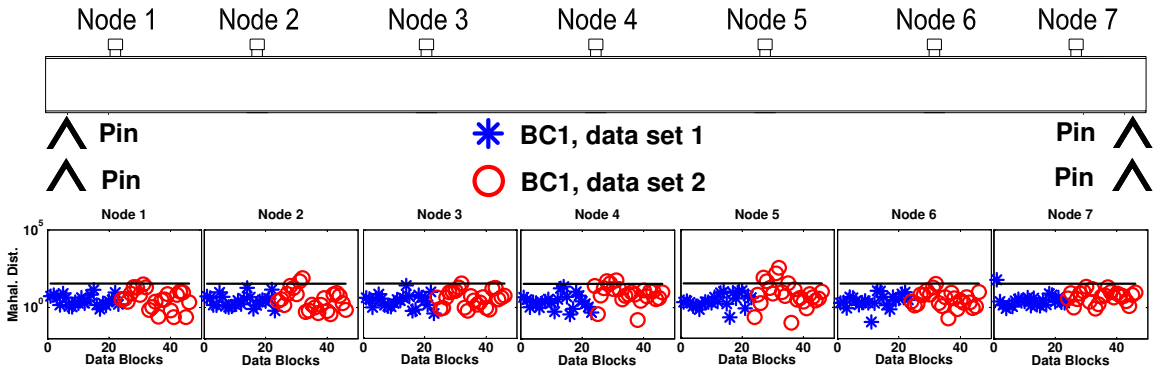

Figure 51. Verification of the threshold with experimental data

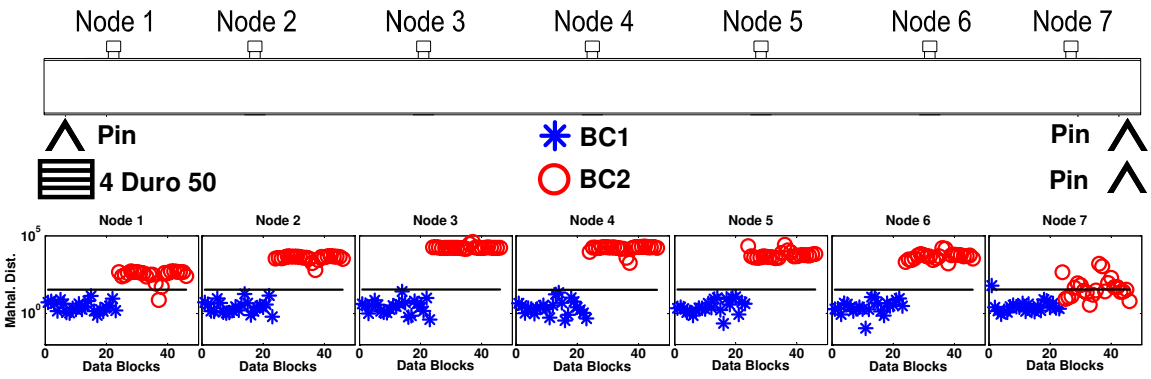

Figure 52. Mahalanobis distances for BC1 vs. BC2

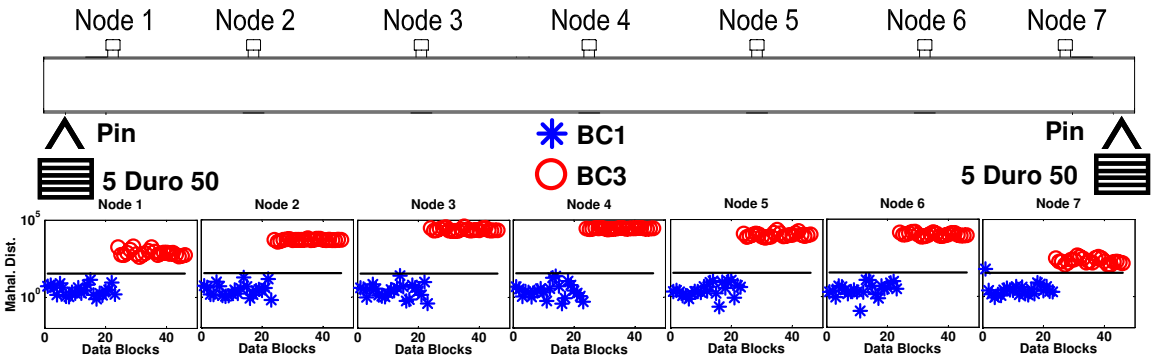

Figure 53. Mahalanobis distances for BC1 vs. BC3

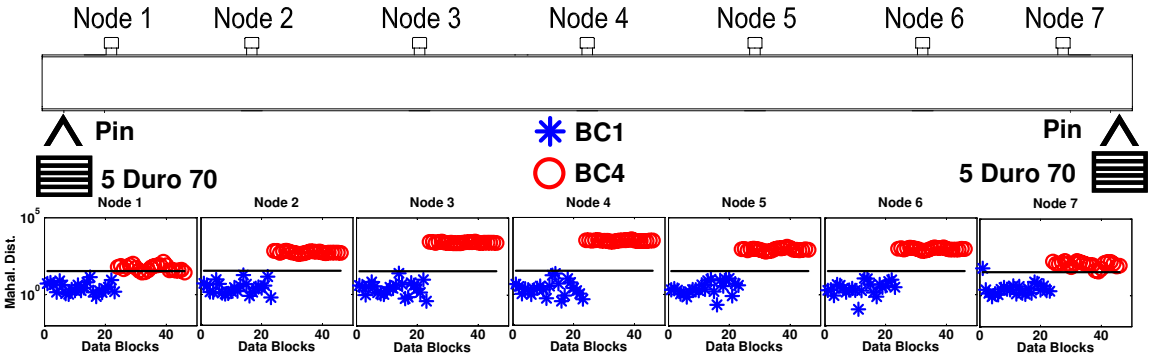

Figure 54. Mahalanobis distances for BC1 vs. BC4

In order to demonstrate the improvement when AR modeling is used in conjunction with the RD approach, the same data sets are analyzed with and without using RD. When RD is not employed, the data is normalized simply by subtracting the mean from the data and dividing it to the standard deviation in order to minimize the loading effects on the data (Sohn et al. 2001). All other parameters are kept the same as the case where RD is used. Figure 55-Figure 58 illustrate the results of the analysis without using RD before constructing the AR model. Comparing these figures with Figure 51-Figure 54, it is observed that the separation between baseline and damaged data is better when RD is used for the data analysis.

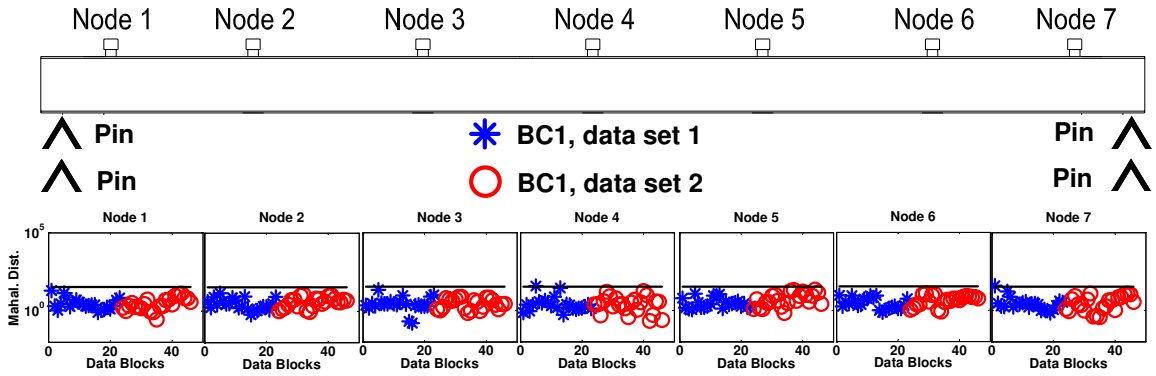

Figure 55. Verification of the threshold with experimental data (when RD is not used)

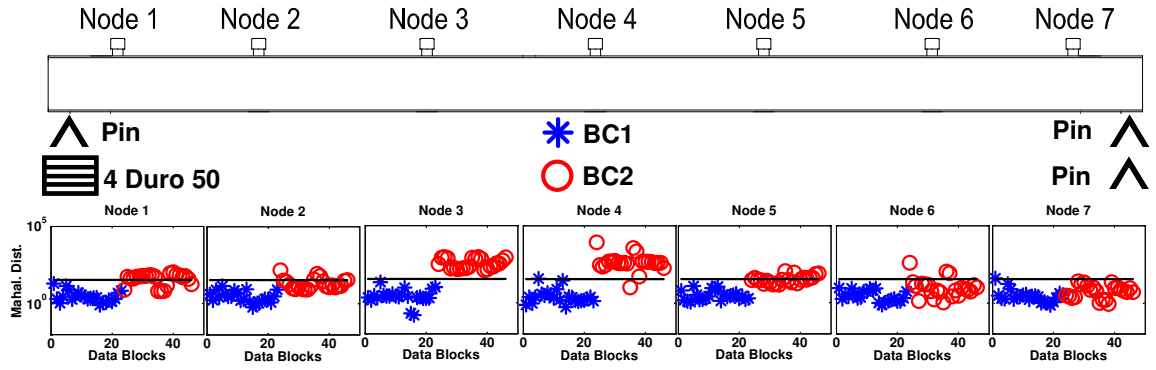

Figure 56. Mahalanobis distances for BC1 vs. BC2 (when RD is not used)

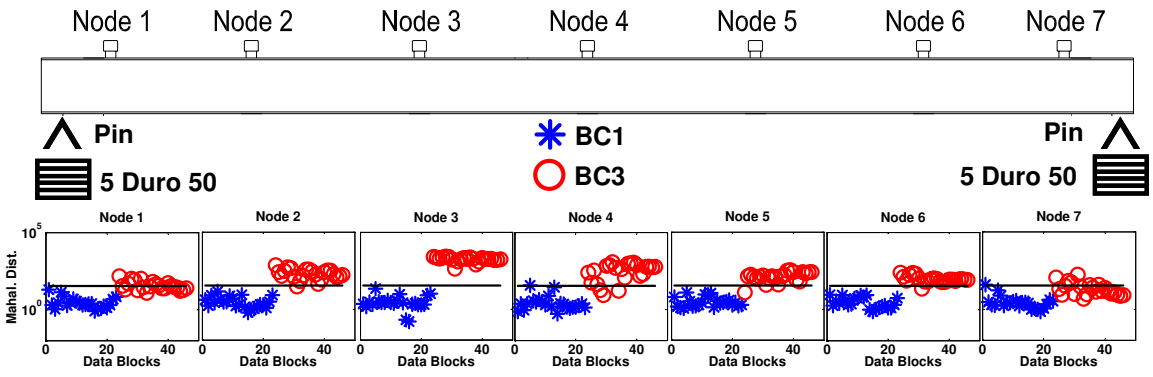

Figure 57. Mahalanobis distances for BC1 vs. BC3 (when RD is not used)

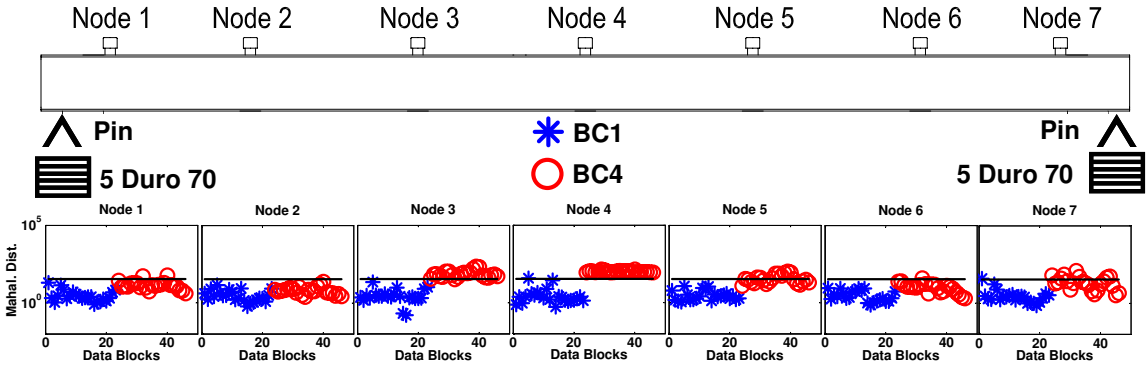

Figure 58. Mahalanobis distances for BC1 vs. BC4 (when RD is not used)

3.4.2. Test Grid

For this part of the study, the same grid structure discussed in previous chapter was used. Damage cases are also same as the ones discussed in the previous chapter. The test grid is excited by random hand tapping of two researchers simultaneously, as in the test beam case, to create ambient excitation. Sampling rate is 400 Hz for the experiments. There are 23 data blocks for each case. The acceleration data is averaged by using RD where the reference channel for RD process is Node 2 (the location of Node 2 can be seen in Figure 59). The model order for the AR models has been determined to be 10. The threshold is calculated as 180.

Baseline Case (BC0)

Before the analysis of the data from the damage cases, it is investigated whether the data coming from the baseline (healthy) grid structure is under the determined threshold value or not. Figure 59 shows analysis results of the baseline data acquired on the same day (first and second half of one data set). It is seen from the figure that all the values are under the threshold value (no false positives). Furthermore, another baseline data, which was acquired three months before the tests, is also used for this part of the analysis. It is shown in Figure 60 that all the data points are again under the threshold values. This indicates that the numerically evaluated threshold value is consistent with the experimental results.

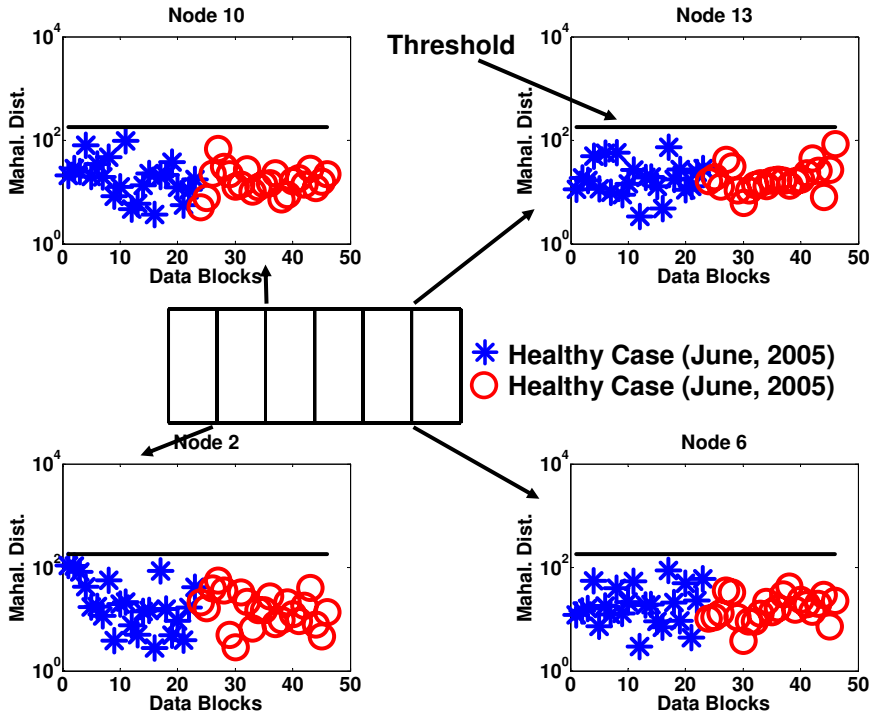

Figure 59. Verification of the threshold value with experimental data (both data sets acquired in the same day)

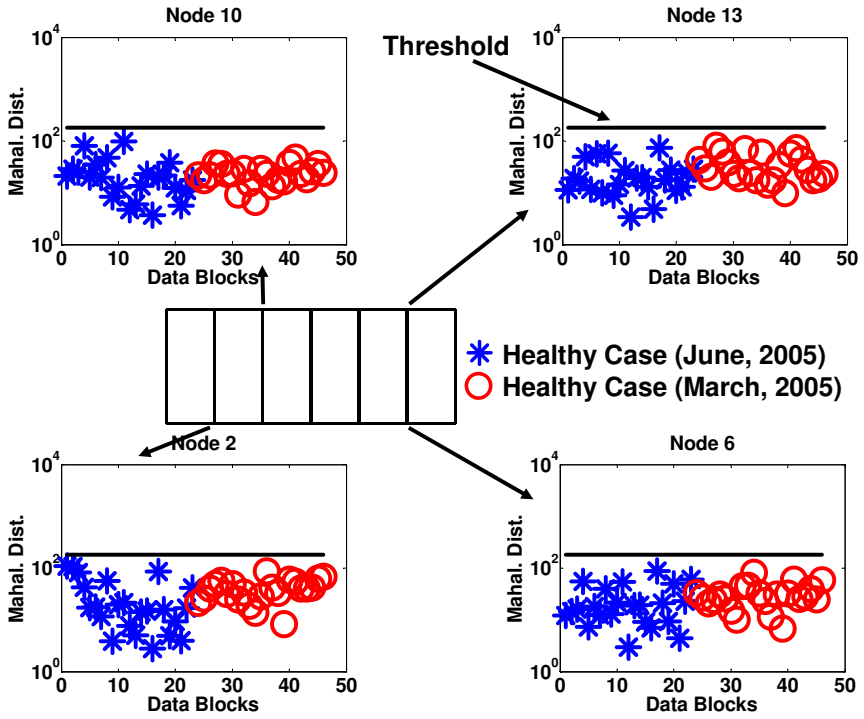

Figure 60. Verification of the threshold value with experimental data (data sets acquired at different times)

Damage Case 1 (DC1): Moment release at N3 and N10

After the baseline cases, the data from the damaged structure is examined. Figure 61 shows that around 50% of the damage features are above the threshold for DC1. It is noted that the number of false negatives is close to unacceptable levels, whereas a distinction between healthy and damaged cases is still somewhat observable. It should be emphasized at this point that although the same damage was identified using modal curvature with impact test data in the previous chapter, this damage case was not successfully identified using pseudo-flexibility where ambient data was used. Comparing Figure 40 and Figure 61, it is seen that both of the methodologies show some difference between BC0 and DC1, however, it is not very clear if this change can be attributed to damage.

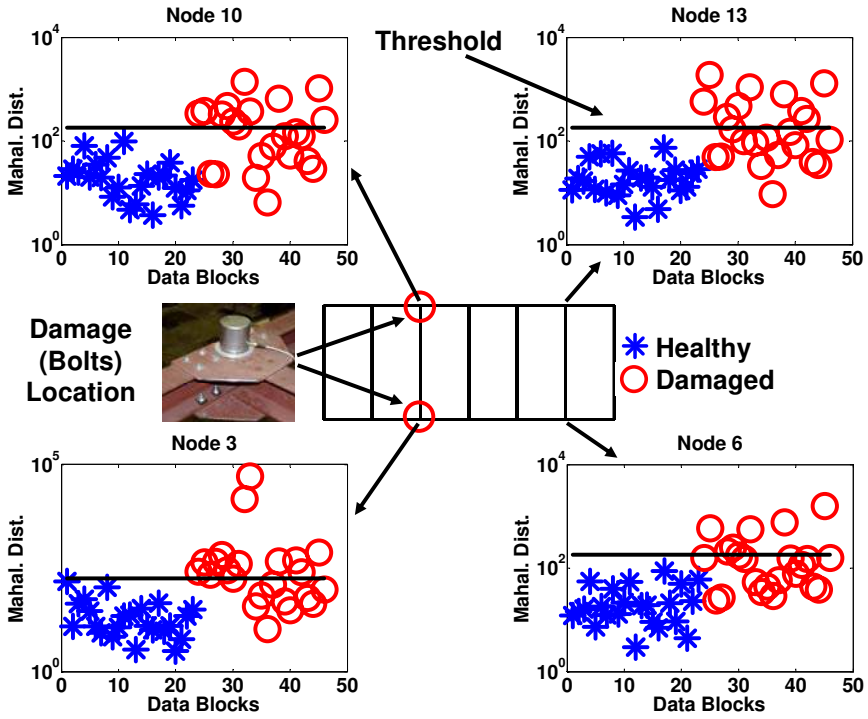

Figure 61. Mahalanobis distance plots for Reduced Stiffness case

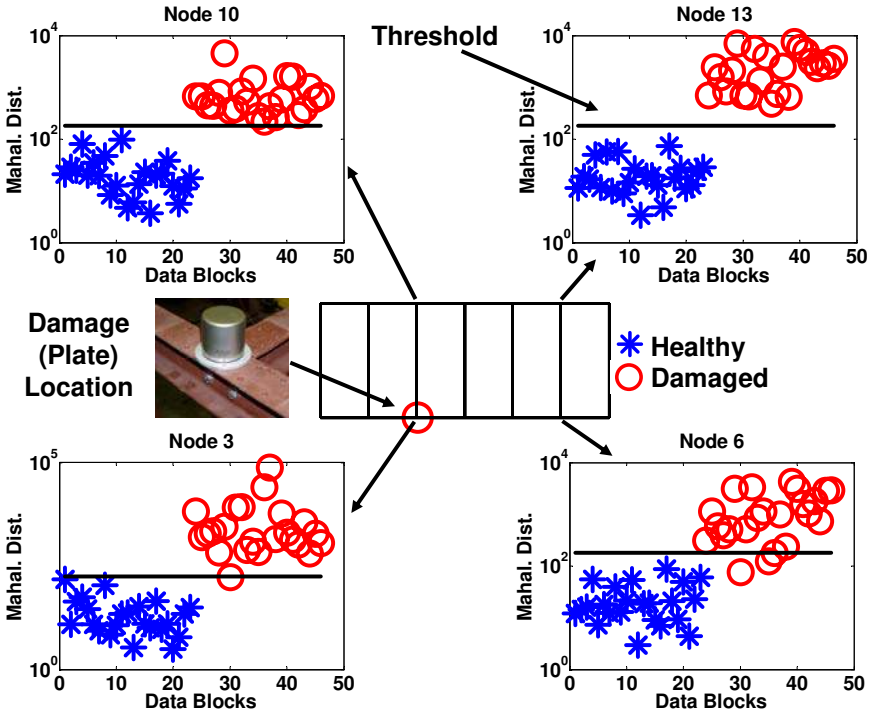

Figure 62. Mahalanobis distance plots for Plate Removal case

Damage Case 2 (DC2): Moment release and plate removal at N3

Figure 62 shows the same plots for DC2 where it is seen that a clearer separation of the features is achieved. These results are noteworthy since the damage was not successfully identified by using the ambient data in the previous chapter.

Damage Case 3 (DC3): Scour at N4

For the scour case, again the features coming from the damaged state can be separated from the baseline case as seen in Figure 63. One point that should be observed from the figure that, the Mahalanobis distances for N3 is higher than those for N4. This is one of the disadvantages of the methodology since it does not give any information about the location of the methodology.

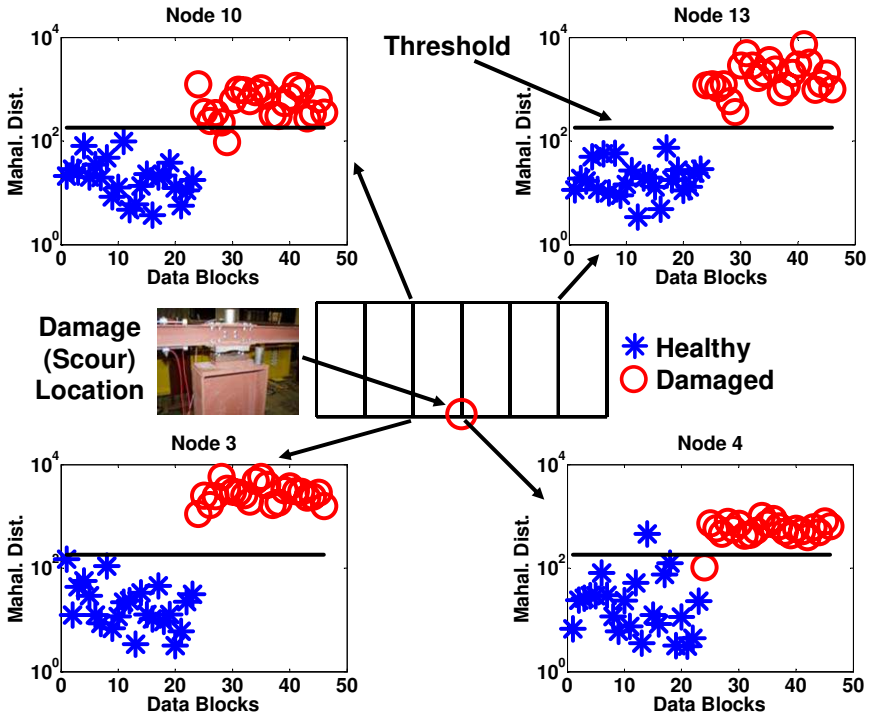

Figure 63. Mahalanobis distance plots for the Scour case

Damage Case 4 (DC4): Boundary restraint at N7 and N14

As for DC4 (Figure 64), the majority of the values are still above the threshold value; however, some false negatives are also observed. This is not an expected situation since as it was shown in the previous chapter; the configuration of the structure is changed considerably for DC4. It was previously shown that the damage was identified and located by using pseudo-flexibility.

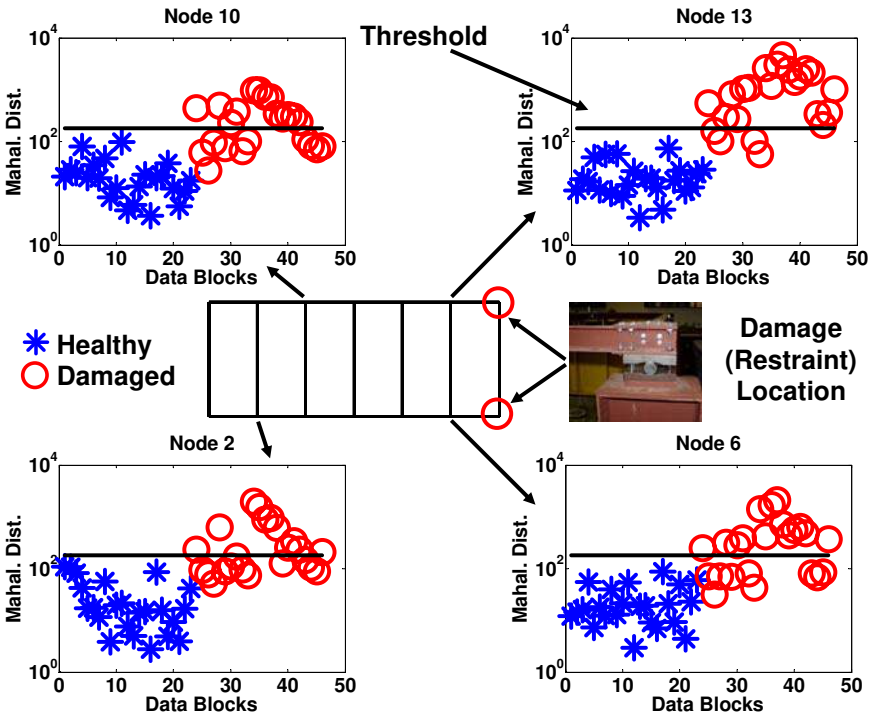

Figure 64. Mahalanobis distance plots for Restraint Supports case

3.4.3. Discussions on Experimental Studies

The results presented above sections show that the methodology is capable of detecting changes in the test structures for most of the cases. However, the methodology does not provide enough information to locate the damage. It should also be noted that there are a number of

issues to be solved before the methodology can be successfully applied to real life structures in an automated SHM system.

First, it was noted that determining the right threshold value is one of the important issues to solve. The threshold value depends on both the length of the feature vector and the number of the features in the vector. Therefore, a different threshold value might be obtained when a different model order is used since the AR model order determines the length of the feature vector. It was also noted that determining this threshold is not a trivial problem and it might require some trial and error process during the monitoring process. If the threshold is set too low, most of the healthy data can be identified as outliers, increasing the number of the false positives. On the contrary, if the threshold value is set too high, data coming from damaged structure can be classified as inliers. This is not a desired situation, either. Further investigation is needed for demonstration of the threshold value for an automated SHM application.

Second, determining the order of the AR model in an automated SHM system might be difficult. A high model number might be required for complex structures (and therefore a longer feature vector) and this can make it more difficult to identify the outliers because of 'the curse of the dimensionality'. For example, it is shown in this study that the model order p for the beam structure is three whereas it is ten for the grid structure suggesting that the model order number increases as the complexity of the structure increases. This number might be quite high for a real life structure such as a long span bridge.

Next, it is also seen from the results that for an automated SHM system it might be necessary to set certain rules about the number of outliers so that a decision can be made whether damage has occurred in the structure or not. For example, if a certain number of the new data

points are determined as outliers, then it might indicate a possible structural change and then further precautions can be taken. After determining that a structural change has occurred, more rigorous analyses can be conducted by using different methodologies to determine the location, severity, and the nature of the change.

Another issue is the effect of environmental and operational changes. It should be noted that using an AR model, a model of the signal rather than the structure itself is created. Therefore, the model might be affected by these exogenous outputs, and some discrepancies might be encountered in outlier detection process. However, the use of RD before constructing the AR models mitigates the effects caused by the ambient loading and allows creating more consistent models. For further verification of the methodology for environmental and operation effects, the methodology should be tested with experiments where these effects are also included. Ultimately, the methodology should be verified by using data coming from different real life structures.

3.5. Summary

In this chapter, a statistical pattern recognition methodology was investigated in the context of SHM by using different laboratory structures. AR modeling is used in conjunction with Mahalanobis distance-based outlier detection algorithm to identify the damage in the structures. RD method is used for data normalization (averaging) and AR models are fitted to the averaged data. The use of RD method enables elimination of the random loading effects on the structure and it makes it easier to fit the AR model to the data.

A simply supported steel beam and a complex steel grid structure are used for the laboratory experiments. A number of different tests are conducted by applying various damage scenarios to the structures. It is shown that different boundary conditions in the beam were identified successfully by using the methodology. Furthermore, comparative analyses showed that using RD for averaging improves the methodology and a better separation is obtained during the outlier detection process. The methodology gave successful results for the grid structure most of the time. However, it was also observed that the methodology did not perform as successful for some cases, such as the DC4.

CHAPTER 4. A NEW METHODOLOGY FOR IDENTIFICATION, LOCALIZATION AND QUANTIFICATION OF DAMAGE

4.1. Introduction

As it was mentioned in the previous chapter, one common approach to extract damage sensitive features (or damage features) from SHM data is to use *time series analysis.* Time series analysis employed as a non-parametric method (also known as data driven methods) has gained considerable attention recently since their implementation for an automated SHM system is relatively more feasible compared to other damage detection methodologies such as parametric (physics-based) or model updating. This analysis approach mainly fits time series models to the vibration data and then aim to detect the damage by extracting features such as curve fit coefficients or error terms. In other words, some of these methodologies directly compare the time series models whereas some of them use the residual errors when the new data is used with the previously created model. These methodologies usually make use of AR (Auto-Regressive) and ARX models (Auto-Regressive models with eXogenous outputs) to detect the damage in a statistical manner (Sohn et al. 2000; Sohn et al. 2001; Chang et al. 2003; Nair et al. 2006; Omenzetter and Brownjohn 2006; Zhang 2007; Zheng and Mita 2007; Carden and Brownjohn 2008; Gul and Catbas 2009). Although these methodologies are generally successful in identifying the presence of the damage (i.e. level 1 damage identification), most of them give limited information about the location and/or severity of the damage (i.e. level 2 and/or level 3 damage identification).

In addition to the studies discussed in the previous chapter, there are a few other studies which are related to the content of this chapter. Lu and Gao (2005) used a modified ARX model

for damage identification and localization. The acceleration response at one location was chosen as the input to their ARX model to predict the outputs at the other locations of the structure. In their study, an ARX model is created for the healthy structure. Then the same model is used to predict the outputs of the damaged structure. The residual error of the model reflects the structural change and the standard deviation of the residual error is selected as the damage sensitive feature. The researchers used two shear-type numerical spring mass models for verification of the methodology and showed that their approach was successful for identification and localization of the damage in those models for noise free data. In another study, a similar methodology was adapted by Monroig and Fujino (2006) where the researchers used a second order multivariate ARX models with data (with 1% additional noise) coming from simulations of a building model. They showed that the methodology was able to identify and locate the damage in the case of numerical study although there are some false-positive and false negative results.

Time series modeling has a great potential for damage detection applications. However, there is still a need for a reliable time series analysis methodology for three levels of damage detection. In this chapter, a robust and practical methodology is developed for identifying, locating, and quantifying the damage by using time series analysis. In order to achieve this goal, ARX models are created for different sensor clusters and different damage sensitive features are extracted from these models. These features are then used for identifying, locating and quantifying the damage.

4.2. Theoretical Background: Time Series Modeling for Structural Dynamics

The equation of motion for an N Degrees of Freedom (DOF) linear dynamic system can be written as in Eqn. (42).

$$M\ddot{x}(t) + C\dot{x}(t) + Kx(t) = f(t) \tag{42}$$

where $M \in \Re^{N\times N}$ is the mass matrix, $C \in \Re^{N\times N}$ is the damping matrix and $K \in \Re^{N\times N}$ is the stiffness matrix. The vectors $\ddot{x}(t), \dot{x}(t)$ and $x(t)$ are acceleration, velocity and displacement, respectively. The external forcing function on the system is denoted with $f(t)$. The same equation can be written in matrix form as shown in Eqn. (43) (t for time is omitted).

$$\begin{bmatrix} m_{11} & \cdots & m_{1N} \\ \vdots & \ddots & \vdots \\ m_{N1} & \cdots & m_{NN} \end{bmatrix} \begin{Bmatrix} \ddot{x}_1 \\ \vdots \\ \ddot{x}_N \end{Bmatrix} + \begin{bmatrix} c_{11} & \cdots & c_{1N} \\ \vdots & \ddots & \vdots \\ c_{N1} & \cdots & c_{NN} \end{bmatrix} \begin{Bmatrix} \dot{x}_1 \\ \vdots \\ \dot{x}_N \end{Bmatrix} + \begin{bmatrix} k_{11} & \cdots & k_{1N} \\ \vdots & \ddots & \vdots \\ k_{N1} & \cdots & k_{NN} \end{bmatrix} \begin{Bmatrix} x_1 \\ \vdots \\ x_N \end{Bmatrix} = \begin{Bmatrix} f_1 \\ \vdots \\ f_N \end{Bmatrix} \tag{43}$$

The equality in Eqn. (44) is obtained if the first row of Eqn. (43) is written separately. By rearranging Eqn. (44), it is seen in Eqn. (45) that the output of the 1st DOF can be written in terms of the excitation force on 1st DOF, the physical parameters of the structure, and the outputs of the other DOFs (including itself). Furthermore, in case of free response, the force term can be eliminated and the relation is written as shown by Eqn. (46).

$$\left(m_{11}\ddot{x}_1 + \cdots + m_{1N}\ddot{x}_N\right) + \left(c_{11}\dot{x}_1 + \cdots + c_{1N}\dot{x}_N\right) + \left(k_{11}x_1 + \cdots + k_{1N}x_N\right) = f_1 \tag{44}$$

$$\ddot{x}_1 = \frac{f_1 - \left(m_{12}\ddot{x}_2 + \cdots + m_{1N}\ddot{x}_N\right) - \left(c_{11}\dot{x}_1 + \cdots + c_{1N}\dot{x}_N\right) - \left(k_{11}x_1 + \cdots + k_{1N}x_N\right)}{m_{11}} \tag{45}$$

$$\ddot{x}_1 = -\frac{\left(m_{12}\ddot{x}_2 + \cdots + m_{1N}\ddot{x}_N\right) + \left(c_{11}\dot{x}_1 + \cdots + c_{1N}\dot{x}_N\right) + \left(k_{11}x_1 + \cdots + k_{1N}x_N\right)}{m_{11}} \tag{46}$$

It is seen from Eqn. (46) that if a model is created to predict the output of the first DOF by using the DOFs connected to it (neighbor DOFs); the change in this model can reveal important information about the change in the properties of that part of the system. Obviously, similar equalities can be written for each row of Eqn. (43) and different models can be created for each equation. Each row of Eqn. (43) can be considered as a sensor cluster with a reference DOF and its neighbor DOFs. The reference DOF for Eqn. (46), for example, is the first DOF and neighbor DOFs are the DOFs that are directly connected to the first DOF. Therefore, it is proposed that different linear time series models can be created to establish different models for each sensor cluster and changes in these models can point the existence, location and severity of the damage. The details of the methodology are explained in the following sections.

As explained in the previous chapter, a general form of a time series model can be written as in Eqn. (47) and an ARX model is shown in Eqn. (48).

$$A(q)y(t) = B(q)u(t) + D(q)e(t) \tag{47}$$

$$A(q)y(t) = B(q)u(t) + e(t) \tag{48}$$

The core of the methodology presented in this part is to create different ARX models for different sensor clusters and then extract damage sensitive features from these models to detect the damage. In these ARX models, the *y(t)* term is the acceleration response of the reference channel of a sensor cluster, the *u(t)* term is defined with the acceleration responses of all the DOFs in the same cluster while *e(t)* is the error term. Eqn. (49) shows an example ARX model to estimate the 1st DOF's output by using the other DOFs' outputs for a sensor cluster with *k* sensors.

$$A(q)\ddot{x}_1(t) = B(q)\left[\ddot{x}_1(t) \quad \ddot{x}_2(t) \quad \cdots \quad \ddot{x}_k(t)\right]^T + e(t) \tag{49}$$

To explain the methodology schematically, a simple 3-DOF model is used as an example. Figure 65 shows the first sensor cluster for the first reference channel. The cluster includes first and second DOFs since the reference channel is connected only to the second DOF. The input vector u of the ARX model contains the acceleration outputs of first and second DOFs. The output of the first DOF is used as the output of the ARX model as shown in the figure. When the second channel is the reference channel, Figure 66, the sensor cluster includes all three DOFs since they are all connected to the second DOF. The outputs of the first, second and third DOFs are used as the input to the ARX model and then the output of the second DOF is used as the output of this model. Likewise, for the reference channel three, Figure 67, the inputs to the ARX model are the output of the second and third channels and the output of the model is the third channel itself. The equations of the ARX models created for the example system are shown in Eqns. (50)-(52).

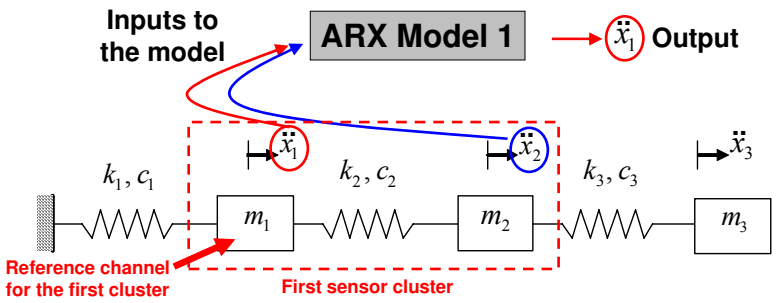

Figure 65. Creating different ARX models for each sensor cluster (first sensor cluster)

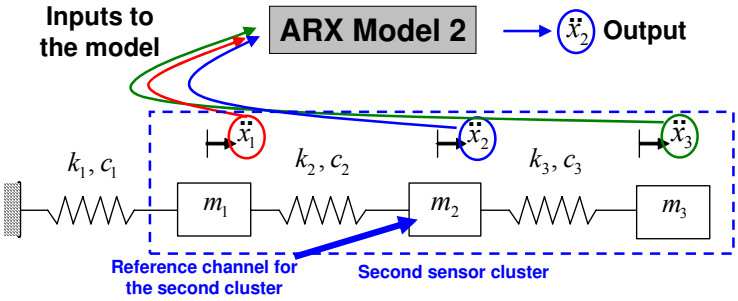

Figure 66. Creating different ARX models for each sensor cluster (second sensor cluster)

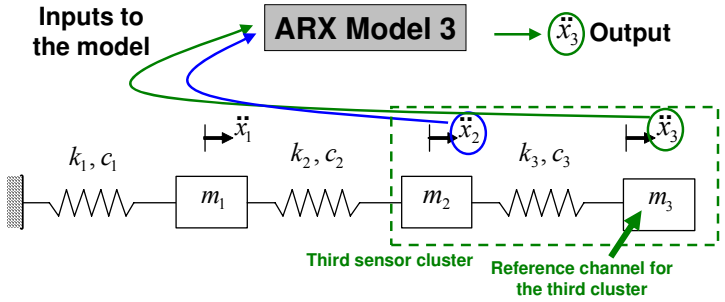

Figure 67. Creating different ARX models for each sensor cluster (third sensor cluster)

$$A_1(q)\ddot{x}_1(t) = B_1(q)\left[\ddot{x}_1(t) \quad \ddot{x}_2(t)\right]^T + e_1(t) \tag{50}$$

$$A_2(q)\ddot{x}_2(t) = B_2(q)\left[\ddot{x}_1(t) \quad \ddot{x}_2(t) \quad \ddot{x}_3(t)\right]^T + e_2(t) \tag{51}$$

$$A_3(q)\ddot{x}_3(t) = B_3(q)\left[\ddot{x}_2(t) \quad \ddot{x}_3(t)\right]^T + e_3(t) \tag{52}$$

After creating the ARX models for the baseline condition, two different approaches are presented for detecting damage. Approach I is based on the assumption that the comparison of the coefficients of the ARX models for each sensor cluster before and after damage (Figure 68) will give information about the existence, location and severity of the damage. For Approach II, the fit ratios of the baseline ARX model when used with new data is employed as a damage sensitive feature. The details about the two approaches are presented in the next sections.

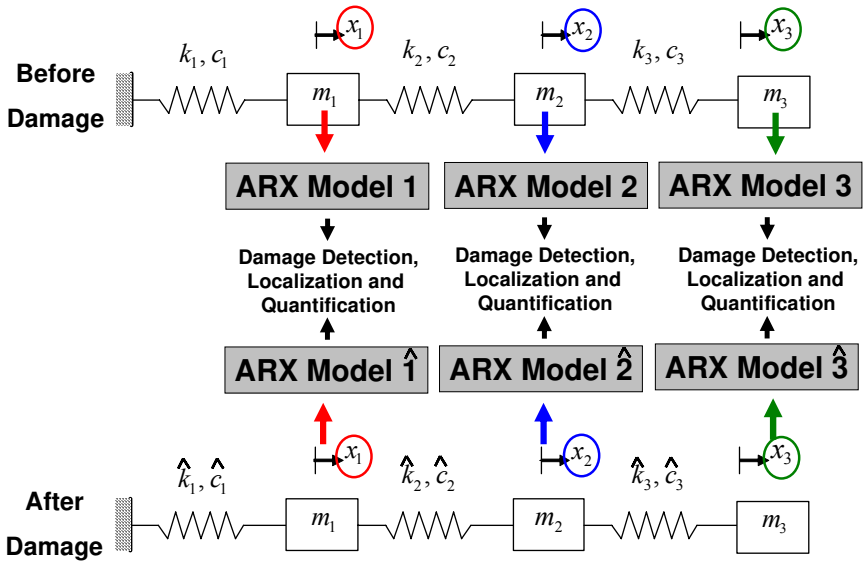

Figure 68. Comparing the ARX models for each reference channel to identify, locate and quantify the damage

4.3. Approach I: Ratio of the ARX model coefficients as the Damage Feature (DF)

As explained in the previous sections, two different approaches are used for comparison of the ARX models, i.e. two different Damage Features (DF) are extracted from these models. For Approach I, the "*B*" term coefficients of the ARX models are selected as the DF (Gul and Catbas 2008). It is shown that the change in these coefficients can be attributed directly to the stiffness change in the structure for simple and noise free models. This practical analysis gives exact identification, localization, and quantification and damage. However, it is also observed that when there is noise in the data, this approach will not perform satisfactorily and it needs to be modified.

4.3.1. Demonstration with a 4 DOF system

For verification of the Approach I, it is applied to a numerical 4 DOF system. The system

is shown in Figure 69 and its properties can be summarized as: $m_1 = 0.8$, $m_2 = 2$, $m_3 = 1.2$, $m_4 = 0.6$, $k_1 = 20$, $k_2 = 10$, $k_3 = 15$, $k_4 = 10$ and $k_5 = 25$. The damping matrix is defined as $C = 0.001 \times M + 0.0001 \times K$. The structural system being used in this study is very similar to the system that was used by Lus et al. (2003).

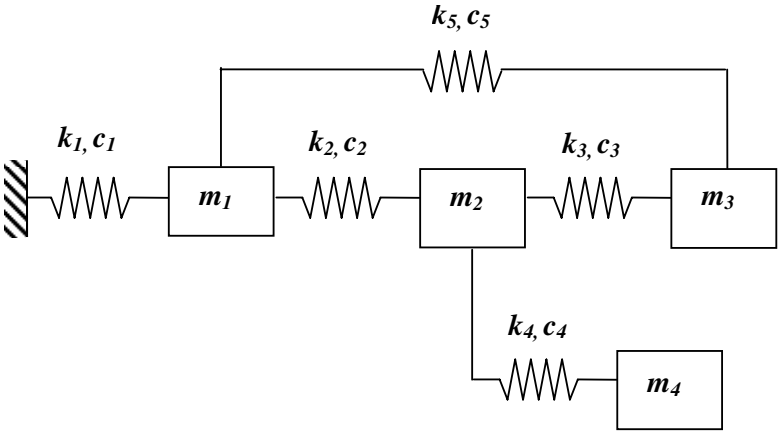

Figure 69. The numerical model to generate data from simulations (similar to the model used in Lus et al. (2003))

First, the free response (acceleration) of the healthy system is simulated. Then four ARX models are created for four sensor clusters for the baseline case. The models for each sensor cluster are given in Eqns. (53)-(56). The model orders for the ARX models are selected as n_a=1, n_b=2. Since it is a simple model without any noise in the data, these model orders are observed to be sufficient to obtain a very accurate model. Figure 70 shows the measured free response of the first DOF and the output of the ARX model for the first sensor cluster. It is seen that there is a perfect match meaning that the output of the first DOF can be estimated without any error by using the ARX model. The damage simulations and the results are discussed in the following sections.

$$A_1(q)\ddot{x}_1(t) = B_1(q)\left[\ddot{x}_1(t) \quad \ddot{x}_2(t) \quad \ddot{x}_3(t)\right]^T + e_1(t) \tag{53}$$

$$A_2(q)\ddot{x}_2(t) = B_2(q)\left[\ddot{x}_1(t) \quad \ddot{x}_2(t) \quad \ddot{x}_3(t) \quad \ddot{x}_4(t)\right]^T + e_2(t) \tag{54}$$

$$A_3(q)\ddot{x}_3(t) = B_3(q)\left[\ddot{x}_1(t) \quad \ddot{x}_2(t) \quad \ddot{x}_3(t)\right]^T + e_3(t) \tag{55}$$

$$A_4(q)\ddot{x}_4(t) = B_4(q)\left[\ddot{x}_2(t) \quad \ddot{x}_4(t)\right]^T + e_4(t) \tag{56}$$

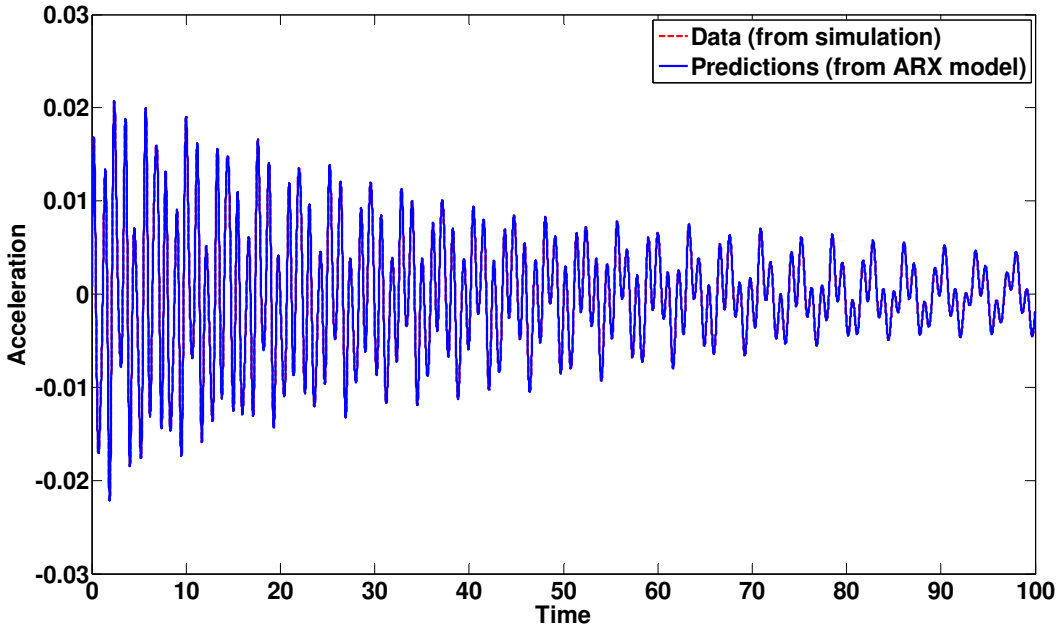

Figure 70. "Measured" vs. predicted output response of the 1st DOF

Case 1-1: 10% stiffness reduction at k_3 (k_3=13.5), noise free data

For this damage scenario, the stiffness coefficient of the spring between m_2 and m_3 is reduced by 10% (k_3=13.5). Then, four new ARX models are created as it was done for the baseline case. The model orders are kept same, i.e. n_a=1, n_b=2. The *B* term coefficients of each ARX model of the damaged structure are compared to the counterparts obtained with the baseline data. The results are summarized in Table 3.

Table 3. DF change (%) with respect to location when k_3=13.5 (10% stiffness loss between DOFs 2 and 3)

Measurement Location	DOF 1	DOF 2	DOF 3	DOF4
DOF 1	0.00	0.00	0.00	n/a
DOF 2	0.00	0.00	**-10.00**	0.00
DOF 3	0.01	**-10.00**	0.00	n/a
DOF4	n/a	0.00	n/a	0.00

The first row of the table shows the change in the mean of the *B* term coefficients (there are two *B* term coefficients since the n_b is 2) of the ARX model for the first sensor cluster. The 'n/a' in the fourth column of the first row indicates that fourth DOF is not included in the first sensor cluster. Looking at the table, it is observed that the DF between m_2 and m_3 has decreased whereas the other coefficients have remained constant. Moreover, it is seen that the decrease is 10% indicating the extent of the damage exactly. The results shown in the table clearly indicate that the methodology was successful for identifying, locating and quantifying the damage for the 4 DOF system. Finally, note that there are no false positives, i.e. there is no change in DF for other DOFs.

Case 1-2: Multiple damage at three locations, noise free data

Having showed that the proposed methodology was successfully applied to identify, locate and quantify the damage, a multi damage scenario is applied to the same model. Stiffness reductions at three different locations are applied simultaneously, i.e. k_2=9, k_3=12.75, k_4=9.5 (10%, 15% and 5% stiffness losses, respectively). It is seen in Table 4 that the DF between first

and second DOFs, first and third DOFs; and second and fourth DOFs have changed almost exactly as the applied damage ratios. Results indicate that the methodology was very successful for three levels of damage identification when there is multiple damage.

Table 4. DF change (%) with respect to location when k_2=9, k_3=12.75, k_4=9.5 (multiple damage with 10%, 15% and 5% stiffness losses)

Measurement Location	DOF 1	DOF 2	DOF 3	DOF4
DOF 1	0.00	**-9.97**	0.02	n/a
DOF 2	**-10.00**	0.01	**-15.00**	**-5.00**
DOF 3	0.00	**-14.99**	0.01	n/a
DOF4	n/a	**-5.00**	n/a	0.00

Case 1-3: 10% stiffness reduction in k_3 (k_3=13.5), with 5% noise

Although very successful results have been obtained with noise free data, Approach I is not successful in identifying the damage when noise is present in the data. To show this handicap, Case 1-1 is now repeated with 5% artificial white noise added to the data. Table 5 shows that the DF changes do not give meaningful information about the damage, its location or severity.

The findings presented in Table 5 do not improve by increasing the model order number although a better fit to the data is obtained. The results obtained by Approach I for noisy data might be caused by the fact that linear regression solution assumes that the data in the Y and X

matrix in Eqn. (38) are noise-free. Other techniques for the numerical solution may further be explored to obtain better results but it is not pursued in this study since Approach II, which will be discussed later, provided very satisfactory results. Another disadvantage of Approach I is that it does not work properly for complex models. Considering these shortcomings, it is clear that the methodology will have limitations in real life applications. Therefore, Approach I is improved in the next section to consider the effect of noise and model complexity. The modified approach is referred as Approach II and is discussed in the next sections.

Table 5. DF change (%) with respect to location when k_3=13.5 (10% stiffness loss) with 5% noise added to the simulation data

Measurement Location	DOF 1	DOF 2	DOF 3	DOF4
DOF 1	65.94	952.78	195.45	n/a
DOF 2	-4.37	-15.10	-159.51	-671.44
DOF 3	-57.04	-27.13	-21.27	n/a
DOF4	n/a	60.02	n/a	-9.21

4.4. Approach II: Fit ratio of the data as the Damage Feature (DF)

For this approach, the first step of the methodology remains same, i.e. ARX models are created for each sensor cluster for the baseline case. Then these models are used to predict the output of the damaged structure for the same sensor clusters. The difference between the fit ratios of the models is used as the DF (Gul and Catbas 2009). The Fit Ratio (FR) of an ARX model is calculated as given in Eqn. (57).

$$Fit\ Ratio\,(FR) = \left(1 - \frac{\|\{y\} - \{\hat{y}\}\|}{\|\{y\} - \{\bar{y}\}\|}\right) \times 100 \tag{57}$$

where $\{y\}$ is the measured output, $\{\hat{y}\}$ is the predicted output, $\{\bar{y}\}$ is the mean of $\{y\}$ and $\|\{y\} - \{\hat{y}\}\|$ is the norm of $\{y\} - \{\hat{y}\}$. The DF is calculated by using the difference between the FRs for healthy and damaged cases as given in Eqn. (58).

$$Damage\ Feature\,(DF) = \frac{FR_{healthy} - FR_{damaged}}{FR_{healthy}} \times 100 \tag{58}$$

4.4.1. Demonstration with a 4 DOF system

The second approach is demonstrated with the same numerical model used in the previous section. Different cases are created to show that Approach II is successful at identifying, locating and quantifying the damage for noisy cases. The cases are explained below.

Determining the threshold

Before damage identification with noisy data, the threshold for the DF under noisy conditions should be established so that the change in the DF due to the noise can be separated from the change due to damage. To define the threshold level, a method similar to one used in the previous chapter is adapted. For this case, 10% random noise is added to two healthy data sets separately. There is no additional damage applied to the structure. Then the change in the DF is computed. This process is repeated 1000 times independently to create a statistically meaningful threshold level. To create a 99.9% confidence level for the threshold, the 999th highest DF is selected as threshold.

By calculating this threshold, we ensure that not every change in the DF is attributed to damage. If the change in DF is under the threshold level, this change could have been caused by noise in the data or by the damage. The results for the threshold are shown in Figure 71. It is observed that the threshold values for each DOF are very close to each other and it is around 0.5. Although the threshold is different for each channel, the highest one (0.5239) will be used as the threshold of each channel for the sake of simplicity.

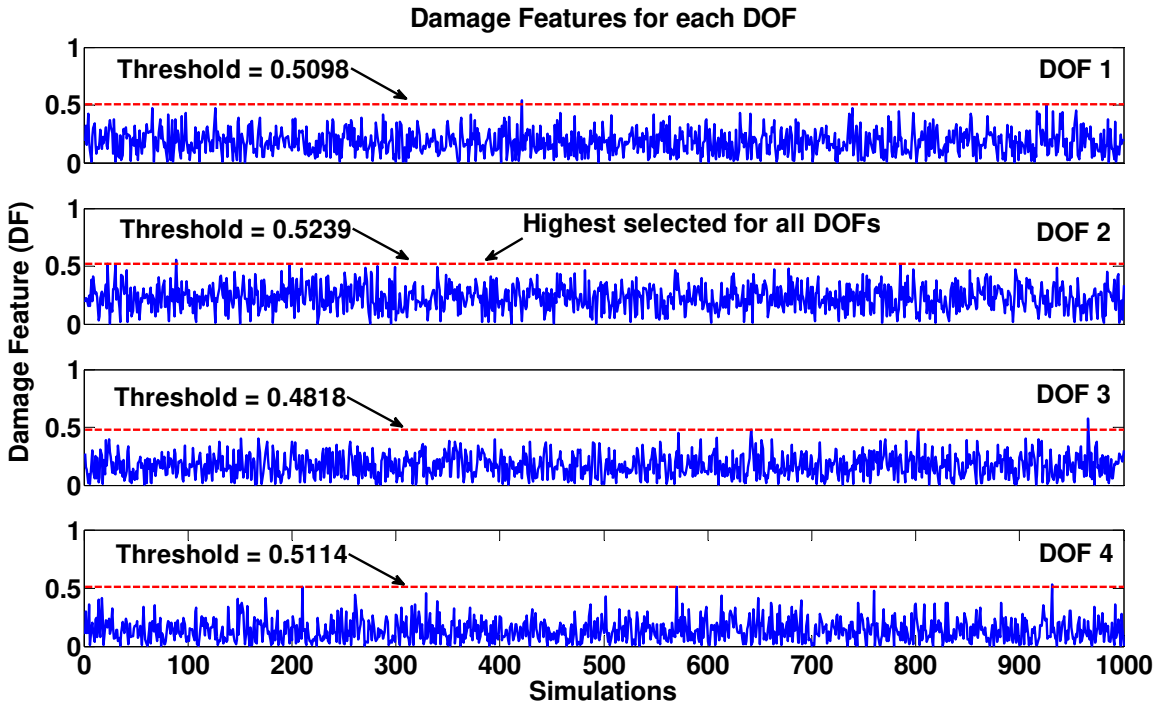

Figure 71. Thresholds for each DOF

Case 2-1: 10% stiffness loss in k_3 (k_3=13.5), with 10% noise

After setting up the threshold value, damage simulations are conducted. For this case, the stiffness value of the spring between m_2 and m_3 is decreased by 10% as in Case 1-1. In addition, 10% random white noise is added to the data. Then the DFs are calculated for each DOF by

using Approach II. This process is repeated independently 100 times. Figure 72 shows that the highest DF values are obtained for DOF 3 and it is considerably higher than the threshold value. Moreover, DFs for DOF2 are higher than the threshold value (except five points out 100). Finally, the DFs for DOF1 and DOF4 are under the threshold value for all the simulations. These results clearly show that there is a structural change and it is occurred close to DOF 2 and DOF 3. This is consistent with the applied damage where the stiffness value between m_2 and m_3 is decreased by 10%. The change in the DF for DOF 3 is higher than DOF 2 because DOF 3 is connected to two other DOFs and a change in one of those connections affects it more compared to DOF 2, which is connected to three DOFs. From this case, it is observed that damage is identified and located successfully for noisy data.

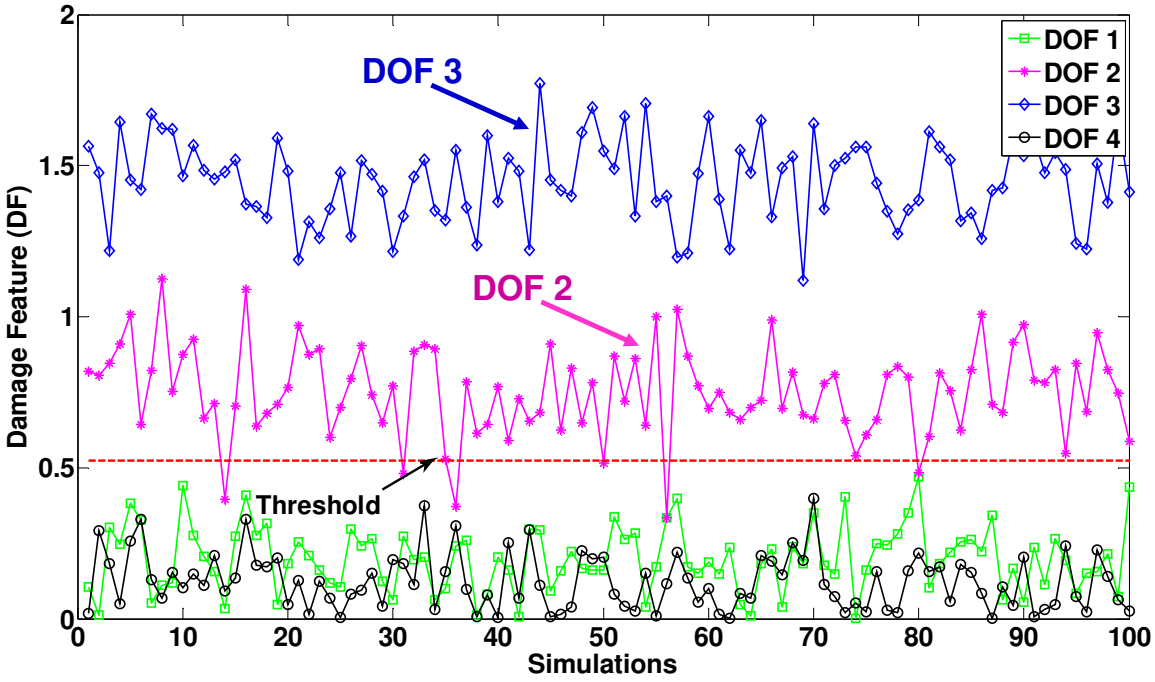

Figure 72. DFs for Case 2-1

Case 2-2: 20% stiffness loss in k_3 (k_3=12), with 10% noise

After showing that damage can be identified and located with noisy data by using Approach II, the stiffness reduction is doubled to see if the severity of the damage can be determined by using the second approach. In this case, the stiffness coefficient between m_2 and m_3 is decreased 20%. Comparing Figure 72 and Figure 73, the DFs for DOF 2 and DOF 3 increased almost 2-3 times, which is consistent with the increase in the damage induced to the structure. It is observed that, in addition to existence and location, the severity of the damage can be observed by using Approach II. Also note that, increasing the damage between DOF 2 and DOF 3 did not increase the DFs for DOF 1 and DOF 4 and they are still under the threshold.

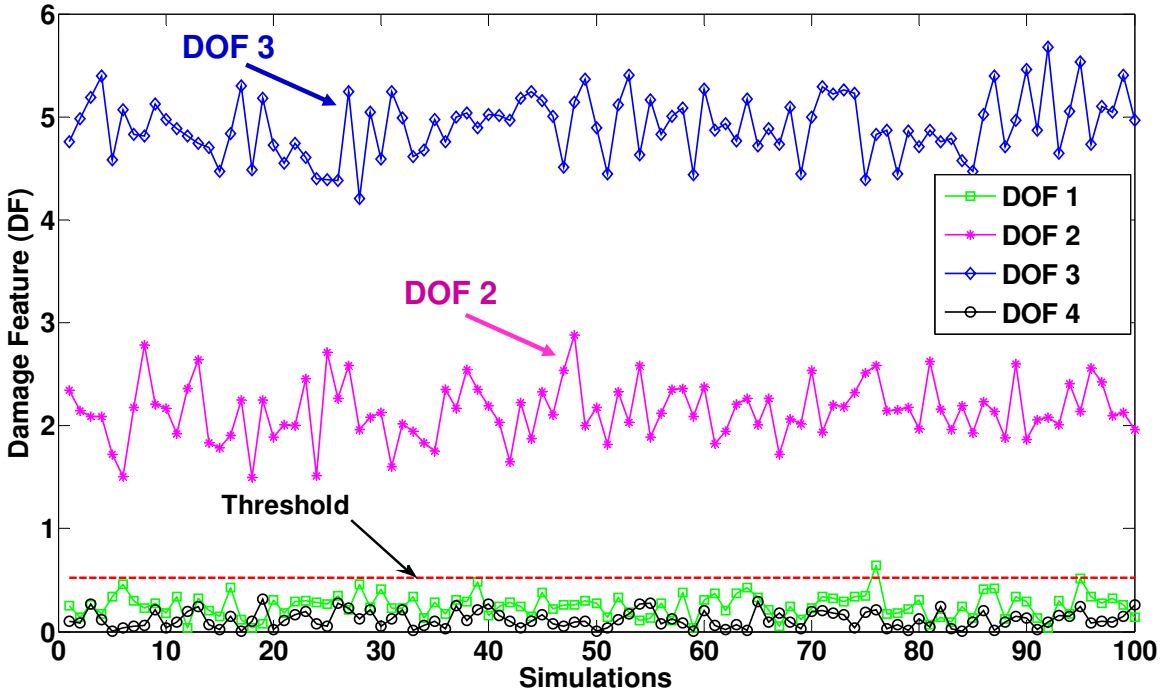

Figure 73. DFs for Case 2-2

Case 2-3: Multiple damage case, with 10% noise

This is the final case for the 4 DOF system where multiple stiffness reductions are applied to the structure simultaneously to investigate the capability of the methodology to identify multiple damage cases using noisy data. For this case, a 40% stiffness reduction is applied to k_1 (k_1=12) and 20% stiffness reduction is applied to k_3 (k_3=12) at the same time where the noise ratio is 10%. It is clearly apparent from Figure 74 that the severe damage at the first DOF is identified and located successfully. Furthermore, the DFs for DOFs 2 and DOF 3 are at about the same level with the ones shown in Figure 73. Also, note that the DFs for DOF 1 are almost two times as DFs for DOF 3 showing that the severity of the damage is determined successfully, too. Finally, it is observed from the figure that DFs for DOF 4 are still under the threshold and very close to zero giving no false positives about DOF 4.

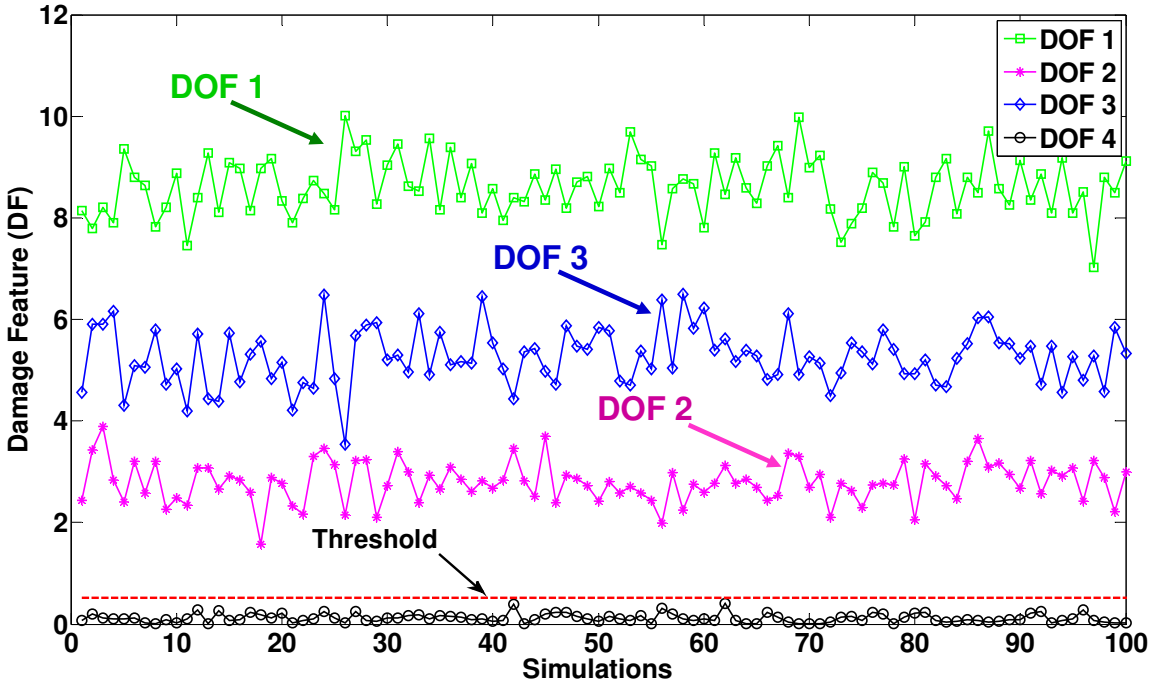

Figure 74. DFs for each DOF for Case 2-3

4.4.2. Application of the Methodology to Numerical Benchmark Data

After showing that Approach II is successfully used to identify the damage induced to the 4 DOF numerical model, its capability with a more complex model is investigated. For this part of the study, the numerical model of the first phase of a Bridge Health Monitoring Benchmark Problem (Catbas et al. 2006) was used.

The numerical benchmark problem was prepared by using a detailed Finite Element (FE) model of the test specimen. The FE model consists of 181 elements, 176 nodes, and 1056 degrees of freedom. A number of different damage cases with different levels can be simulated with the model such as reduced stiffness at connections, boundary condition change and scour. The damage cases simulated with the numerical model are slightly different from the experimental cases discussed in the previous sections. However, similar cases are selected for the numerical studies to be able to make better comparisons. Different types of sensors, such as accelerometers, strain gages and displacement gages, can be placed on the model to collect static and dynamic data under various loading conditions, e.g. static, impact, random, and traffic loading. Caicedo et al. (2007) discusses more details about the numerical model and benchmark study. The user interface of the benchmark program can be seen in Figure 75.

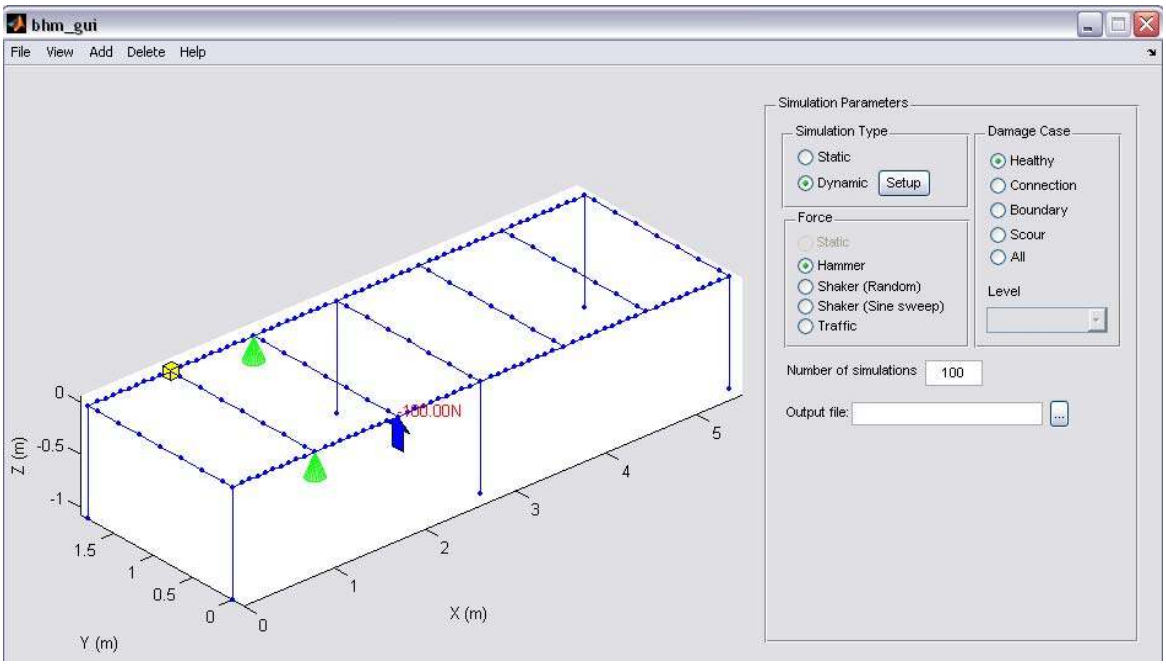

Figure 75. The user interface of the benchmark program

Eight accelerometers are placed on the model to collect the vertical acceleration at all of the corner nodes except supports (N2, N3, N5, N6, N9, N10, N12, and N13 in Figure 76). The free response data was obtained from the impact test simulations. The accelerations of the support nodes are not included in the model since they were practically zero and this created instability in the ARX models. Eight different sensor clusters were created for each reference channel and these clusters are shown in Table 6. The inputs and outputs of the ARX models for each sensor cluster are also shown in the table.

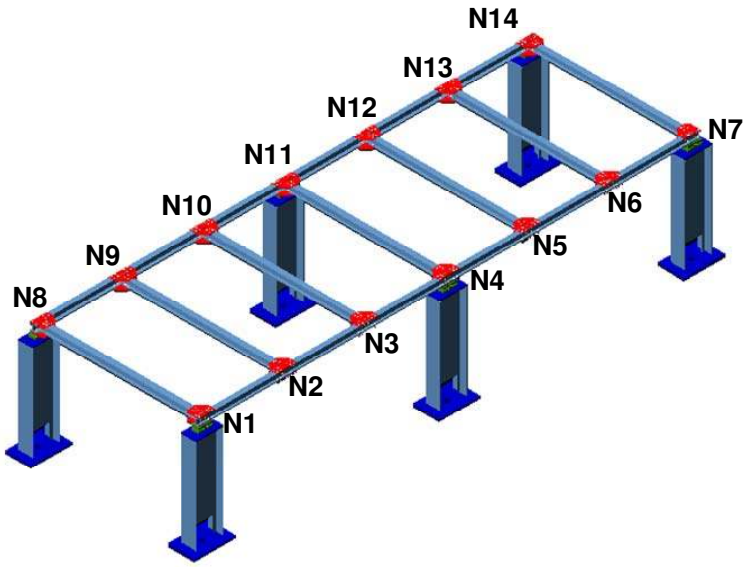

Figure 76. Node numbers for the numerical benchmark problem

Table 6. The inputs and outputs of the ARX models created for the benchmark problem

Sensor Cluster	Output of the ARX Model (Reference Channel)	Inputs of the ARX Model
1	N2	N2, N9, N3
2	N3	N2, N3, N10, N5
3	N5	N3, N5, N12, N6
4	N6	N5, N6, N13
5	N9	N9, N2, N10
6	N10	N9, N10, N3, N12
7	N12	N10, N12, N5, N13
8	N13	N12, N13, N6

Determining the Threshold

The threshold for the benchmark problem is also calculated as explained in the previous sections. One thousand independent simulations were carried out with 10% noise added to data and the 999th highest DF is selected as the threshold with a confidence level of 99.9%. The threshold value for each node is very close yet different from each other and it is about 0.7. The threshold is set to the highest value (0.7108) as shown in Figure 77.

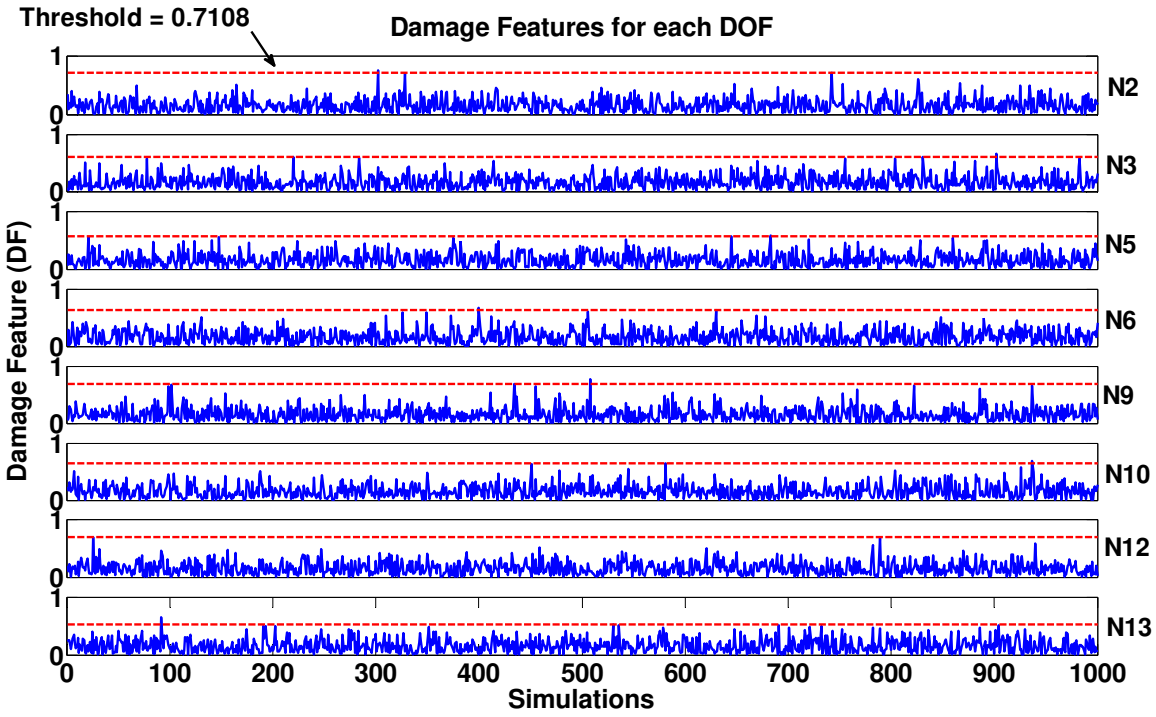

Figure 77. Threshold for the Benchmark Problem

Case 3-1: Moment release at N3, with 10% noise

For this damage scenario, the moment connection of the transverse member at N3 is released. In real life, this damage case corresponds to slight local stiffness loss due to loosening or removing the bolts at one connection. Then the DFs are calculated by using the ARX models

for each sensor cluster. The results are shown in Figure 78. It is seen from the figure that almost all the DFs are under the preset threshold value. This result is rather reasonable since removing just eight bolts in a highly redundant structure does not impact the operational response of the structure, thus does not create significant difference in the data especially when there is 10% artificial noise.

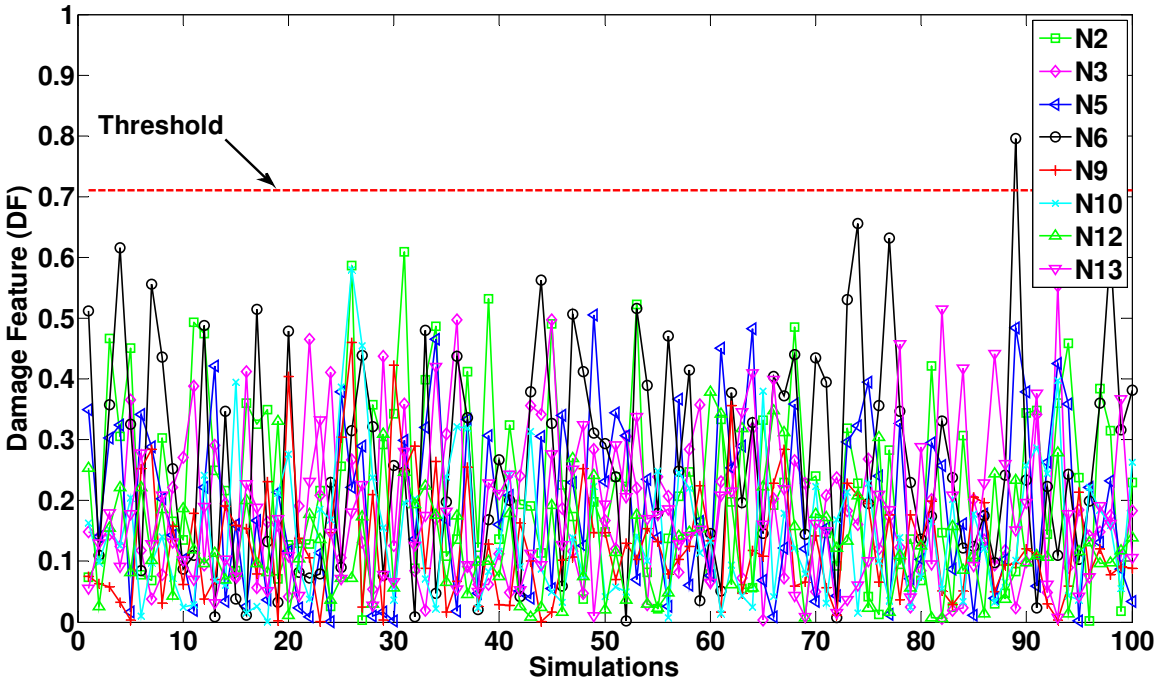

Figure 78. DFs for Case 3-1

Case 3-2: Moment release and plate removal at N3, with 10% noise

This case may be considered as a more severe version of Case 3-1 because the gusset plate at node N3 is removed in addition to the bolts. This case is the numerical version of the experimental DC2 discussed in the previous chapters. The DFs for this case are calculated and plotted in Figure 79. It is observed that DFs coming from N3, N2, N10 and N5 are higher than the threshold indicating there is a change in the structure around these nodes. Since the DFs for

N3 are considerably higher than the other ones, it can be concluded that damage has occurred very close to this node. Also, note that the DFs for N2 are well above the threshold, too. The DFs for N5 and N10 are also above the threshold. This is because these three nodes are the neighbor nodes of N3 (i.e. they are in the same sensor cluster) and removing the gusset plate at N3 affects the stiffness between N2 and N3, N3 and N5; and finally N3 and N10. The highest effect is seen between N2 and N3 since they are on the main girder. Finally, note that the DFs for the other nodes are under the threshold level. Hence, it is evidenced that the methodology is successful at detecting and locating the damage in the benchmark problem for this case.

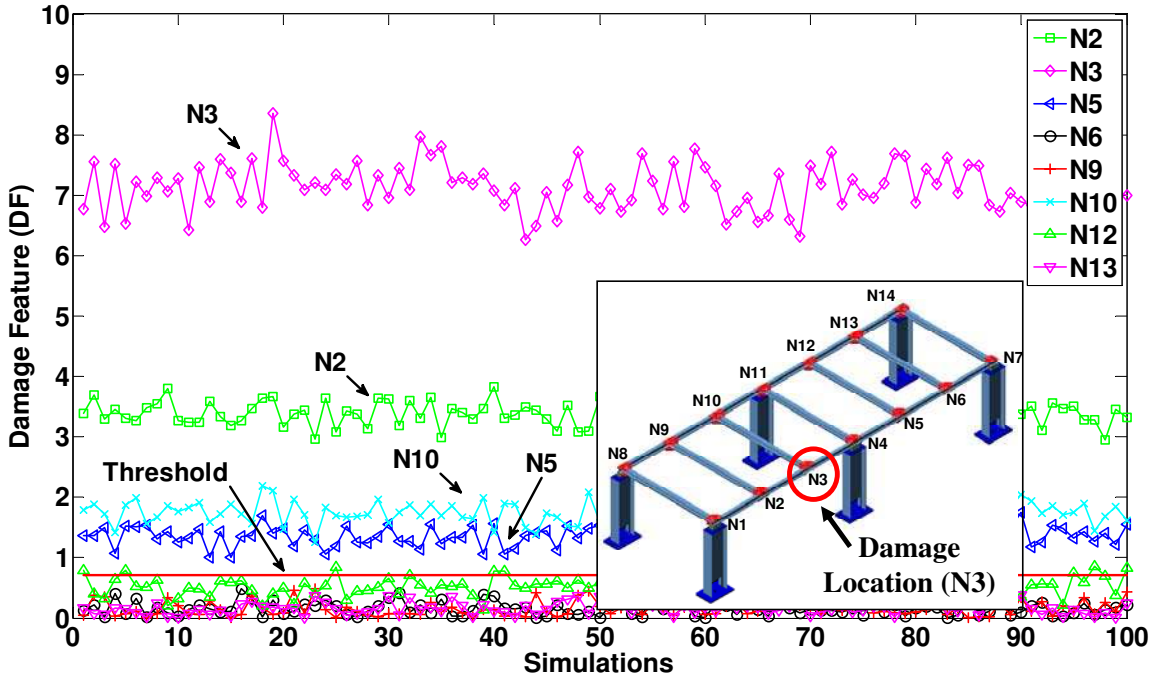

Figure 79. DFs for Case 3-2

Case 3-3: Moment Release and plate removal atN3 and N10, with 10% noise

For this damage case, the bolts and gusset plates at nodes N3 and N10 are removed at the same time. As shown in Figure 80, similar results to the previous case are obtained. However,

this time it is seen that the DFs for N10 have gone up to the same level as N3 since the gusset plate at that node is also removed. Furthermore, the DFs for N9 are now also higher than the threshold since removing the gusset plate at N10 creates a stiffness loss between N9 and N10. Another difference is that for this case the DFs for N5 are not above the threshold since the damage is now more symmetrical, the effect of the stiffness reduction at N5 is not as obvious as the previous case. This is also partly because there is a support between N3 and N5.

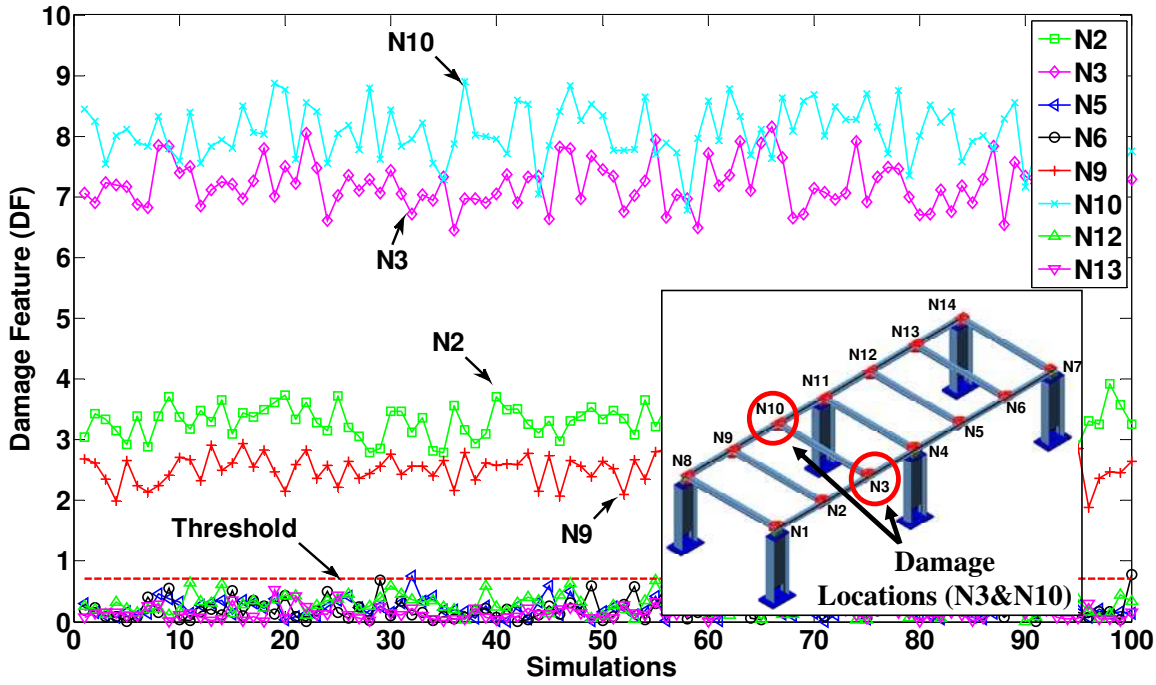

Figure 80. DFs for Case 3-3

Case 3-4: Boundary restraint at N7, with 10% noise

This damage scenario is simulated in the model by removing the moment release at node N7, i.e. making it a fixed support. This damage case is created to simulate some unintended rigidity at a support caused by different reasons such as corrosion or frozen bearings. Figure 81 shows that the DFs for all nodes are now above the threshold. DFs for N6 and N5 have increased

dramatically showing that damage is very close to N6 and N5 (note that data from the support nodes including N7 was not used in the models). DFs for the other nodes are considerably less than these two nodes but higher than the threshold value since the boundary condition change affects the structure as a whole.

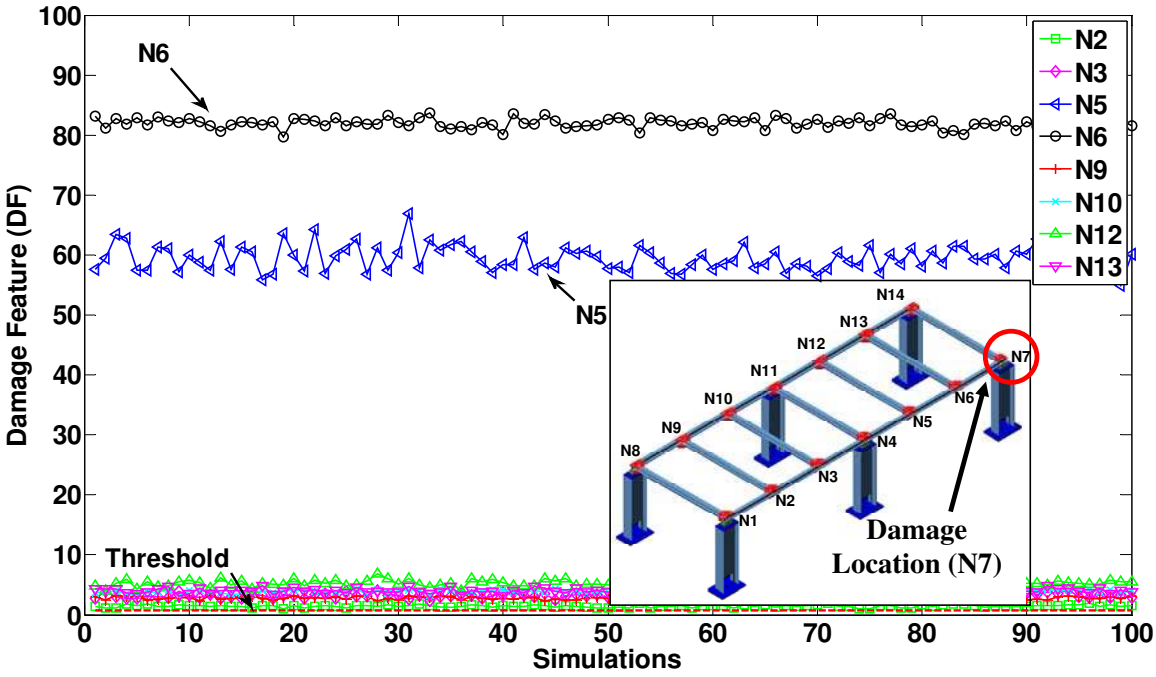

Figure 81. DFs for Case 3-4

Case 3-5: Boundary restraint at N7 and N14, with 10% noise

This case can be considered as the numerical version of the experimental DC4. It should be re-emphasized here again that the data coming from N7 and N14 are not used in the ARX models since they were practically zero. Figure 82 shows that the DFs for N6 and N13 are very close to each other because they are the closest nodes to the damage location (N7 and N14). Another observation is that the DFs for N5 and N12 are also very high because they are in the same span with the changed boundary condition. Finally, the nodes in the other span (N2, N3,

N9 and N10) are also above threshold since they are affected by the boundary condition change however they are considerably less than the other nodes. The log scale plot in Figure 83 illustrates the DFs for N2, N3, N9 and N10 better, where it is clearly observed that N2 and N9 have the smallest DFs since they are the furthest away nodes from the damaged nodes.

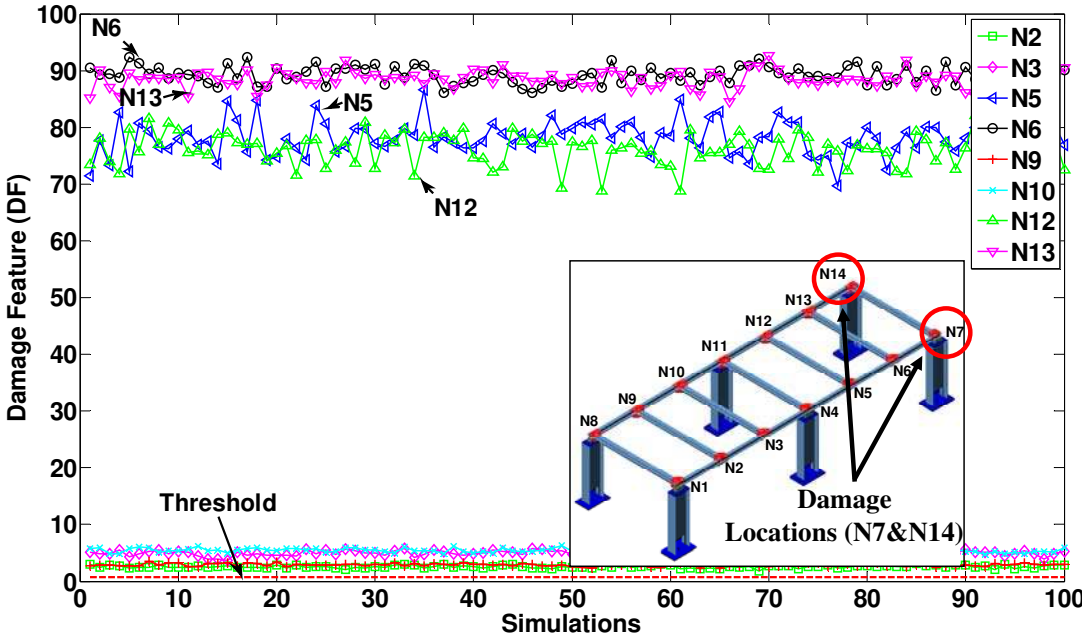

Figure 82. DFs for Case 3-5 (linear scale to show the general view of the DFs)

4.5. Application of the New Methodology to Experimental Data

After showing that the methodology is successfully applied to different numerical models for damage detection, its capability for damage detection with experimental data is investigated. In this part, the experimental data, which was used in the previous two chapters, is used. The results are explained in the following sections. The model orders ARX models are determined as n_a=1, n_b=10. The numerical threshold calculated in the numerical case is used for the experimental data. The validity of the numerical threshold was shown previously.

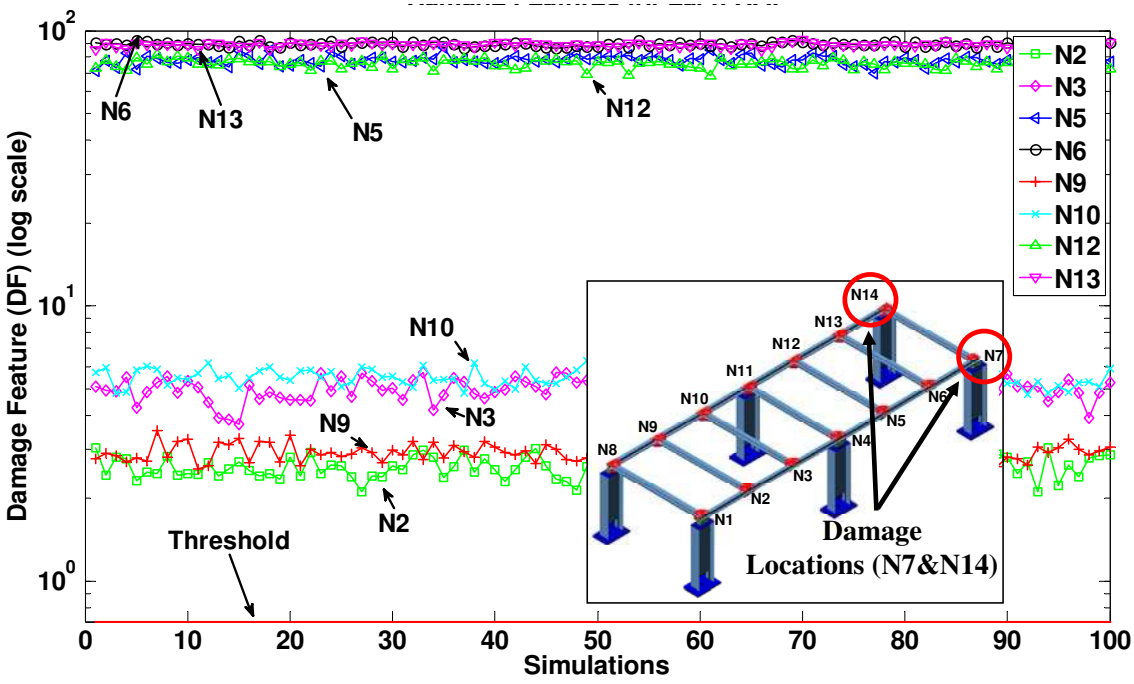

Figure 83. DFs for Case 3-5 (log scale to show the details)

4.5.1. Analysis Results of the Experimental Free Response Data

For this part, the free responses that are obtained from the impact tests are used. The first 100 points (out of 4096 data points), which covers the duration of the impulse, of each data set is removed so that the impact data can be treated as free responses. Five impact data sets were used for each case.

Damage Case 1 (DC1): Moment release at N3 and N10

The DFs for DC1 is plotted in Figure 84. It is seen from the figure that the DFs for N9, N10 and N3 are higher than the other nodes. This information is showing us that some changes have happened around these nodes. This indeed is the case since the bolts connecting the transverse member to N3 and N10 are removed, which is affecting these nodes. The effects should also be seen on N2 and N9 since these are the closest neighbor nodes. Furthermore, a

slight change in the DFs of N5 and N12 is also expected since these nodes are also neighbor nodes to N3 and N10. The effect on N9 is clearly apparent from the figure however, the effect on N2 is not observed. Furthermore, the DFs for N12 are higher than the threshold and other nodes. The effect is seen to a lesser extent because there is the support between N10 and N12. One point that should be noted that the DFs for N2 and N5 are not higher than the other nodes although they are expected to be. However, if the curvature plots for the same case in the second chapter is investigated again (Figure 26), it can be seen that the curvature change at N3 is around 3% whereas the change is around 13% for N10. Therefore, it can be commented that the experimental damage applied at N3&N10 did not create the same effect on both nodes. The results obtained with different methodologies consistently show the difference at these nodes.

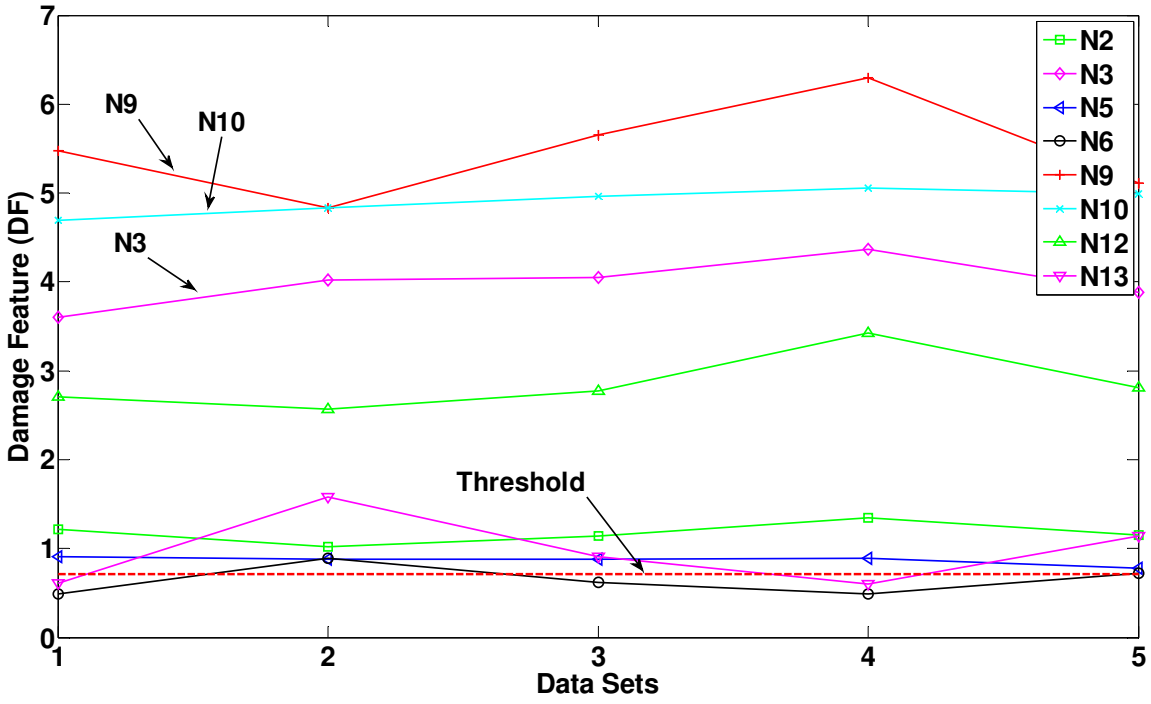

Figure 84. DFs for DC1 using free response data

Damage Case 2 (DC2): Moment release and plate removal at N3

For DC2, Figure 85 shows that the DFs for N3 are considerably higher than the threshold and other nodes. This fact is due to the plate removal at this node. It is also observed from the figure that the DFs for N2 are also relatively high since N2 is the closest neighbor of N3. Finally the secondary effect of the damage on N5 and N10 is also seen. Therefore, the methodology was very successful at detecting and locating the damage for this experimental damage case. Another note is that since the DFs for N3 considerably higher than the ones presented in Figure 84, it can be concluded that a more severe damage has occurred. This is actually the case, since the removal of the plate and bolts at N3 has a bigger effect on the structure than just removing the bolts. Finally note that the DFs for other nodes are around the threshold showing us that these nodes are not affected significantly from the localized damage.

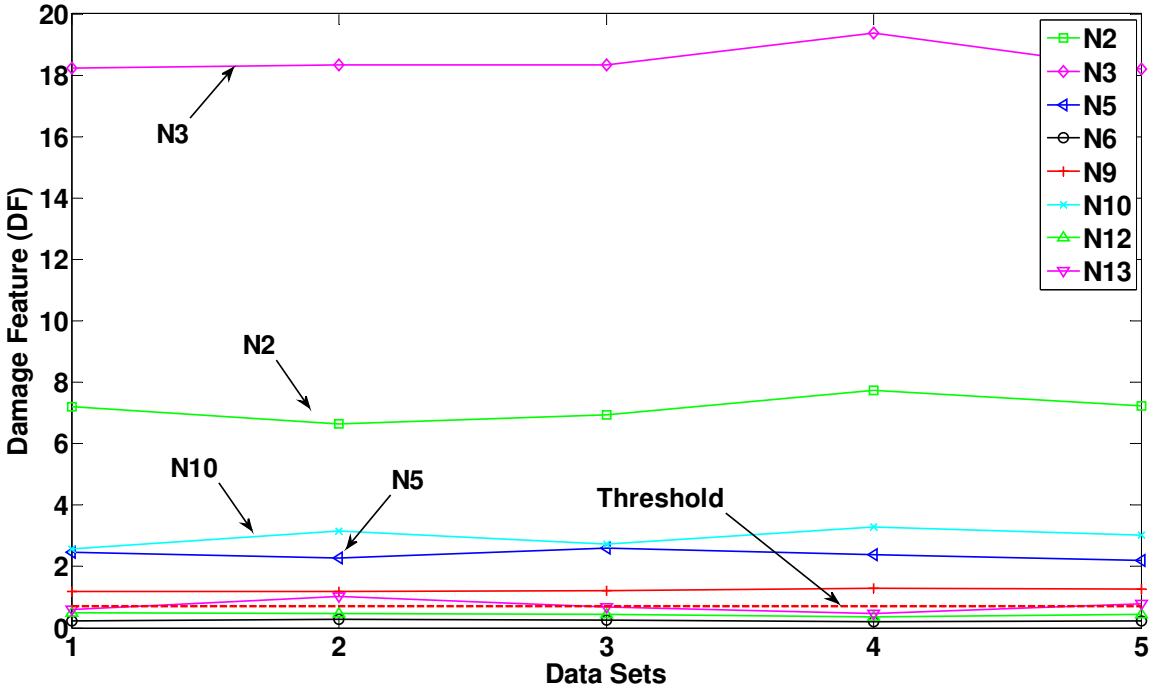

Figure 85. DFs for DC2 using free response data

Damage Case 3 (DC3): Scour at N4

Looking at Figure 86, it is apparent that a very important structural change has occurred close to N3 and N5. Note that the DFs for these two nodes are around 100. This is because the roller support at N4 was removed and this caused the DFs for the two neighbor nodes to increase significantly (remember that the data from the support nodes are not used in the analysis). The secondary effects of the damage on N2 and N6 are also clearly seen since these nodes are on the same girder where the support was removed. Also note that the DFs for other nodes are also higher than the threshold since the support removal changes the global condition of the structure rather than being a localized damage case like DC1 and DC2.

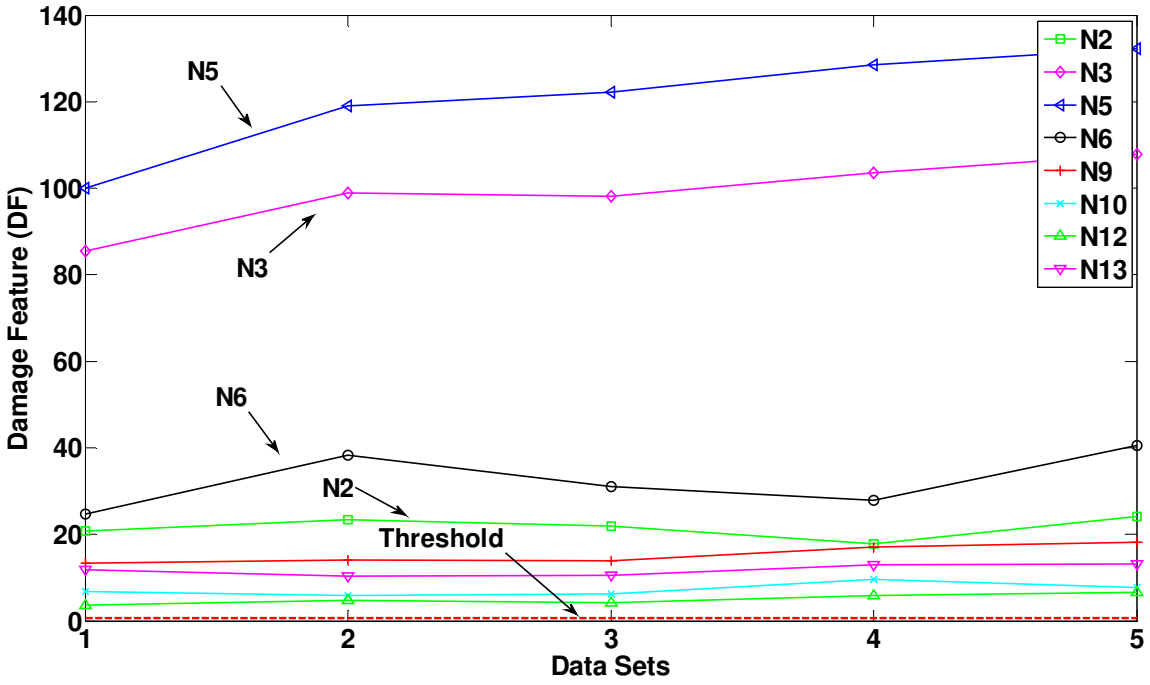

Figure 86. DFs for DC3 using free response data

Damage Case 4 (DC4): Boundary restraint at N7 and N14

The results for the final damage case, DC4, are presented in Figure 87. It is seen that the DFs for N6 and N13 are considerably higher than the other nodes. This is because of the fact that they are the closest nodes to the restrained supports (N7 and N14). The DFs for N5 and N12 are also high since they are also affected by the damage. The DFs for the remaining nodes are also slightly higher than the threshold since the structure is changed globally for DC4. Finally, note that the DFs for N6 and N13 are around 40 which shows that the damage is less severe than DC3 but more severe than DC1 and DC2. This information is also consistent with the damage cases.

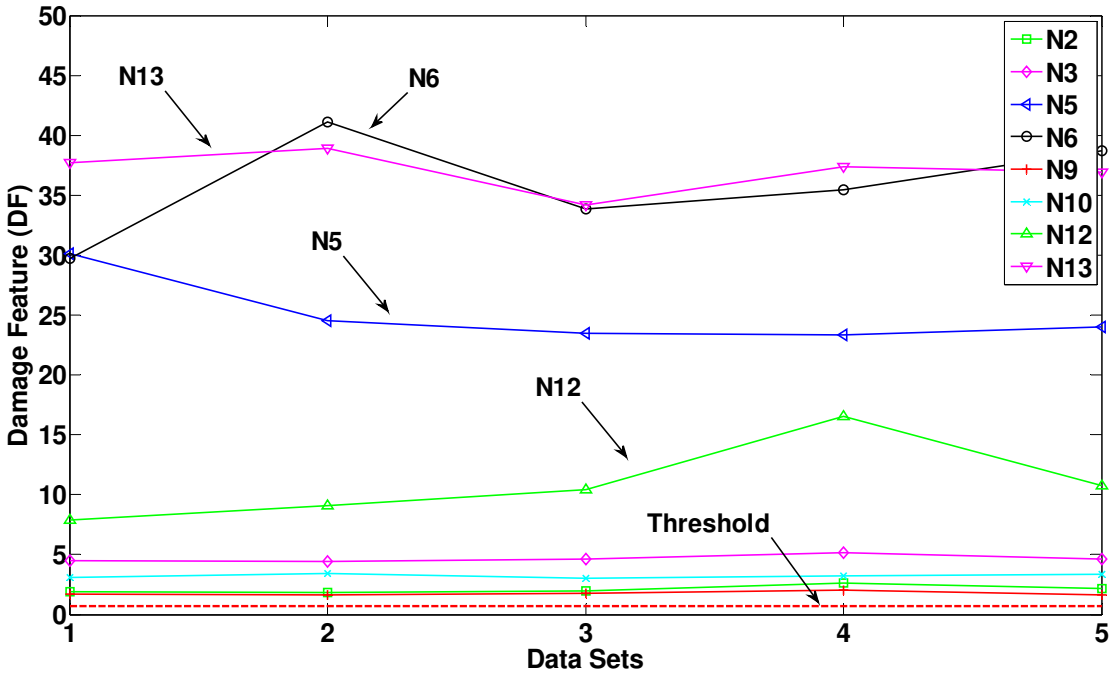

Figure 87. DFs for DC4 using free response data

4.5.2. Analysis Results of the Experimental Ambient Vibration Data

In this part, the methodology is used in conjunction with RD method for damage detection with ambient data. As discussed in previous sections, RD is used to obtain the pseudo-

free responses from the ambient data. After obtaining these pseudo-free responses, the methodology is applied for damage detection. The 5 min long ambient data sets for each case are divided into 5 data blocks and then RD is applied to average the data. The number of point used for RD is 4096. The model orders for the ARX models are same as the previous section (i.e. n_a=1, n_b=10). The results are presented in the following figures.

Damage Case 1 (DC1): Moment release at N3 and N10

The DFs for DC1 obtained by using ambient vibration data are presented in Figure 88. It is observed that the damage is not clearly apparent from the figure. However, it is also noted that the DFs for N3 and N10 (the damaged nodes) are higher than the other nodes in average. It should be reminded at this point that this damage case was not clearly identified by using other methodologies in the previous chapters (Figure 40 and Figure 61) when the ambient vibration data was employed. Comparing the three methodologies, it can be seen that the new methodology performed better than the other two.

Damage Case 2 (DC2): Moment release and plate removal at N3

The DFs for DC2 obtained with ambient vibration data are presented in Figure 89. It is seen that there is a clear sign showing that there has been a change at N3 (where the plate was removed). Also, note that the DF values are in good agreement with the free response case (Figure 85). Therefore, it can be commented that the damage for DC2 is successfully identified and located by using ambient vibration data with the new methodology.

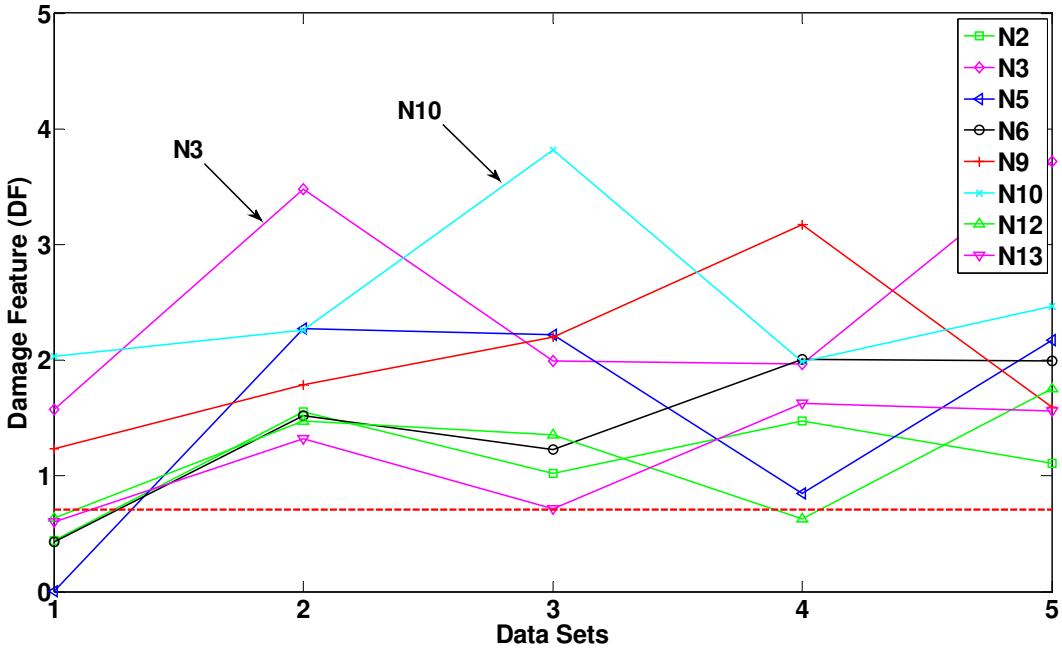

Figure 88. DFs for DC1 using ambient data

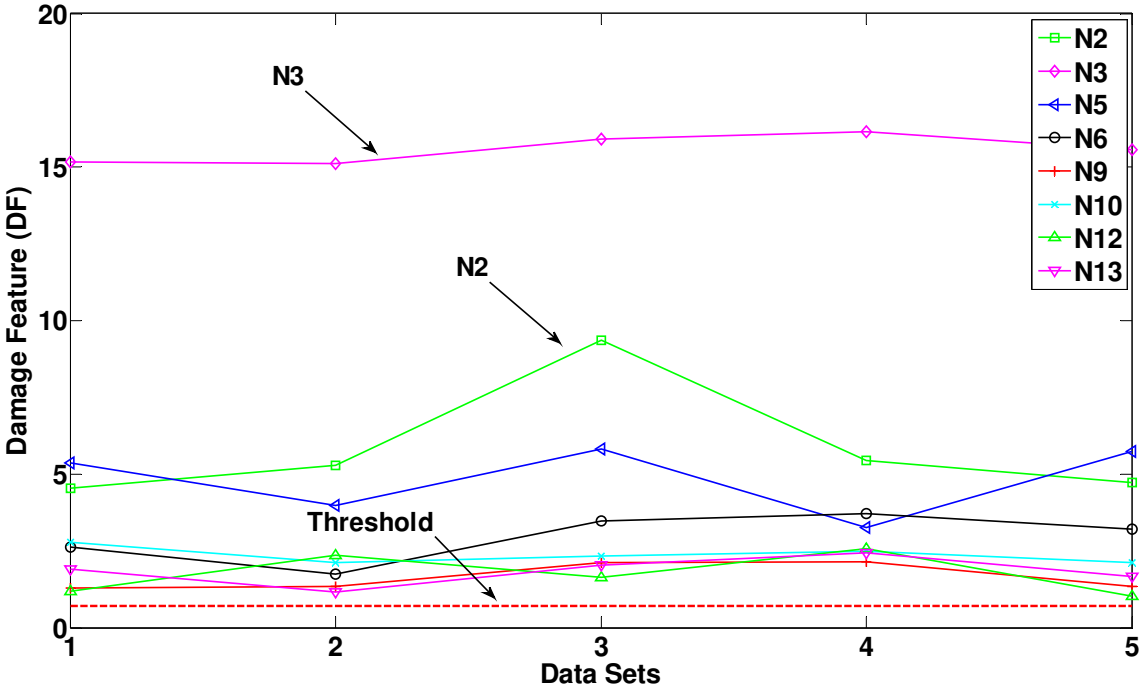

Figure 89. DFs for DC2 using ambient data

Damage Case 3 (DC3): Scour at N4

Figure 90 shows that the DFs for N3 and N5 are significantly high hinting the fact that there has been a major change around these nodes (the roller support at N4 is removed). Furthermore, the DFs for N2 and N6 are also high because these nodes are on the same girder. Therefore, it can be stated the damage for DC3 is also successfully located and quantified by using the ambient vibration data.

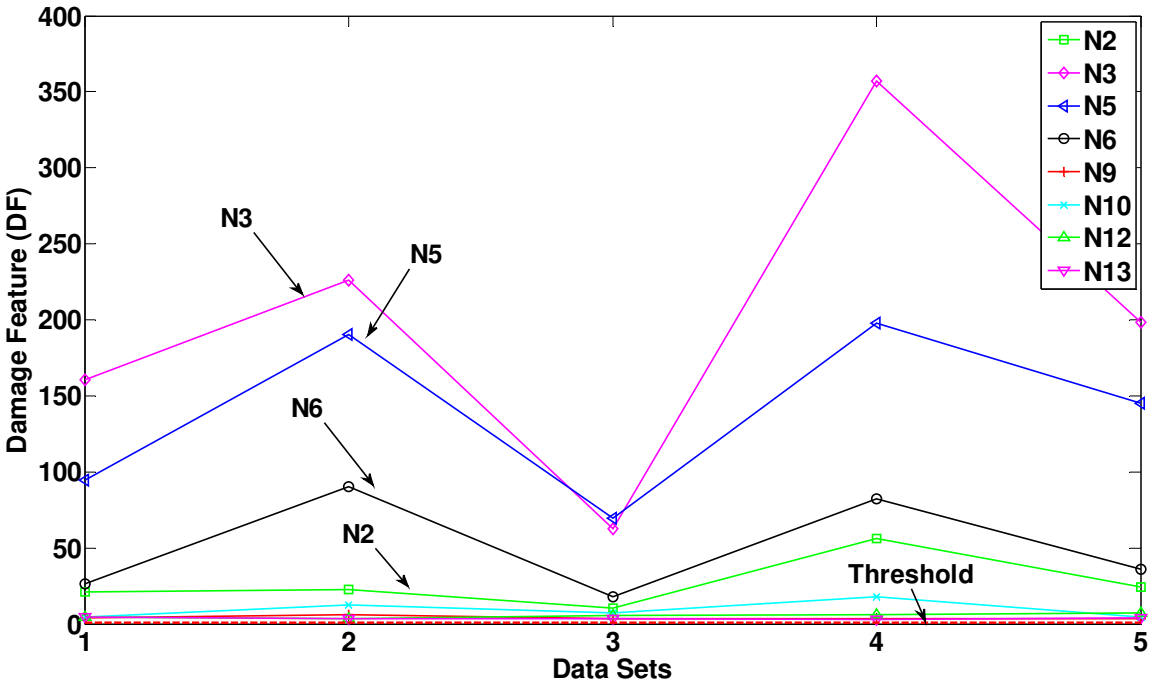

Figure 90. DFs for DC3 using ambient data

Damage Case 4 (DC4): Boundary restraint at N7 and N14

The same plot for the final damage case DC4 is presented in Figure 91. It is observed that the DFs for N6 and N13 are noticeably higher than the other nodes since they are the closest nodes to restrained supports. Furthermore, the effect of the restrained supports is also seen on N5

and N12 since they are on the same span. Again, the consistency of the ambient results with free response results (Figure 87) should be noted.

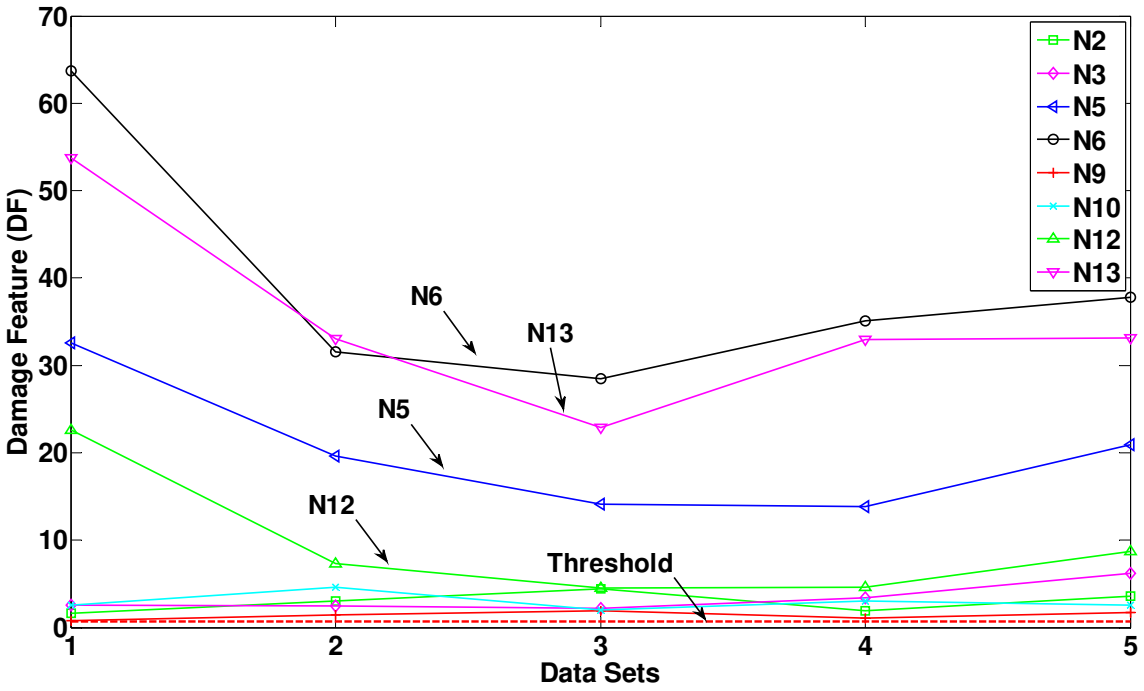

Figure 91. DFs for DC4 using ambient data

4.6. Summary

In this part of the study, a new methodology based on time series analysis is presented for damage detection, localization and quantification. In this methodology, ARX models for different sensor clusters are created and different Damage Features (DFs) are extracted from these models. Two different approaches are introduced where different types of DFs are extracted from the ARX models created for the different clusters.

Approach I is based on direct comparison of the "*B*" term coefficients of the ARX models. This approach is applied to a 4-DOF model for noise-free case and it is shown that

Approach I is very successful at giving exact information about the existence, location and severity of the damage for simple and noise-free models.

In the second part of the study, Approach II is introduced to consider the effects of the noise and model complexity. For Approach II, the fit ratios of the ARX models are used as the DFs. This approach is applied to a 4 DOF and to numerical data of an international benchmark study. Finally, the methodology is applied to experimental data from the steel grid impact and ambient vibration tests. The same damage cases used in previous chapters are used. It is demonstrated the damage can be identified, located and quantified by using Approach II for noisy numerical data and experimental data.

CHAPTER 5. REAL LIFE APPLICATIONS

5.1. General Remarks

One of the proposed studies for this dissertation was the implementation of different methodologies on laboratory structures (discussed in previous chapters) and a real bridge that our research team was planning to start at the time of the proposal defense. The SHM design, instrumentation, the data and analysis results from this bridge (Sunrise Bridge), which is a movable bridge in Ft. Lauderdale, Florida, was to be presented. Since the project was still ongoing during the compilation of this dissertation, it was decided to present the design and instrumentation of the Sunrise Bridge. For the analysis of real data Professor Guido De Roeck was contacted to obtain data from a past study on the Z24 Bridge in Switzerland. The next sections in this chapter will present SHM design and instrumentation of the Sunrise and Z24 bridges along with analysis of the Z24 data.

5.2. Monitoring of a Movable Bridge (On-going Project)

The Florida Department of Transportation owns and operates the largest number of movable bridges in the U.S. The 98 movable bridges in Florida are complex structures utilizing machinery to open a portion of the bridge allowing for the passage of waterborne traffic. The majority of the movable bridges in Florida are of the bascule type, having interior spans called "leaves" that rotate upward and away from the centerline of the waterway thus providing a clear passage for the marine traffic.

Movable bridges are commonly used over the waterway especially in flat terrain. These bridges also present significant drawbacks and problems associated with the operation and

performance. Movable bridge rehabilitation and maintenance costs are considerably higher than that of fixed bridges. Deterioration and damage is observed due to the proximity of these bridges to waterways, moving parts, friction, and wear and tear of the structural and mechanical components. If there are breakdowns, these cause problems for both land and maritime traffic. Maintenance costs associated with the operation system and mechanical parts require special expertise and may cause extensive repair work. Finally, difficulty in repair works is an issue for movable bridges. A malfunction of any component can cause an unexpected failure of bridge operation. Electrical and mechanical problems may require experts and may be difficult and time consuming to fix.

Structural health monitoring can be considered as an approach to continuously monitor the structural, mechanical, and even electrical components of a movable bridge mainly for bridge maintenance and predicting possible problems in advance. Such a monitoring program can generate flags and warnings for maintenance to indicate a worsening condition according to industry standards, manufacturer recommendations, and/or preset thresholds. Methods and approaches discussed in previous chapters can be implemented to track the performance of the structure. In addition, root causes of the structural and mechanical problems can be determined, and future designs can be improved using the information generated using the monitoring system.

In this part of the dissertation, the design and implementation of a monitoring system on a movable bridge in Ft. Lauderdale (Figure 92) will be presented. The selected representative movable span (constructed in 1989) is the west-bound span of two parallel spans on Sunrise Boulevard in Ft. Lauderdale (Catbas et al. 2009). It has double bascule leaves, with a total length

of 117 ft, width of 53.5 ft each 70-ft long, and 40-ft wide, carrying three traffic lanes. The bridge opens every 30 minutes when requested and about 10 times a day.

Figure 92. Sunrise Bridge in Ft. Lauderdale, FL

5.2.1. Design of the Sensor Network

The data acquisition system (DAS) is a critical component of a structural health monitoring system that includes sensors, data acquisition systems, signal processing, synchronization, and storage of the data. In this real-life bridge monitoring application, the data acquisition equipment is installed in permanent protective and temperature-humidity-controlled-enclosures located in both machinery rooms at each side of the bridge. The sensors are connected by weatherproof cables and specially designed connectors. Since the two leaves of the movable bridge are physically separated from each other, wireless communication is provided to ensure the data transmission between the leaves of the bridge, and two GPS units are used for synchronization. Figure 93 shows the scheme used for the data transmission.

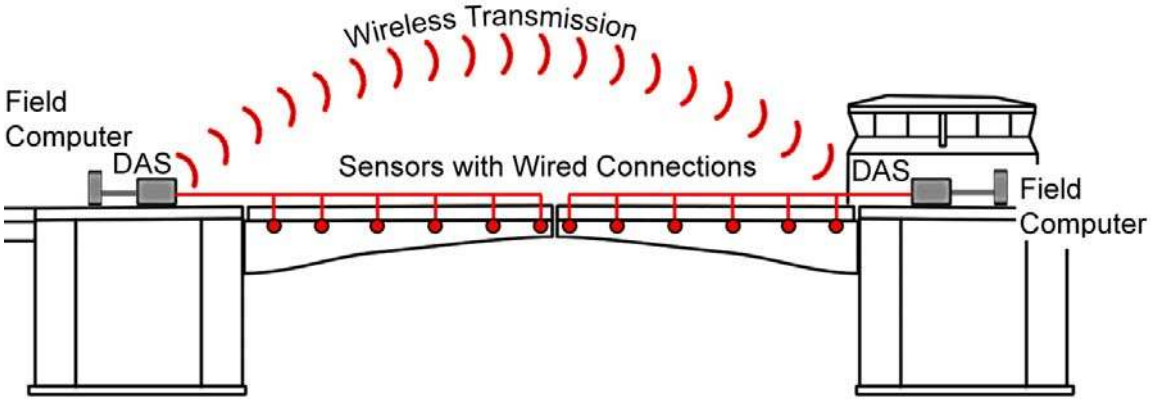

Figure 93. Data transmission scheme

The instrumentation plan is designed to monitor the most critical electrical, mechanical, and structural components. The current installation consists of an array of 162 channels/sensors. These sensors are installed to monitor structural, mechanical, and electrical components of the bridge. In addition, a weather station to monitor the environmental factors is also installed. A summary of the sensors used in the study is shown in Table 7.

Details about the sensing units and other data acquisition components can be given as follows. *Accelerometers:* A total of 40 PCB accelerometers are installed. Sixteen sensors (eight on the girders of each leaf) are installed to measure vertical (12) and horizontal (4) acceleration. Another six are placed on each gearbox and four accelerometers are installed on the electric motors to monitor the performance of the mechanical and electrical components. Also, two accelerometers are placed on each rack and pinion base for detecting excessive vibration. *Dynamic strain gages:* A total of 36 Hitec weldable dynamic strain gages have been deployed on main girders, floor beams, and stringers. *Vibrating wire strain gages:* 36 Geokon VWSG are installed, collecting slow speed temperature and strain data continuously.

Table 7. Summary of the installed sensors

Sensor type	Structural	Mech. and Elect.	Total
High-speed Strain Gage	36	0	36
Vibrating Wire Strain Gage	36	0	36
Strain Rosette	6	16	22
Tiltmeter	4	4	8
Accelerometer	16	24	40
Pressure Gage	4	0	4
Microphone	0	6	6
Infrared Temperature	0	2	2
Video Camera	0	2	2
Ampmeter	0	6	6
Total	102	60	162

Strain Rosettes: 22 Hitec strain rosettes are used in total. Four of these sensors are placed on girders at the live-load shoe locations to correlate with traffic loads, another two at the receiving encasing for the span locks, and eight sensors at the trunnions vicinities for studying the shear on these critical regions. Eight sensors are installed at the main shafts to correlate with tiltmeters and monitor the torque/balance on each opening/closing operation. *Tiltmeters:* A total of eight uniaxial Tuff tiltmeters are used. Four are located at the trunnion regions to correlate with the torque and calculate the friction/balance of the bridge, and another four are placed at the tip of each girder for checking the alignment of both leaves.

Pressure gages: Four TPS sensors are placed at the span-lock hydraulic system for detecting problems related to alignment between the span-lock bar and the receiver. *Infrared Temperature sensors:* Two noncontact IT Omega transmitters are for measuring anomalies on the motor brakes. *Amperage meters:* Six current sensors are placed to monitor the amperage consumption of the motors during the opening/closing operations. *Video cameras:* Two fire wire cameras collect video stream data; one is dedicated to monitor the traffic and the other to detect corrosion on the open gears. *An Orion weather station* is also installed to monitor temperature, humidity, rain, and wind intensity/direction to correlate with all the other measurements.

The SHM system is controlled by two personal computers. All the dynamic sensors are connected to two National Instruments SCXI 1001 signal conditioning chassis with its corresponding modules: SCXI 1520, SCXI 1102B, SCXI 1531; for strain, voltage, and acceleration respectively. The VWSG are controlled by two units CR1000 by Campbell Scientific. The sensor and data acquisition system are schematically shown in Figure 94.

5.2.2. Instrumentation and Data Collection

The technical challenges associated with field implementation of a structural health monitoring program for bridges are commonly related to installation, operation, and maintenance of the various components of the monitoring system. Ideally, a structural health monitoring system should be designed to operate accurately and reliably with minimal maintenance for the entire duration for which the bridge will be monitored. Meeting this standard requires careful consideration of the various issues and incorporating some degree of flexibility and redundancy to the system during its initial design.

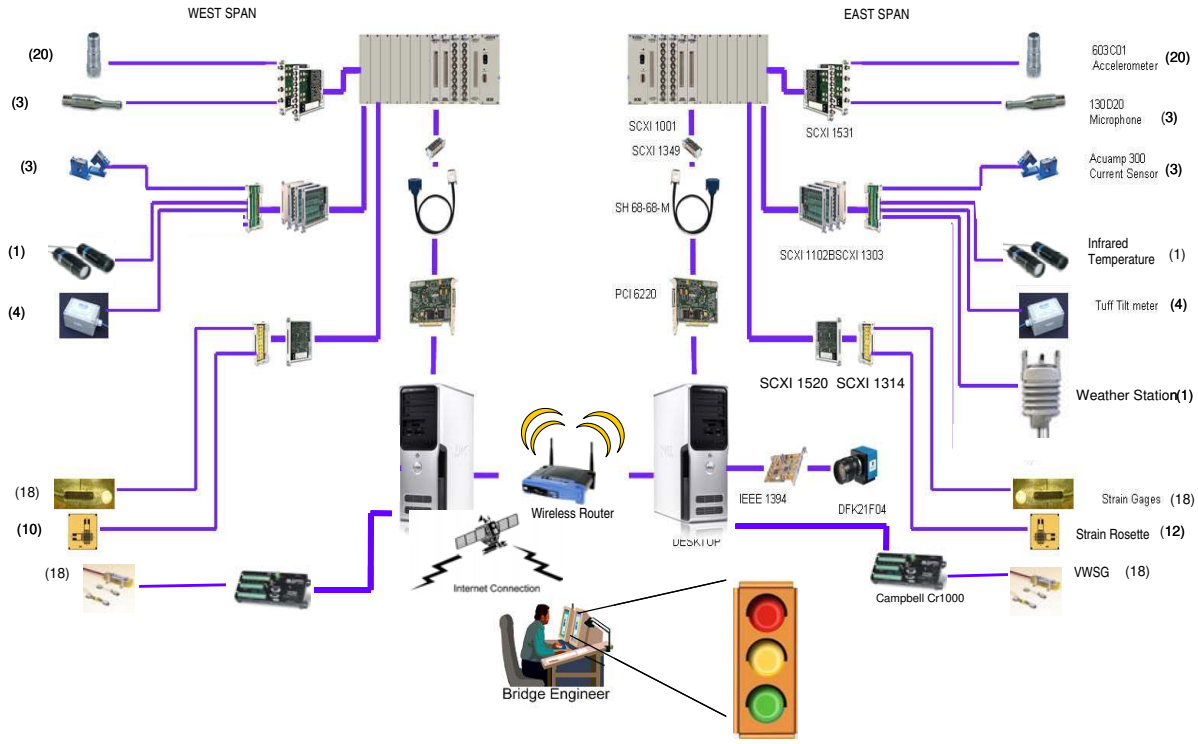

Figure 94. A graphical representation of the DAS components used in the movable bridge project

Another major challenge in the implementation of SHM system in real life is the coordination of fieldwork with infrastructure owners in such a way that sensor and cable installation impact the land and maritime traffic minimally. The sensors on the structural elements are installed by the help of a snooper truck (Figure 95). An example picture showing the installed sensors at the live load shoe area is presented in Figure 96. The same figure provides close-up pictures showing some of the vibrating wire and high-speed strain gages and specially designed connectors. Finally, Figure 97 (a) and (b) shows the instrumentation at the mechanical parts.

5.2.3. Data Analysis Strategies

As discussed above, different components of the bridge are monitored such as the main girders, floor beams, stringers, gearbox, electrical motor, trunnion, brakes, live load shoe, and electrical components. It is clear that different methodologies should be employed to obtain the most useful information about the safety, reliability, and maintenance of the bridge. First, threshold levels for each component during its normal operation will have to be established with a statistical confidence interval. Then, the data will be analyzed with different methods to obtain the performance features, which are to be continuously compared with the threshold values during the monitoring program. The methods investigated and developed in this dissertation can be implemented to track the performance and possible damage/deterioration of the movable bridge as discussed in the following.

Figure 95. Sensor installation at the movable bridge

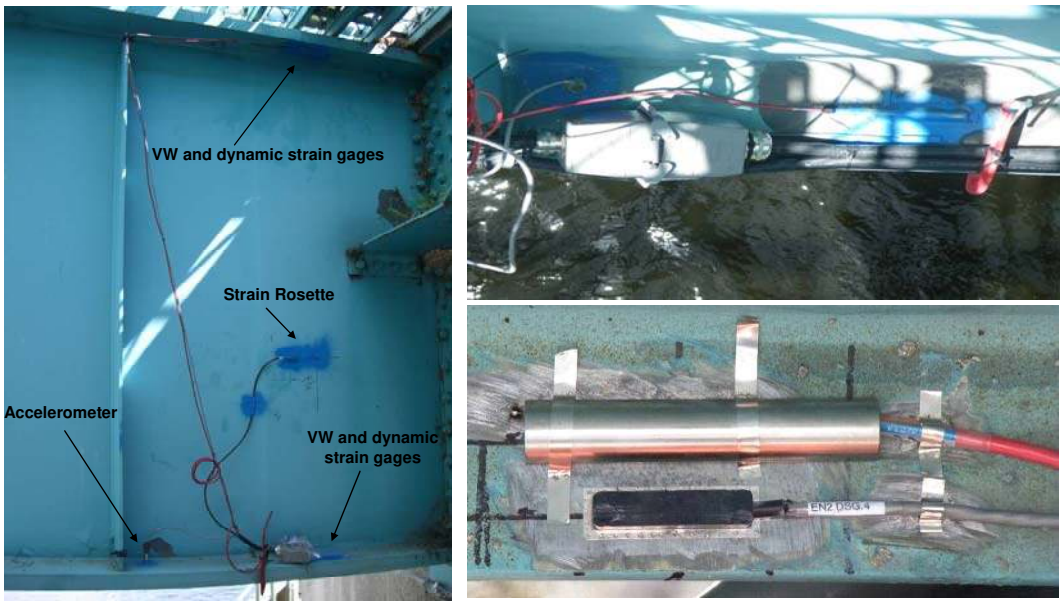

Figure 96. Vibrating wire and high speed strain gages and specially designed connectors

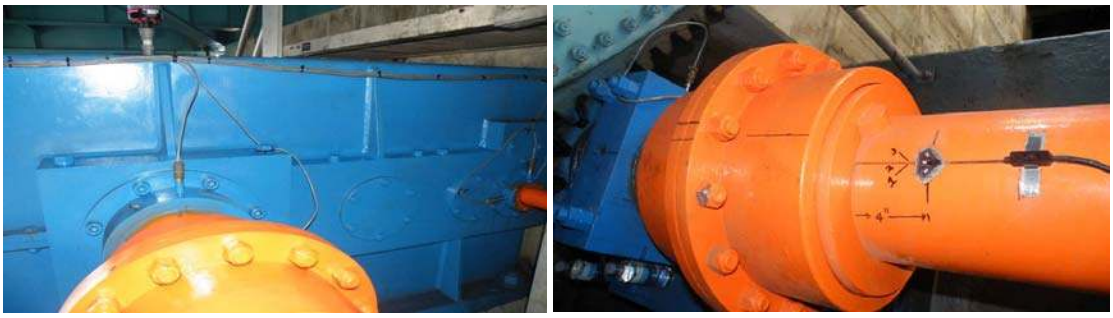

Figure 97. Instrumentation of the mechanical parts: accelerometers at the gearbox and strain rosettes at the drive shaft

The parametric methodologies discussed in Chapter 2 can be used for the assessment of the structural integrity. The vibration data from the structural elements is employed for modal parameter estimation. The modal parameters and modal parameter based damage features such as modal flexibility, modal curvature and pseudo-flexibility are continuously identified and evaluated for structural damage detection. Second, the proposed ARX based damage detection method discussed in Chapter 4 is also implemented as a complement to the parametric methods.

These two approaches are combined for a reliable condition assessment strategy.

The statistical pattern recognition methodologies discussed in Chapter 3 are utilized mainly for the assessment of the mechanical and electrical parts. Different types of data (acceleration, high-speed strain, sound etc.) will be employed for time series analysis based outlier detection. Figure 98 illustrates a conceptual analysis framework to combine the methodologies described in this study for implementation to the SHM system of the movable bridge.

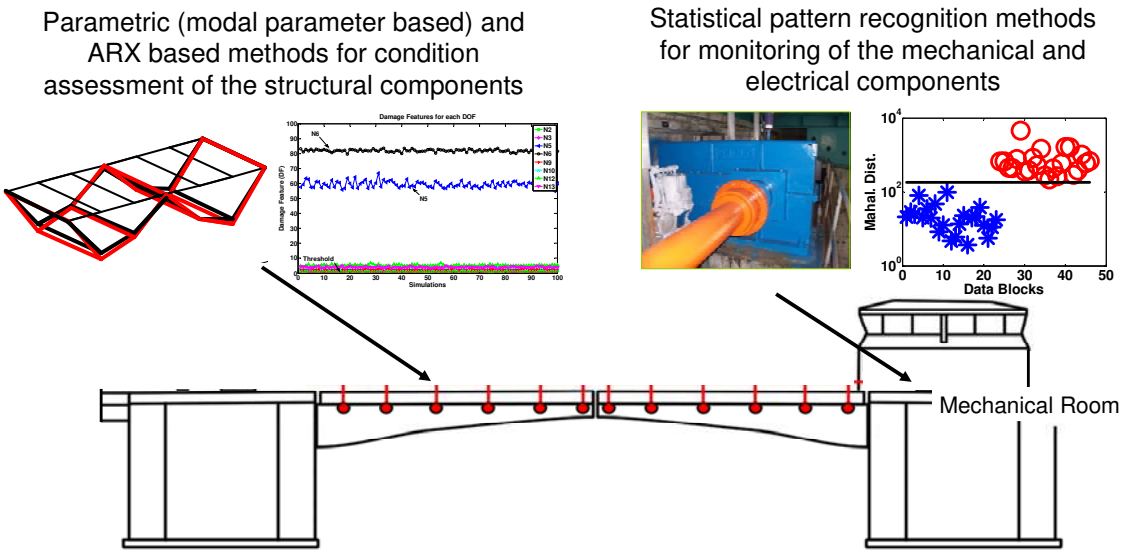

Figure 98. Different analysis strategies for different components of the movable bridge

Since the movable bridge project is still on-going and the installation of the system was not complete at the time of writing this dissertation, the implementation of the methodologies for real life data was not available from the movable bridge. Therefore, the data from Z24 bridge benchmark problem was used to demonstrate the capabilities and limitations of the damage detection methods for a real life application. The details about the application and analysis

results are given below.

5.3. Z24 Bridge Benchmark

5.3.1. Description of the Bridge and Data Sets

The Z24 Bridge benchmark is one of the most commonly used benchmark problems by researchers in SHM and experimental dynamics. The description of the benchmark will be briefly discussed here. More details about the benchmark problem and damage detection studies can be found in the literature (Kramer et al. 1999; Brincker et al. 2001; Kullaa 2003; Maeck and De Roeck 2003; Maeck and De Roeck 2003; Peeters and Ventura 2003; Catbas et al. 2006).

Z24 Bridge is located in Canton Bern, Switzerland, linking Koppigen and Utzenstorf. The bridge is a highway overpass of the A1, which connects Bern and Zurich. Z24 has three spans with two lanes and approximately 60m overall length. It is a prestressed concrete bridge. The bridge was constructed in 1963 and demolished at the end of 1998 after this research study for the benchmark problem. The overall geometry of the bridge is shown in Figure 99.

A series of progressive damage cases were carried out as a part of this study. The full description of the damage cases can be found in Kramer et al. (1999). In this study, three levels of pier settlement are investigated as shown in Table 8. The levels of the settlements are 40 mm, 80 mm and 95 mm. The damaged pier is referred as the Koppigen pier and it is shown in Figure 99.

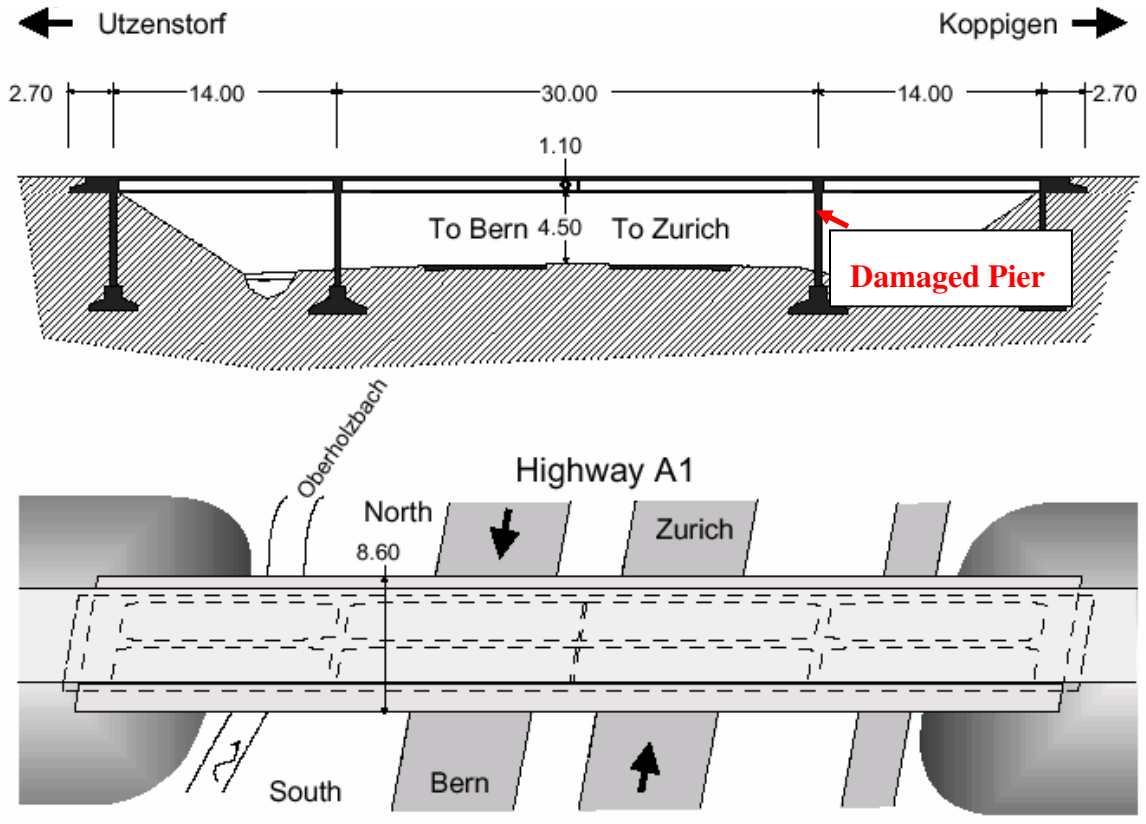

Figure 99. The geometry of the bridge; top and plan view (modified from the Z24 benchmark documents)

Table 8. Damage cases employed in this study

Scenario	Description
Baseline	3rd reference, 'No Damage'
40 mm settlement	Koppigen pier lowered 40 mm
80 mm settlement	Koppigen pier lowered 80 mm
95 mm settlement	Koppigen pier lowered 95 mm

The measurements consisted of ambient and forced vibration tests. The sources of the ambient vibration data on the bridge were mainly the wind and traffic that was passing under the bridge. The forced vibration data was measured by using two shakers simultaneously. The shakers generated random vibration on the bridge at locations Reference 1 (R1) and Reference 2 (R2) in Figure 100. The data from the whole bridge was measured by nine setups of 33 accelerometers in vertical, lateral, and transversal directions. The setups are shown Figure 100. The data was collected with a 100 Hz sampling rate. Each data set contains 65536 data points.

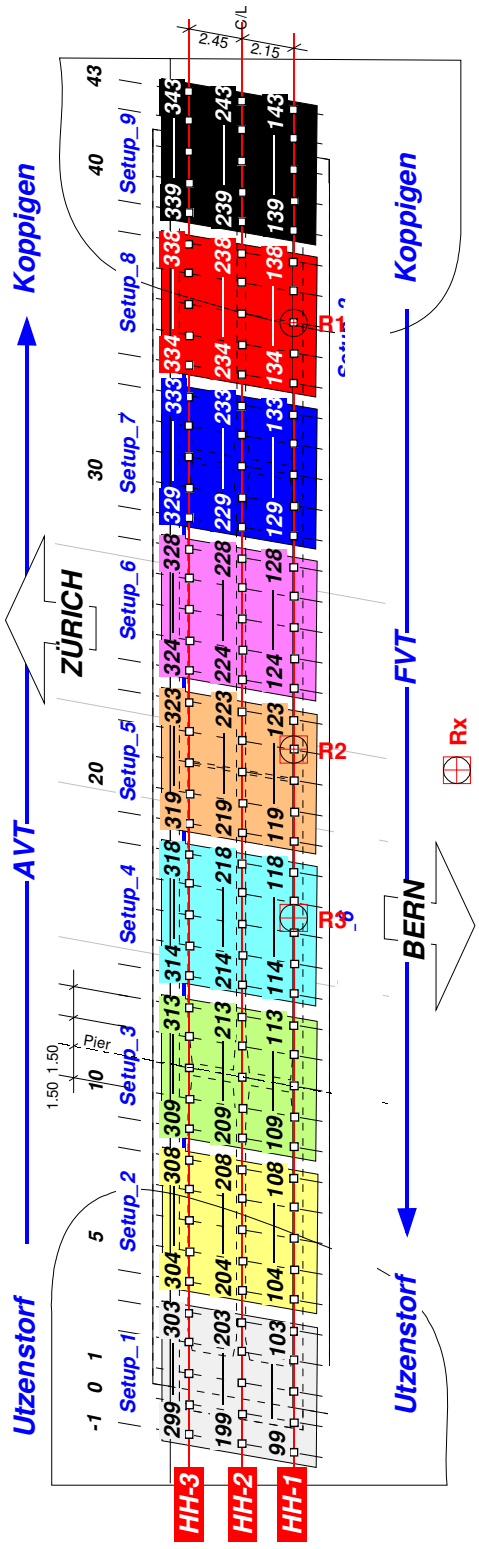

Figure 100. The measurement setups (modified from the Z24 benchmark documents)

5.3.2. Analysis and Results

Ambient Vibration Analysis and Pseudo-Flexibility

The first part of the analysis includes modal identification with the ambient vibration data and using pseudo-flexibility based deflections for damage detection. As mentioned above, the ambient vibration on the bridge was caused mainly by wind and the traffic passing under the bridge. Therefore, the measured vibration level was usually very low, especially for the data from the ends of the bridge. An example of ambient vibration data is shown in Figure 101.

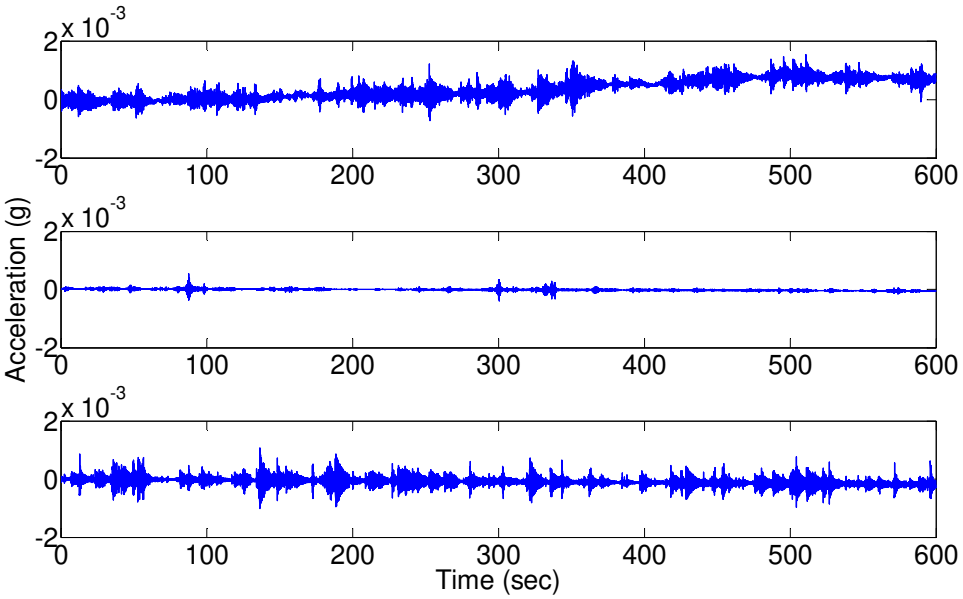

Figure 101. Example ambient data (sample data with some drift-top, good quality low level vibration data-center and good quality data-bottom)

In this study, data from 90 vertical accelerometers at two sides of the bridge are used for the ambient vibration analysis. These sensors shown as 99, 100, …, 143 and 299, 300, …, 343 in Figure 100 are vertical sensors and used for the analyses. Power spectral densities are used instead of Random Decrement since some of the poorly excited modes were not clearly visible with RD. The modal parameters are identified by using CMIF, which was discussed in the

previous chapters. An example CMIF plot for the baseline case is presented in Figure 102. The first five mode shapes of the baseline case that are used in the pseudo-flexibility calculations are shown in Figure 103-Figure 108. The second mode was not used in the calculations of the pseudo-flexibility since it is a highly lateral mode and the vertical contribution of this mode was negligible.

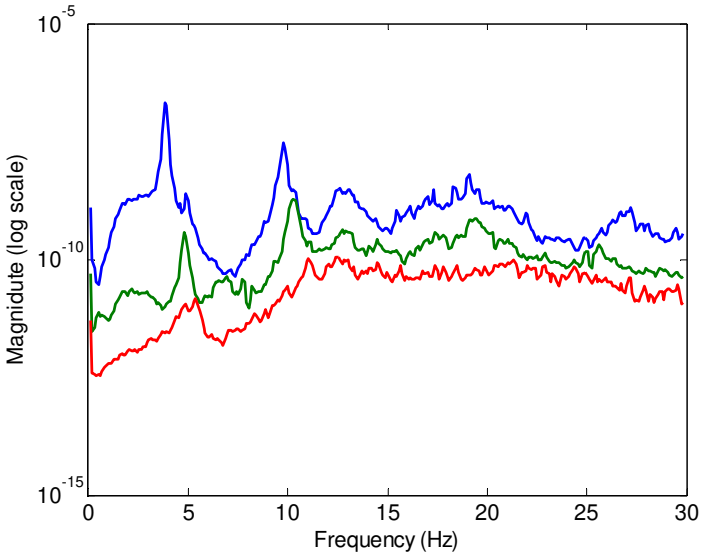

Figure 102. An example of CMIF plot for the baseline case

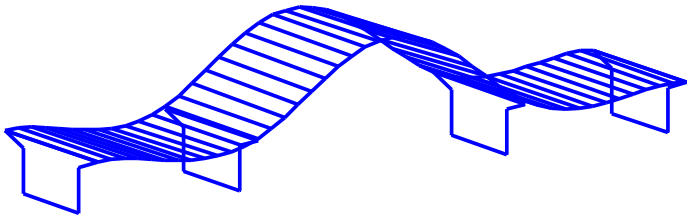

Figure 103. The first mode at 3.86 Hz

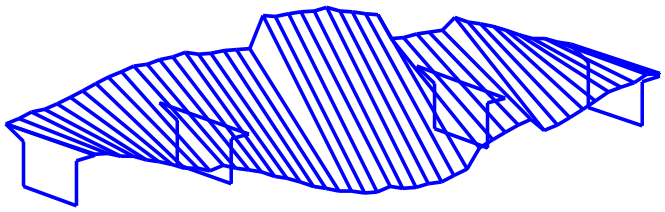

Figure 104. The second mode at 4.89 Hz

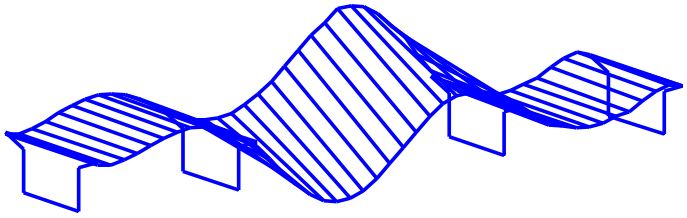

Figure 105. The third mode at 9.78 Hz

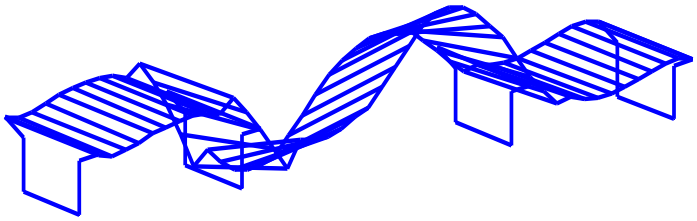

Figure 106. The fourth mode at 10.24 Hz

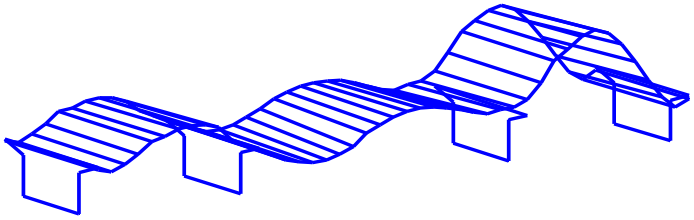

Figure 107. The fifth mode at 12.64 Hz used

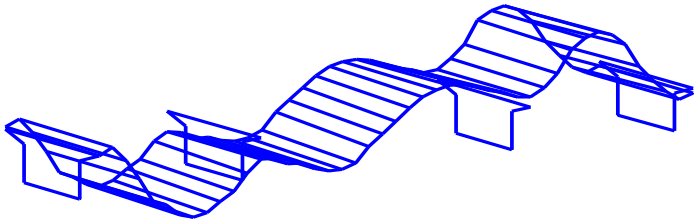

Figure 108. The sixth mode at 13.21 Hz

The pseudo-flexibilities for each case are computed by using the identified modal parameters. Then, the deflected shapes under a uniform loading were calculated. Figure 109 and Figure 110 show the deflected shape of the Bern and Zurich sides respectively. It is observed from the deflected shapes that the flexibility of the Koppigen side (where the settlement occurred) is slightly higher for the damaged cases. Although the distinction is not very clear, this information is consistently illustrating a higher flexibility at the Koppigen side. These findings may not be a direct indicator of the damage and its location however they are suggesting a further more localized investigation. By conducting a more detailed analysis, the impact of this change as damage on the structure can be determined more reliably.

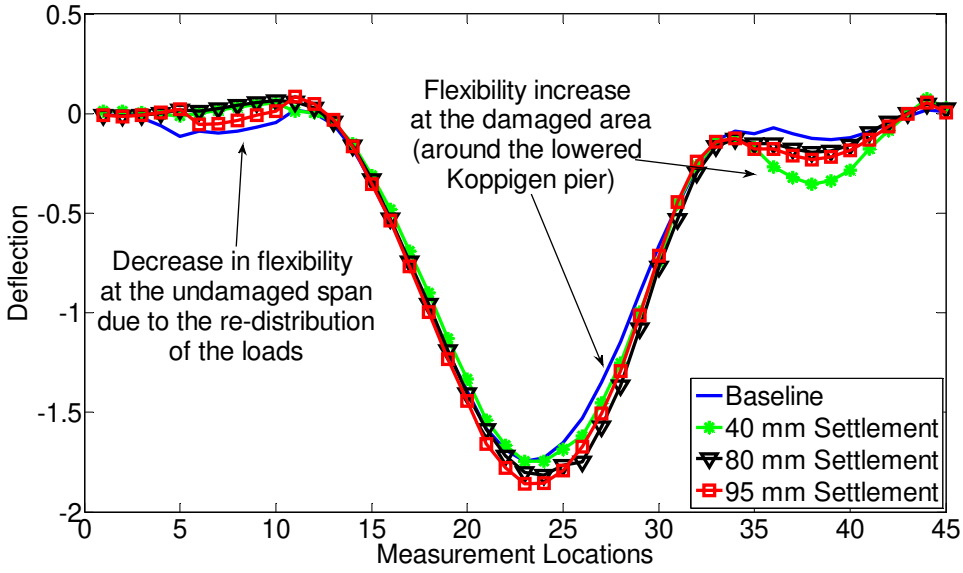

Figure 109. The deflection profile obtained using pseudo-flexibility (Bern side)

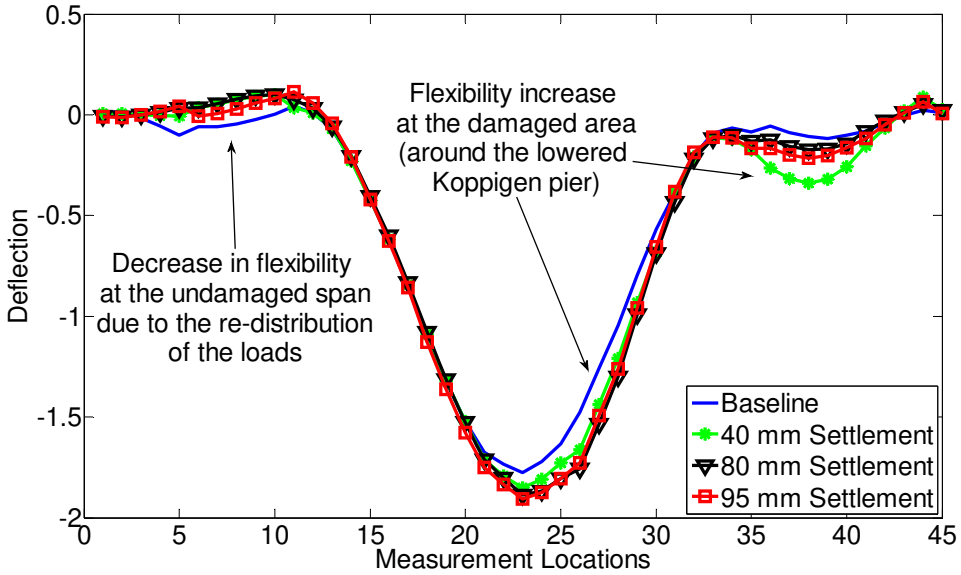

Figure 110. The deflection profile obtained using pseudo-flexibility (Zurich Side)

Outlier Detection with AR Modeling

After investigation of the pseudo-flexibility for damage detection with ambient data, the statistical pattern recognition approaches are explored. Since the level of the ambient vibration data was very low, which sometimes caused instability in the time series models, the time series analysis was conducted by using the response of the forced vibration tests. The excitation force information was not used; i.e. only the acceleration response data was used. Sample forced vibration data is shown in Figure 111. The comparison of the vibration levels of the forced tests with ambient tests (Figure 101) shows that the maximum vibration level from the ambient vibration monitoring are order of magnitude lower than the forced vibration tests.

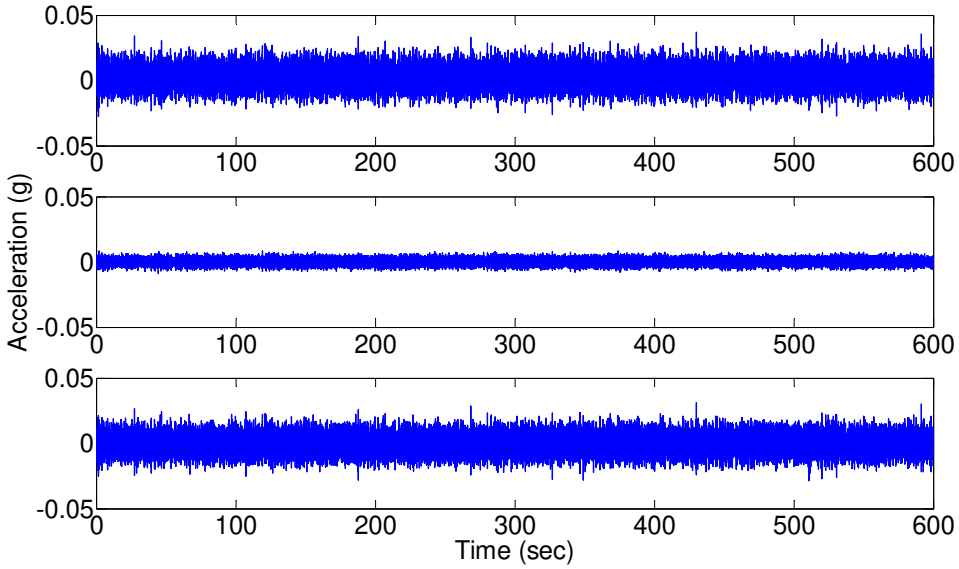

Figure 111. Example of random vibration for the same channels as in Figure 101

For the time series modeling part, four corner sensors from each setup was used, e.g. sensors 99, 103, 299 and 303 for Setup 1. The time history data was averaged by using RD. Then AR models are fitted to each data set. The model order for the AR model is 10. The coefficients of the AR models are used for calculating the Mahalanobis distance of each damage case from the baseline case. For each setup, the Mahalanobis distances for four sensors are averaged.

Figure 112 shows the results for the 95 mm settlement case. Although the Mahalanobis distance for some setups, e.g. Setup 2 and Setup 6, 7 show some change, it is observed that there is no clear separation between the healthy and damaged case. The results are for the other two damage cases (40mm and 80 mm settlement) are not significantly different from this case and they are not shown here.

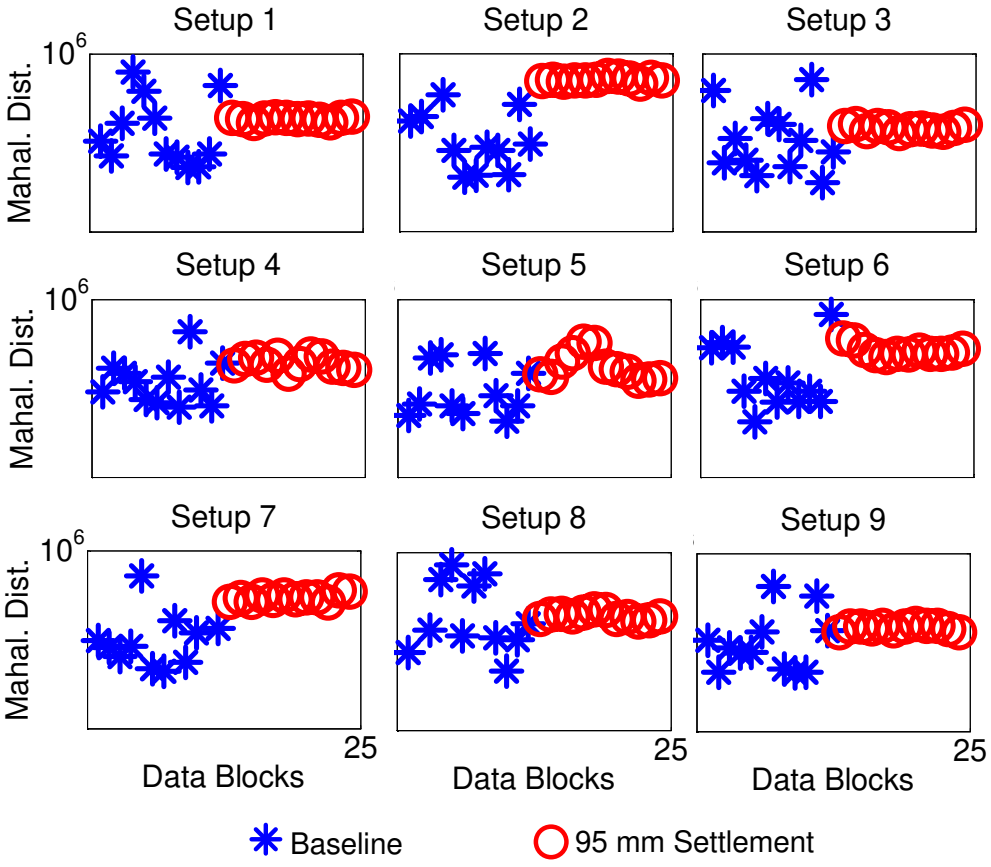

Figure 112. The Mahalanobis distances for each setup for 95 mm settlement case

Application of the New ARX Based Methodology

Finally, the proposed ARX based methodology is applied for damage detection. The damage features are calculated by using the forced vibration data for each setup as well. It should be re-emphasized however that the input excitation was not used in the calculations. Again, four corner sensors are used for each setup. The first sensor is selected as the reference channel (e.g. measurement point 99 in Setup 1) and the four measurements are used to predict the reference measurements after applying RD. The ARX model order is determined as 20.

The Damage Features (DFs) computed for baseline and damaged cases are shown in Figure 113. It is observed that the DFs are higher for Setups 6-9 where the pier settlement occurred. A closer view of the same plot is shown in Figure 114, where the outlier for 80 mm settlement for Setup 90 is excluded. This figure represents a better illustration of the increase in the DFs for the damaged locations. Furthermore, the plots also give an idea about the severity of the damage, as the DFs get higher with increased settlement. It is observed that the DFs for 95 mm settlement are higher than DFs for 80 and 40 mm settlement (except two points) and the DFs for 80 mm settlement are higher than that of 40 mm settlement.

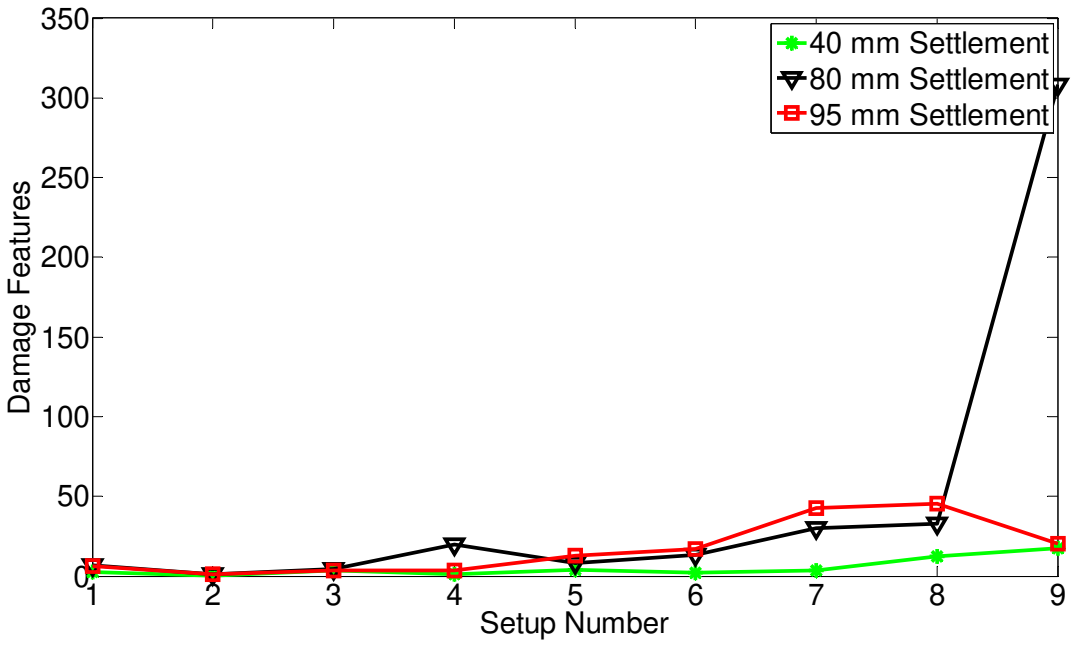

Figure 113. The damage features for each setup

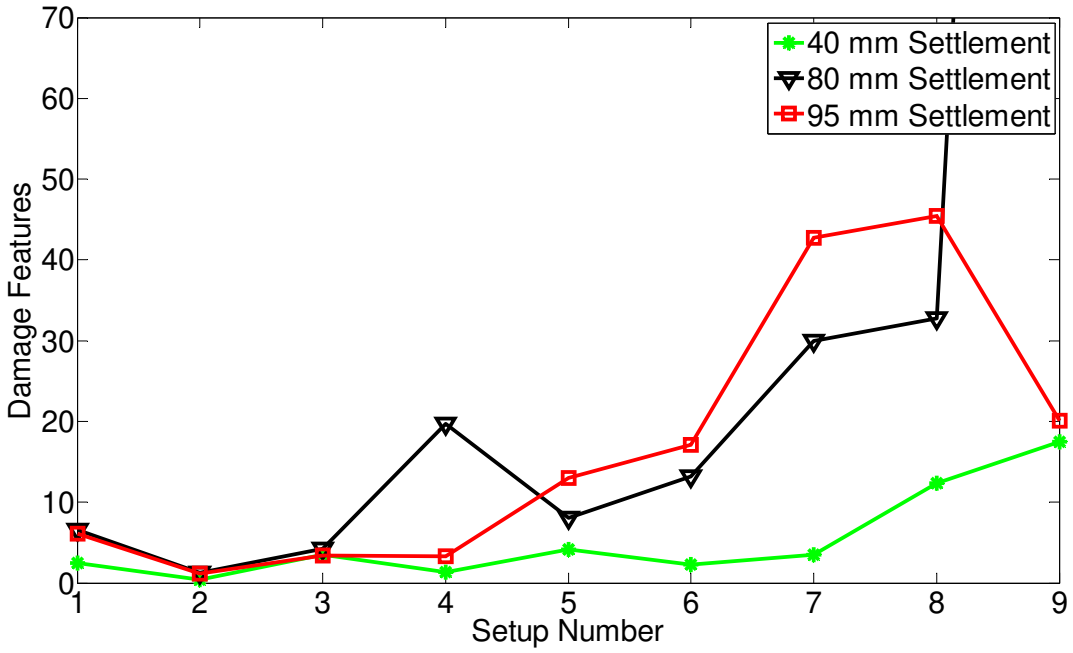

Figure 114. The damage features for each setup (a closer view)

The same analysis is also conducted by using ambient vibration data and it was observed that some false negatives and false positives were obtained although the trends of the DFs provided hints for damage detection. The reason for this is probably the fact that the level of the ambient vibration was very low for some sensors and this created instability in the ARX models, which in return may give higher DFs for locations where damage is not present.

5.4. Summary

In this chapter, two real life SHM applications are discussed. In the first part of the chapter, the design and implementation of a comprehensive SHM system for a movable bridge is presented. Different aspects of the sensor network design for monitoring the structural, mechanical and electrical components are discussed. Since the project is still on-going and the data from this study is not available, the methodologies investigated in this study could not be

employed for implementation on this structure. However, the monitoring for damage detection strategy that will be implemented in the later phases of the monitoring study is discussed along with the instrumentation plan for damage detection techniques explored in this study.

Since the damage detection could not be performed with the movable bridge due to unavailability of data, Z24 bridge benchmark data was used. First, the ambient vibration data analysis was conducted by identifying the modal parameters and obtaining the pseudo-flexibility from the identified parameters. The comparison of the deflected shapes obtained with pseudo-flexibility for baseline and damaged cases showed slight change, which could not be directly attributed to damage. However, these results suggested a more localized analysis. Second, the statistical pattern recognition approach with AR model based outlier detection was employed for damage detection using the forced vibration data. Results of the outlier detection process did not give conclusive results about the existence or location of the damage. Investigation of the results showed weak signs of the separation for the damage features to confidently detect the damage. Finally, the proposed ARX based damage detection method was applied to the forced vibration data. The results showed that the method performed satisfactorily for this case by showing more clear signs of the location and severity of the damage except a few false negatives and false positives.

CHAPTER 6. CONCLUSIONS

The main objective of this dissertation is to investigate different damage detection methods in the context of Structural Health Monitoring (SHM). The dissertation can mainly be summarized in four parts: 1) *the evaluation of parametric methods and damage features* 2) *investigation of statistical pattern recognition techniques for damage detection* 3) *development of a new methodology for damage detection, localization and quantification* and 4) *implementation and demonstration of the methodologies* with laboratory experiments and real life data.

For the parametric damage evaluation approach, different data analysis and feature extraction methods are investigated. A robust and practical frequency domain method for modal parameter identification for Multiple Input Multiple Output (MIMO) and ambient vibration (output only) data is presented. For the MIMO case, the Complex Mode Indicator Function (CMIF) is used to obtain the modal parameters by utilizing Frequency Response Functions (FRFs). For the ambient vibration case, the Random Decrement (RD) method is used for estimating the un-scaled MIMO FRFs to feed to CMIF. Different modal parameter based damage features are extracted from the identified modal parameters, i.e. modal flexibility, modal curvature and pseudo-flexibility. After discussing the theoretical background, the performances of these damage features are evaluated by using experimental data from a steel grid for different damage scenarios.

The experimental studies show that both modal flexibility and modal curvature performed well for localized and global damage cases. It is also noted that change in the modal

curvature is a better indicator for the localized damage cases. For damage detection with output only analysis, the deflection profiles obtained from the un-scaled (pseudo) flexibility is presented as a conceptual damage indicator. It is shown that the pseudo-flexibility performed satisfactorily for global damage cases however, it is not successful at identification of the localized damage cases for the set of laboratory experiments in the scope of this study. The reason might be that the higher modes, which are usually the modes affected by the localized damage, cannot be estimated precisely with ambient vibration analysis because of various reasons such as low excitation of the higher frequency modes or suppressing these modes during the averaging progress.

Statistical pattern recognition approaches for damage detection is presented in the third chapter. Time series analysis along with its implementation with outlier detection for damage detection is discussed. AR modeling is used in conjunction with Mahalanobis distance-based outlier detection algorithm to identify the damage in the structures. The methodologies presented in this chapter can be considered as a complement to commonly employed damage detection methods.

Two different set of experimental studies are conducted for the demonstration of the approach. The first set of experiments is conducted with a simply supported steel beam for different boundary conditions and it is shown that changes in the boundary conditions were identified successfully by using the statistical pattern recognition approach. Furthermore, comparative analyses show that the methodology yields improved results when RD is used for averaging and a better separation is obtained during the outlier detection. The method gives successful results for the steel grid experiments in general. However, it is also observed that the

success rate of the methodology is not as high for some damage cases. This might be caused by the fact that the AR models fitted to the signals coming from the sensors individually might not always capture the effect of the structural change adequately. For some of the cases, the change in the structure might be identified better when different combinations of the sensors are used in the analysis process.

Next*, a new non-parametric damage detection methodology* using ARX analysis of vibration data is introduced. The capability of the proposed method for identifying the existence, location and severity of the damage is discussed. Two different approaches (Approach I and Approach II) are introduced where different types of Damage Features (DFs) are extracted from the ARX models created for the different sensor clusters.

Approach I is based on direct comparison the ARX models and it is very successful at identifying the exact information about the existence, location and severity of the damage for simple and noise-free models. Approach II is introduced to consider the effects of the noise and model complexity, where the fit ratios of the ARX models are used as the DFs. After these models, more complicated numerical and experimental evaluations using the steel grid structure demonstrated the damage can be identified, located and quantified by using Approach II for noisy numerical data and experimental data.

Finally, *real life applications* of SHM are presented in the last part of the dissertation. First, design of an SHM system for a movable bridge is discussed. Different aspects of the design of the sensor network for monitoring of the structural, mechanical and electrical components are discussed along with the damage detection strategy that will be implemented in the later phases

of the study.

In the second part of the real life applications, forced and ambient vibration data from the Z24 Bridge tests were used. First, the ambient vibration data analysis is carried out to obtain the pseudo-flexibility for damage detection. Although the results obtained with pseudo-flexibility do not directly evidence the damage and its location, it shows signs of the stiffness loss at the damaged area suggesting further exploration. Afterwards, the statistical pattern recognition approach with AR model based outlier detection is employed for damage detection. Results of the outlier detection process did not give a definite sign of the existence or location of the damage. Finally, the proposed ARX based damage detection method is employed for damage detection. The results show that the method yields satisfactory results by showing clear signs of the location and severity of the damage despite a few false negatives and false positives.

The experimental and real life studies conducted in this research clearly show that the performance of a data analysis and/or damage detection methodology might considerably change for different structures, excitation types and damage cases. One of the very important conclusions to be withdrawn from this study is that a combination of different approaches should be adapted for a successful and reliable SHM system.

Another very critical challenge in SHM research is the effect of the environmental and operational effects on the data. Damage detection process may easily get very complicated if there is a considerable change in the operational and environmental conditions during the data collection process. Therefore, robust methodologies for elimination of these external effects should be developed and combined with the damage detection methodologies investigated in this

study.

Finally, it is shown that the proposed method is very promising for damage detection implementation in the context of SHM. One immediate step for the future research is the verification of the proposed methodology with different laboratory and real life structures. The reliability of the method should be verified for damage detection with both forced and ambient vibration data. After improving the method and making sure that it can be used for a variety of structures under different loading and environmental conditions, the methodology can be implemented to a wireless sensor network.

LIST OF REFERENCES

Aktan, A. E., Catbas, F. N., Grimmelsman, K. A. and Tsikos, C. J. (2000). "Issues in Infrastructure Health Monitoring for Management." *Journal of Engineering Mechanics, ASCE*, Vol. 126 (7), 711-724.

Aktan, A. E., Farhey, D. N., Brown, D. L., Dalal, V., Helmicki, A. J., Hunt, V. J. and Shelley, S. J. (1996). "Condition Assessment for Bridge Management." *Journal of Infrastructure Systems, ASCE*, Vol. 2 (3), 108-117.

Allemang, R. J. (1999). "Vibrations: Experimental Modal Analysis". Cincinnati, OH, Course Notes, Structural Dynamics Laboratory, University of Cincinnati.

Allemang, R. J. and Brown, D. L. (1982). Correlation Coefficient for Modal Vector Analysis *1st International Modal Analysis Conference*, Orlando, FL.

Allemang, R. J. and Brown, D. L. (1987). "Modal Parameter Estimation" Experimental Modal Analysis and Dynamic Synthesis, USAF.

Allemang, R. J. and Brown, D. L. (1998). "A Unified Matrix Polynomial Approach to Modal Identification." *Journal of Sound and Vibration*, Vol. 211 (3), pp. 301-322.

Alvandi, A. and Cremona, C. (2005). "Assessment of Vibration-Based Damage Identification Techniques." *Journal of Sound and Vibration*, Vol. 292 (1-2), 179-202.

Asmussen, J. C. (1997). Modal Analysis Based on the Random Decrement Technique-Application to Civil Engineering Structures. Aalborg, University of Aalborg.

Asmussen, J. C., Ibrahim, S. R. and Brincker, R. (1996). Random Decrement and Regression Analysis of Traffic Responses of Bridges. *14th International Modal Analysis Conference*, Dearborn, MI.

Beck, J. L., May, M. W. and Polidori, D. C. (1994). Determination of Modal Parameters from Ambient Vibration Data for Structural Health Monitoring. *Proceedings of the 1st Conference on Structural Control*, Pasadena, CA.

Bernal, D. (2002). "Load Vectors for Damage Localization." *Journal of Engineering Mechanics*, Vol. 128 (1), pp. 7-14.

Bernal, D. and Gunes, B. (2004). "Flexibility Based Approach for Damage Characterization: Benchmark Application." *Journal of Engineering Mechanics*, Vol. 130 (1), 61-70.

Box, G. E., Jenkins, G. M. and Reinsel, G. C. (1994). "Time Series Analysis: Forecasting and Control". New Jersey, Prentice-Hall.

Brincker, R., Andersen, P. and Cantieni, R. (2001). Identification and Level 1 Damage Detection of the Z24 Highway Bridge by Frequency Domain Decomposition. *Proceedings of the IMAC XIX Conference*, Kissimmee, FL.

Brincker, R., Zhang, L. and Andersen, P. (2000). Modal Identification from Ambient Responses Using Frequency Domain Decomposition. *Proceedings of the 8th International Modal Analysis Conference (IMAC)*, San Antonio, TX.

Brownjohn, J. M. (2003). "Ambient Vibration Studies for System Identification of Tall Buildings." *Earthquake Engineering and Structural Dynamics*, Vol. 32 (1), pp. 71-95.

Brownjohn, J. M., Tjin, S.-C., Tan, G.-H. and Tan, B.-L. (2004). A Structural Health Monitoring Paradigm for Civil Infrastructure. *1st FIG International Symposium on Engineering Surveys for Construction Works and Structural Engineering*, 28 June–1 July, Nottingham, UK.

Brownjohn, J. M., Zasso, A., Stephen, G. A. and Severn, R. T. (1995). "Analysis of Experimental Data from Wind-Induced Response of a Long Span Bridge." *Journal of Wind Engineering and Industrial Aerodynamics*, Vol. 54/55), pp. 13-24.

Burkett, J. L. (2005). Benchmark Studies for Structural Health Monitoring using Analytical and Experimental Models. Department of Civil and Environmental Engineering. Orlando, FL, University of Central Florida.

Caicedo, J. M., Catbas, F. N., Gul, M. and Zaurin, R. (2007). Phase I of the Benchmark Problem for Bridge Health Monitoring: Numerical Data. *Proceedings of the 18th Engineering Mechanics Division Conference of the ASCE*, June 3-6, 2007, Virginia Tech, Blacksburg, VA.

Caicedo, J. M., Catbas, F. N., Gul, M., Zaurin, R. and Dyke, S. J. (2006). Benchmark Problem for Bridge Health Monitoring: Definition Paper. *Proceedings of the World Conference on Structural Control and Monitoring*, July 11-13, San Diego, CA.

Caicedo, J. M., Dyke, S. J. and Johnson, E. A. (2004). "Natural Excitation Technique and Eigensystem Realization Algorithm for Phase I of the IASC-ASCE Benchmark Problem-Simulated Data." *Journal of Engineering Mechanics*, Vol. 130 (1), pp. 49-60.

Carden, E. P. and Brownjohn, J. M. (2008). "ARMA Modelled Time-Series Classification for Structural Health Monitoring of Civil Infrastructure." *Mechanical Systems and Signal Processing*, Vol. 22 (2), pp. 295-314.

Carden, E. P. and Fanning, P. (2004). "Vibration Based Condition Monitoring: A Review." *Structural Health Monitoring*, Vol. 3 (4), pp. 355-3777.

Casas, J. R. and Cruz, P. J. S. (2003). "Fiber Optic Sensors for Bridge Monitoring." *Journal of Bridge Engineering, ASCE*, Vol. 8 (6), 362-373.

Catbas, F. N. and Aktan, A. E. (2002). "Condition and Damage Assessment: Issues and Some Promising Indices." *Journal of Structural Engineering, ASCE*, Vol. 128 (8), pp. 1026-1036.

Catbas, F. N., Brown, D. L. and Aktan, A. E. (2004). "Parameter Estimation for Multiple-Input Multiple-Output Modal Analysis of Large Structures." *Journal of Engineering Mechanics ASCE* Vol. 130 (8), 921-930.

Catbas, F. N., Brown, D. L. and Aktan, A. E. (2006). "Use of Modal Flexibility for Damage Detection and Condition Assessment: Case Studies and Demonstrations on Large Structures." *Journal of Structural Engineering, ASCE*, Vol. 132 (11), 1699-1712.

Catbas, F. N., Caicedo, J. M. and Dyke, S. J. (2006). Development of a Benchmark Problem for Bridge Health Monitoring. *Proceedings of the International*

Conference on Bridge Maintenance, Safety and Management, IABMAS, July 16-19, Porto, Portugal.

Catbas, F. N., Ciloglu, S. K., Hasancebi, O., Grimmelsman, K. A. and Aktan, A. E. (2007). "Limitations in Structural Identification of Large Constructed Structures." *Journal of Structural Engineering, ASCE*, Vol. 133 (8), pp. 1051-1066.

Catbas, F. N., Gul, M. and Burkett, J. L. (2008). "Conceptual Damage-Sensitive Features for Structural Health Monitoring: Laboratory and Field Demonstrations." *Mechanical Systems and Signal Processing*, Vol. 22 (7), pp. 1650-1669.

Catbas, F. N., Gul, M. and Burkett, J. L. (2008). "Damage Assessment Using Flexibility and Flexibility-Based Curvature for Structural Health Monitoring." *Smart Materials and Structures*, Vol. 17 (1), 015024 (12 pp).

Catbas, F. N., Gul, M., Zaurin, R., Terrel, T., Dere, Y., Ansley, M., Frangopol, D. M. and Grimmelsman, K. (2009). Structural Health Monitoring for the Safety of Bridges: Fundamental, Application and Organizational Considerations. *ASCE Structures Congress '09*, Apr. 30-May 2, Austin, TX.

Catbas, F. N., Lenett, M., Brown, D. L., Doebling, S., Farrar, C. R. and Turer, A. (1997). Modal Analysis of Multi-Reference Impact Test Data for Steel Stringer Bridges. *Proceedings of the 15th International Modal Analysis Conference*, Orlando, FL.

Catbas, F. N., Shah, M., Burkett, J. and Basharat, A. (2004). Challenges in Structural Health Monitoring. *Proceedings of the 4th International Workshop on Structural Control*, June 10-11, Columbia University, New York.

Chang, C. C., Chang, T. Y. P. and Zhang, Q. W. (2001). "Ambient Vibration of Long-Span Cable-Stayed Bridge." *Journal of Bridge Engineering, ASCE*, Vol. 6 (1), 46-53.

Chang, P. C., Flatau, A. and Liu, S. C. (2003). "Review Paper: Health Monitoring of Civil Infrastructure." *Structural Health Monitoring*, Vol. 2 (3), pp. 257-267

Chapra, S. C. and Canale, R., P. (2002). "Numerical Methods for Engineers with Software Programming Applications", McGraw Hill.

Ciloglu, S. K., Catbas, F. N., Pervizpour, M., Wang, A. and Aktan, A. E. (2001). Structural Identification of Phenomenological Physical Models with Controlled Mechanisms of Uncertainty. *Proceedings of SPIE, Smart Systems for Bridges, Structures, and Highways-Smart Structures and Materials*, March 5-7, Newport Beach, CA.

Cole, H. A. (1968). "On-The-Line Analysis of Random Vibrations." *American Institute of Aeronautics and Astronautics*, Vol. 68 (288.

Doebling, S. W., Farrar, C. R., Prime, M. B. and Shevitz, D. W. (1996). Damage Identification in Structures and Mechanical Systems Based on Changes in Their Vibration Characteristics: A Detailed Literature Survey. Los Alamos, NM, Los Alamos National Laboratory Report No. LA-13070-MS.

Dyke, S. J., Bernal, D., Beck, J. L. and Ventura, C. (2001). An Experimental Benchmark Problem in Structural Health Monitoring. *Proceedings of the 3rd International Workshop on Structural Health Monitoring*, Stanford, CA.

Dyke, S. J., Caicedo, J. M., Turan, G., Bergman, L. A. and Hague, S. (2003). "Phase I Benchmark Control Problem for Seismic Response of Cable-Stayed Bridges." *ASCE Journal of Structural Engineering*, Vol. 129 (7), pp. 857-872.

Enright, M. P. and Frangopol, D. M. (1999). "Condition Prediction of Deteriorating Concrete Bridges Using Bayesian Updating." *Journal of Structural Engineering, ASCE*, Vol. 125 (10), 1118-1125.

Ewins, D. J. (2000). "Modal Testing, Theory, Practice and Application ", Research Studies Press Ltd.

Farhey, D. N., Naghavi, R., Levi, A., Thakur, A. M., Pickett, M. A., Nims, D. K. and Aktan, A. E. (2000). "Deterioration Assessment and Rehabilitation Design of Existing Steel Bridge." *Journal of Bridge Engineering, ASCE*, Vol. 5 (1), 39-48.

Farrar, C. R., Duffey, T. A., Doebling, S. W. and Nix, A. D. (1999). A Statistical Pattern Recognition Paradigm for Vibration-Based Structural Health Monitoring. *2nd International Workshop on Structural Health Monitoring*, September 8-10, Stanford, CA.

Farrar, C. R. and Sohn, H. (2000). Pattern Recognition for Structural Health Monitoring. *Workshop on Mitigation of Earthquake by Advanced Technologies*, Nov. 30-Dec. 1, Las Vegas, NV.

Federal Highway Administration (FHWA) (2008). Deficient Bridges by State and Highway System.

Fladung, W. A., Philips, A. W. and Brown, D. L. (1997). Specialized Parameter Estimation Algorithm for Multiple Reference Testing. *15th International Modal Analysis Conference*, February 3-6, Orlando, FL.

Francoforte, K., Gul, M. and Catbas, F. N. (2007). Parameter Estimation Using Sensor Fusion and Model Updating. *Proceedings of the 25th International Modal Analysis Conference (IMAC)*, February 19 - 22, Orlando, FL.

Fu, Z.-F. and He, J. (2001). "Modal Analysis", Butterworth-Heinermann.

Fujino, Y. (2002). "Vibration, Control and Monitoring of Long-Span Bridges – Recent Developments and Practice in Japan." *Journal of Construction Steel Research*, Vol. 58), 71-97.

Gao, Y. and Spencer, B. F. (2006). "Online Damage Diagnosis for Civil Infrastructure Employing a Flexibility-based Approach." *Smart Material and Structures*, Vol. 15), pp. 9-19.

Giraldo, D. and Dyke, S. J. (2004). Damage Localization in Benchmark Structure Considering Temperature Effects. *7th International Conference on Motion and Vibration Control*, August 8-11, St. Louis, MO.

Gul, M. and Catbas, F. N. (2007). Identification of Structural Changes by Using Statistical Pattern Recognition. *The 6th International Workshop on Structural Health Monitoring* September 11-13, Stanford.

Gul, M. and Catbas, F. N. (2008). "Ambient Vibration Data Analysis for Structural Identification

and Global Condition Assessment." *Journal of Engineering Mechanics*, Vol. 134 (8), pp. 650-662.

Gul, M. and Catbas, F. N. (2008). A New Methodology for Identification, Localization and Quantification of Damage by Using Time Series Modeling. *26th International Modal Analysis Conference (IMAC XXVI)*, Feb. 4-7, Orlando, FL.

Gul, M. and Catbas, F. N. (2009). A Modified Time Series Analysis for Identification, Localization, and Quantification of Damage. *27th International Modal Analysis Conference (IMAC XXVII)*, Feb. 9-12, Orlando, FL.

Gul, M. and Catbas, F. N. (2009). "Statistical Pattern Recognition for Structural Health Monitoring using Time Series Modeling: Theory and Experimental Verifications." *Mechanical Systems and Signal Processing*, Vol. 23 (7), pp. 2192-2204.

Gul, M. and Catbas, F. N. (2009). "Structural Health Monitoring and Damage Assessment using a Novel Time Series Analysis Methodology with Sensor Clustering." *Journal of Sound and Vibration*, Vol. (Under Review).

Gul, M., Catbas, F. N. and Georgiopoulos, M. (2007). Application of Pattern Recognition Techniques to Identify Structural Change in a Laboratory Specimen. *Proceedings of the SPIE Smart Structures and Materials & Nondestructive Evaluation and Health Monitoring Conference* March 18-22, San Diego, CA.

Hogue, T. D., Aktan, A. E. and Hoyos, A. (1991). "Localized Identification of Constructed Facilities." *Journal of Structural Engineering, ASCE*, Vol. 117 (1), 128-148.

Holt, R. and Hartmann, J. (2008). Adequency of the U10 & L11 Gusset Plate Designs for the Minnesota Bridge No. 9340 (I-35W over the Mississippi River) - Interim Report, Federal Highway Administration Turner-Fairbank Highway Research Center.

Huang, C. S., B., Y. Y., Y., L. L. and H., C. C. (1999). "Dynamic Testing and System Identification of a Multi-span Highway Bridge." *Earthquake Engineering and Structural Dynamics*, Vol. 28 (8), pp. 857–878.

Huth, O., Feltrin, G., Maeck, J., Kilic, N. and Motavalli, M. (2005). "Damage Identification Using Modal Data: Experiences on a Prestressed Concrete Bridge." *Journal of Structural Engineering, ASCE*, Vol. 131 (12), 1898-1910.

Ibrahim, S. R. and Mikulcik, E. C. (1977). "A Method for the Direct Identification of Vibration Parameters from the Free Response." *Shock and Vibration Bulletin*, Vol. 47 (4), pp. 183-198.

Juang, J.-N. and Pappa, R. S. (1985). "An Eigensystem Realization Algorithm for Modal Parameter Identification and Model Reduction." *Journal of Guidance Control and Dynamics*, Vol. 8 (5), pp. 620-627.

Kao, C. Y. and Hung, S.-L. (2003). "Detection of Structural Damage via Free Vibration Responses Generated by Approximating Artificial Neural Networks." *Computers and Structures*, Vol. 81), pp. 2631-2644.

Ko, J. M. and Ni, Y. Q. (2005). "Technology Developments in Structural Health Monitoring of Large-scale Bridges " *Engineering Structures*, Vol. 27), pp. 1715-1725.

Kramer, C., De Smet, C. A. M. and De Roeck, G. (1999). Z24 Bridge Damage Detection Tests. *Proceedings of IMAC XVII*, Kissimmee, FL.

Kullaa, J. (2003). "Damage Detection of the Z24 Bridge using Control Charts." *Mechanical Systems and Signal Processing*, Vol. 17 (1), pp. 163-170.

Lee, J., Chang, S. P., Kim, S., Chen, S. S. and Cheong, J. J. (2003). Experimental Investigation of Damage Detection on a Scale Model of the Yeongjong Bridge. *1st International Conference on Structural Health Monitoring and Intelligent Infrastructure*, November 13-15, Tokyo, Japan.

Ljung, L. (1999). "System Identification: Theory for the User". Upper Saddle River, NJ, Prentice-Hall.

Lu, Y. and Gao, F. (2005). "A Novel Time-domain Auto-regressive Model for Structural Damage Diagnosis." *Journal of Sound and Vibration*, Vol. 283), 1031-1049.

Lus, H., Betti, R. and Longman, R. W. (1999). "Identification of Linear Structural Systems Using Earthquake-Induced Vibration Data." *Earthquake Engineering and Structural Dynamics*, Vol. 28), pp. 1449-1467.

Lus, H., De Angelis, M. and Betti, R. (2003). "A New Approach for Reduced Order Modeling of Mechanical Systems Using Vibration Measurements." *Journal of Applied Mechanics*, Vol. 70), 715-723.

Lynch, J. P., Sundararajan, A., Law, K. H., Sohn, H. and Farrar, C. R. (2004). Design of a Wireless Active Sensing Unit for Structural Health Monitoring. *Proceedings of the SPIE, NDE for Health Monitoring and Diagnostics*, San Diego, CA.

Maeck, J. and De Roeck, G. (1999). "Dynamic Bending and Torsion Stiffness Derivation from Modal Curvatures and Torsion Rates." *Journal of Sound and Vibration*, Vol. 225 (1), 157-170.

Maeck, J. and De Roeck, G. (2003). "Damage Assessment Using Vibration Analysis on the Z24-Bridge." *Mechanical Systems and Signal Processing*, Vol. 17 (1), pp. 133-142.

Maeck, J. and De Roeck, G. (2003). "Description of Z24 Benchmark." *Mechanical Systems and Signal Processing*, Vol. 17 (1), pp. 127-131.

Mahalanobis, P. C. (1936). "On the Generalized Distance in Statistics." *Proceedings of the National Institute of Sciences of India*, Vol. 2), 49-55.

Maia, N. M. M. and Silva, J. M. M. (1997). "Theoretical and Experimental Modal Analysis". Taunton, Somerset, UK, Research Studies Press Ltd.

Manson, G., Worden, K. and Allman, D. (2003). "Experimental Validation of a Structural Health Monitoring Methodology. Part II. Novelty Detection on a GNAT Aircraft." *Journal of Sound and Vibration*, Vol. 259 (2), pp. 345-363.

Maxwell, J. C. (1864). "On the Calculation of the Equilibrium and Stiffness of Frames." *Philosophical Magazine*, Vol. 27 (4), 294-299.

Monroig, E. and Fujino, Y. (2006). Damage Identification Based on a Local Physical Model for Small Clusters of Wireless Sensors. *1st Asia-Pacific Workshop on Structural Health*

Monitoring, Dec. 4-6, Yokohama, Japan.

Motavalli, M. and Gsell, D. (2004). Indoor Cable Stayed GFRP-Bridge at EMPA, Switzerland. *1st Conference on Application of FRP Composites in Construction and Rehabilitation of Structures*, Tehran, Iran.

Nair, K. K. and Kiremidjian, A. S. (2005). A Comparison of Local Damage Detection Algorithms Based on Statistical Processing of Vibration Measurements. *Proceedings of the 2nd International Conference on Structural Health Monitoring and Intelligent Infrastructure (SHMII)*, Shenzen, China.

Nair, K. K., Kiremidjian, A. S. and Kincho, H. L. (2006). "Time Series-Based Damage Detection and Localization Algorithm with Application to the ASCE Benchmark Structure." *Journal of Sound and Vibration*, Vol. 291 (1-2), pp. 349-368.

Omenzetter, P. and Brownjohn, J. M. (2006). "Application of Time Series Analysis for Bridge Monitoring." *Smart Material and Structures*, Vol. 15), pp. 129-138.

Pandey, A. K., Biswas, M. and Samman, M. M. (1991). "Damage Detection from Changes in Curvature Mode Shapes." *Journal of Sound and Vibration*, Vol. 145 (2), 321-332.

Pandit, S. M. and Wu, S. M. (1993). "Time Series and System Analysis with Applications". Malabar, FL, Krieger Pub. Co.

Peeters, B. and De Roeck, G. (2001). "Stochastic System Identification for Operational Modal Analysis: A Review." *Journal of Dynamic Systems, Measurements and Control*, Vol. 123), pp. 659-667.

Peeters, B. and Ventura, C. (2003). "Comparative Study of Modal Analysis Techniques for Bridge Dynamic Characteristics." *Mechanical Systems and Signal Processing*, Vol. 17 (5), pp. 965-988.

Ren, W.-X., Zhao, T. and Harik, I. E. (2004). "Experimental and Analytical Modal Analysis of Steel Arch Bridge." *Journal of Structural Engineering, ASCE*, Vol. 130 (7), pp. 1022-1031.

Rodrigues, J., Brincker, R. and Andersen, P. (2004). Improvement of Frequency Domain Output Only Modal Identification from the Application of the Random Decrement Technique *22nd International Modal Analysis Conference*, January 26-29, 2004, Dearborn, MI.

Rytter, A. (1993). Vibration Based Inspection of Civil Engineering Structures. Department of Building Technology and Structural Engineering. Aalborg, Denmark, University of Aalborg. **Doctoral Dissertation**.

Sanayei, M., Bell, E. S., Javdekar, C. N., Edelmann, J. and Slavsky, E. (2006). "Damage Localization and Finite-Element Model Updating Using Multiresponse NDT Data." *Journal of Bridge Engineering*, Vol. 11 (6), pp, 688-698.

Shih, C. Y., Tsuei, Y. G., Allemang, R. J. and Brown, D. L. (1988). "Complex Mode Indication Function and Its Application to Spatial Domain Parameter Estimation." *Mechanical Systems and Signal Processing*, Vol. 2 (4), 367-377.

Shih, C. Y., Tsuei, Y. G., Allemang, R. J. and Brown, D. L. (1988). "A Frequency Domain

Global Parameter Estimation Method for Multiple Reference Frequency Response Measurements." *Mechanical Systems and Signal Processing*, Vol. 2 (4), 349-365.

Sohn, H., Czarnecki, J. A. and Farrar, C. R. (2000). "Structural Health Monitoring Using Statistical Process Control." *Journal of Structural Engineering, ASCE*, Vol. 126 (11), pp. 1356-1363.

Sohn, H. and Farrar, C. R. (2001). "Damage Diagnosis Using Time Series Analysis of Vibration Signals." *Smart Materials and Structures*, Vol. 10), 1-6.

Sohn, H., Farrar, C. R., Hemez, F. M., Shunk, D. D., Stinemates, D. W. and Nadler, B. R. (2003). A Review of Structural Health Monitoring Literature: 1996-2001, Los Alamos National Laboratory Report.

Sohn, H., Farrar, C. R., Hunter, N. F. and Worden, K. (2001). "Structural Health Monitoring Using Statistical Pattern Recognition Techniques." *Journal of Dynamic Systems, Measurement, and Control, ASME*, Vol. 123), 706-711.

Toksoy, T. and Aktan, A. E. (1994). "Bridge Condition Assessment by Modal Flexibility." *Experimental Mechanics*, Vol. 34 (3), 271-278.

Van Overschee, P. and De Moor, B. (1996). "Subspace Identification for Linear Systems: Theory, Implementation and Applications". Dordrecht, The Netherlands, Kluwer Academic Publishers.

Vold, H., Kundrat, J., Rocklin, T. and Russel, R. (1982). "A Multi-Input Modal Estimation Algorithm for Mini-Computers." *SAE Paper Number 820194*, Vol.), 10 pp.

Worden, K., Manson, G. and Fieller, N. R. J. (2000). "Damage Detection Using Outlier Analysis." *Journal of Sound and Vibration*, Vol. 229 (3), pp. 647-667.

Yang, J. N., Lei, Y., Lin, S. and Huang, N. (2004). "Identification of Natural Frequencies and Dampings of In Situ Tall Buildings Using Ambient Wind Vibration Data." *Journal of Engineering Mechanics*, Vol. 130 (5), pp. 570-577.

Zhang, Q. W. (2007). "Statistical Damage Identification for Bridges Using Ambient Vibration Data." *Computers and Structures*, Vol. 85 (7-8), pp. 476-485

Zheng, H. and Mita, A. (2007). "Two-stage Damage Diagnosis Based on the Distance between ARMA Models and Pre-whitening Filters." *Smart Material and Structures*, Vol. 16), pp. 1829-1836.